M.Sc. Dissertation

Atmospheric Boundary Layer Characterizations over Highveld Region South Africa

Philbert Modest Luhunga

A dissertation submitted in partial fulfillment of the requirements for the degree

Master of Science in Meteorology

Department of Geography, Geoinformatics and Meteorology

February 2013

Declaration of Originality

I declare that this dissertation is my own unaided work. It is being submitted for the degree of Master of Science in Meteorology at the University of Pretoria, Pretoria, South Africa. It has not been submitted previously for any degree or examination in any other universities for a similar or any other degree award. I also declare that all the sources I have quoted have been indicated and acknowledged by complete references.

Signed _____

Date _____

Dissertation Supervisors

Main Supervisor: Professor George Djolov

Department of Geography, Geoinformatics and Meteorology, University of Pretoria

Co-Supervisor: Professor Sivakumar Venkataraman

Department of Physics, University of Kwa-Zulu Natal, Durban 4000, South Africa

ACKNOWLEDGEMENTS

First and foremost, I would like to express my gratefulness and appreciation to my supervisor Professor George Djolov, for financial support and encouragement, through his guidance, constructive comments and useful suggestions during the preparation of this study. It gives me a special pleasure to thank my research co-supervisor, Professor Sivakumar Venkataraman for financial support and assistance, numerous ideas and vital contributions to this study, with whom this research would not have been successful. You made a difference in my professional career.

Finally, I would like to say a sincere word of thanks to my wife Ester Msigwa and my children, Daniel and Anastasia Philbert without their unconditional love, devotion and encouragement; I certainly could not have seen this work through. They really deserve countless thanks for putting up with my long absence.

Above all things, the unconditional love, help, protection and guidance that I received from God, the most Gracious and Merciful, has been so profound. Let His name to be praised.

PUBLISHED MATERIAL FROM THIS DISSERTATION PEER REVIEWED PAPERS

P. Luhunga, I. Esau, G. Djolov, A Study of Stable Atmospheric Boundary Layer over Highveld South Africa, International Conference on Planetary Boundary Layer and Climate Change, IOP Conf. Series: Earth and Environmental Science 13 (2010) 012012doi:10.1088/1755-1315/13/1/012012.

Philbert Luhunga, George Djolov, Venkataraman Sivakumar, 2011:Stable atmospheric boundary layer characterization over Highveld region of South Africa, South African Society for Atmospheric Sciences, 27th Annual Conference 22- 23 September 2011 North-West Province, South Africa, Peer reviewed conference proceedings, , Hartbeespoort, North-West Province, South Africa, ISBN 978-0-620-50849-0

Igor Esau1, **Philbert Luhunga**, George Djolov, and C. J. deW, Rautenbach and Sergej Zilitinkevich, 2012: Links between scales of observed micro-meteorological variability and the land use pattern in Highveld Priority Area of South Africa, Meteorol Atmos Phys DOI 10.1007/s00703-012-0218-4

ABSTRACT

Atmospheric Boundary Layer (ABL) characteristics can be highly complex; the links between spatial and temporal variability of ABL meteorological quantities and existing land use patterns are still poorly understood due to the non-linearity of air-land interaction processes. This study describes the results from Monin Obukhov similarity theory and statistical analysis of meteorological observations collected by a network of ten Automatic Weather Stations (AWSs). The stations were in operation in the Highveld Priority Area (HPA) of the Republic of South Africa during 2008 – 2010. The spatial distribution of stability regimes as presented by both bulk Richardson number (BRN) and Obukhov length (L) indicates that HPA is dominated by strong stability regime. The momentum and heat fluxes show no significant spatial variation between stations. Statistical analysis revealed localization, enhancement and homogenization in the inter-station variability of observed meteorological quantities (temperature, relative humidity and wind speed) over diurnal and seasonal cycles. Enhancement of the meteorological spatial variability was found on a broad range of scales from 20 to 50 km during morning hours and in the dry winter season. These spatial scales are comparable to scales of observed land use heterogeneity, which suggests links between atmospheric variability and land use patterns through excitation of horizontal meso-scale circulations. Convective motions homogenized and synchronized meteorological variability during afternoon hours in the winter seasons, and during large parts of the day during the moist summer season. The analysis also revealed that turbulent convection overwhelms horizontal meso-scale circulations in the study area during extensive parts of the annual cycle

Key words: Micro-meteorology, Atmospheric boundary layer, Air-land interactions, Statistical data analysis, LiDAR

LIST OF ACRONYMS

ABL	Atmospheric Boundary Layer
AP	Air Pollution
ASI	Atmosphere-Surface Intermittency
BL	Boundary Layer
BRN	Bulk Richardson Number
CAC	Clear Air Cooling
CBL	Convective Boundary Layer
CSIR	Council for Scientific and Industrial Research
CWOP	Citizen Weather Observer Program
DAWS	Davis Automatic Weather Stations
DEA	Department of Environmental Affairs
GCM	General Circulation Model
HPA	Highveld Priority Area
K-H	Kelvin-Helmholtz
LiDAR	Light Detection and Ranging
MMEH	Micro-Meteorological Experiment in Highveld
MO	Monin–Obukhov
NBLs	Neutral Boundary Layers
NDVI	Normalized Digital Vegetation Index
NLC	National Laser Centre

NLC	National Laser Centre
NWP	Numerical Weather Prediction
OLR	Outgoing Long wave Radiation
PBL	Planetary Boundary Layer
RL	Residual Layer
RMS	Root Mean Square
SBL	Stable Atmospheric Boundary Layer
TKE	Turbulent Kinetic Energy
TPE	Turbulent Potential Energy
TTE	Total Turbulent Energy

CONTENT

LIST OF FIGURES

LIST OF TABLES

CHAPTER 1

INTRODUCTION

1.1 General Introduction

Stull (1988) defines the Atmospheric Boundary Layer (ABL) as that part of the troposphere that is directly influenced by the presence of the earth's surface, and responds to surface forcing with a time scale of about one hour or less. These forcings include frictional drag, evaporation and transpiration, heat transfer, pollutant emission, and terrain induced flow modification. Surface forcings in the ABL induce significant turbulent fluxes of momentum, heat or matter that are carried by turbulent motions on a scale order of few kilometers or less.

ABL is very important in atmospheric studies since it plays a significant role on the dynamic state of the entire atmosphere. More than 95% of the solar energy is received at the lower part of the ABL where it is transformed and transmitted to different parts of the atmosphere by different processes occurring in the ABL, such as turbulent mixing and molecular diffusion. ABL is important in climate simulation and numerical weather prediction (NWP), where an understanding of surface characteristics, air-surface exchanges, Boundary Layer (BL) thermodynamic fluxes, turbulence friction velocities, and clouds are of great practical importance for BL parameterization processes (Van de Wiel et al., 2001). In reality no climate model can succeed without the consideration of BL processes. Furthermore, in NWP models, a good BL is critical to proper prediction of the diurnal cycle of low-level winds and convergence effect for complex terrain and of timing and location of convection. In air pollution and urban meteorology BL processes are responsible for pollutant dispersal and urban heat island effects. In remote sensing where satellite-based measurements of surface winds, skin temperature, involve the interaction of BL and surface and must often be interpreted in light of a BL model to be useful for NWP. In aviation industries, BL processes such as fog formation and dissipation, dangerous wind shear conditions are imperative for aircraft safety. In agriculture meteorology BL processes are responsible for prediction of frost, dew, evapo-transpiration or evaporation and dispersal of pesticides. BL processes also play a role in plant pollination process.

ABL is uniquely characterized by turbulence processes, which are due to the non-linearity of the processes governing its dynamics. Turbulence is several orders of magnitude more effective at transporting atmospheric quantities in this layer than is the molecular diffusivity. It is defined as the gustiness superimposed on the mean wind, which can be visualized as irregular swirls of motion called eddies (Stull, 1988). Turbulent flows are presented as a superposition of eddies of different sizes and periods, that range from under the millimeter (or second) to few kilometers (or hours). These eddies are generated by thermal convection and mechanically by wind shear, also orography plays an important role on generating or destroying them.

Turbulence play significant role on development of ABL depth over space and time scales (Panofsky and Dutton, 1984; Stull, 1988) ranging from several meters during calm clear nights up to few kilometers on sunny summer days (Mauritsen, 2007). Over the oceans, the depth of the ABL varies relatively slowly in space and time because the sea surface temperature does not change very much over diurnal cycle. On the contrary, over the land, the depth of the BL is more variable in space and time because temperature over the land surface is more variable over the diurnal cycle (Stull, 1988).

ABL structure varies over diurnal cycle (Fig. 1.1). The three components of this structure are; a very turbulent mixed layer, also known as the Convective Boundary Layer (CBL), a less turbulent Residual Layer (RL) containing former mixed-layer air and a Stable Boundary Layer (SBL). The CBL is characterized by vigorous turbulence which tends to stir and uniformly mix variables such as conservative tracer concentrations, potential temperature and momentum (AMS, 2000). After sunset, turbulence decays, leaving a RL in the place of CBL. The RL is neutrally stratified, resulting in turbulence that is nearly of equal intensity in all directions (Stull, 1988). The radiative cooling of the ground leads to development of a shallow SBL. This layer is described in AMS (2000) as a cool layer of air adjacent to a cold surface of the earth, where temperature within that layer is statically stably stratified. The main features as well as the processes that take place in the SBL are quite different to those observed in other ABL regimes. In this dissertation the SBL is studied in depth because of its relevance to the air pollution problem but the data is used for all ABL stability regimes to determine the heterogeneity influence on PBL dynamics.

1.2 The Stable Boundary Layer

The Stable Boundary Layer (SBL) forms when the solar heating ends and the bottom parts of the residual layer is transformed by its contact with a quickly cooling earth's surface into a SBL (Stull, 1988). Turbulence in this layer is mainly generated mechanically usually by wind shear and destroyed by negative buoyancy. Wind shear in the SBL generates Kelvin-Helmholtz (K-H) instabilities. These are waves that propagate upward within the SBL eventually reach the level where their frequencies matches the ambient Brunt-Väisälä frequency, at which level the waves are reflected back toward the ground (Jiménez, 2005). The generated waves are trapped between the ground and the neutral layers or RL aloft, resulting in horizontally propagating waves.

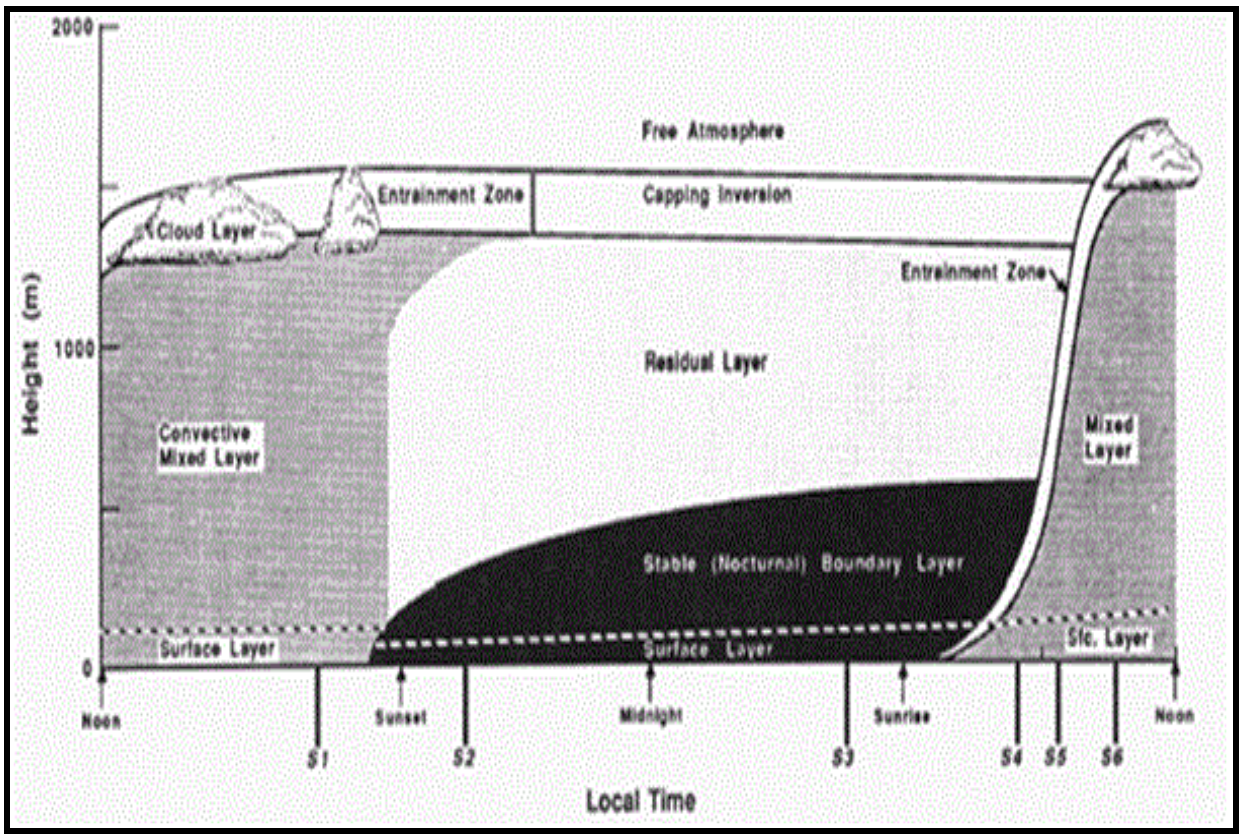

FIGURE 1.1: Diurnal cycle of ABL in high pressure region over the land (Stull, 1988).

The SBL is also characterized by gravity waves. Chimonas (2001) indicated that the SBL at the base of RL supports internal waves that are unambiguously "boundary layer" in character. Some of these waves are instabilities and some are neutrally stable modes, but they all have

critical levels in the RL. When these waves break they may generate drag. Over complex terrain, the generated gravity waves drag may be larger than the conventional drag associated with turbulence processes in this layer (Steeneveld et al., 2008).

According to Verkaik and Holtslag (2007), heterogeneity of the surface complicates the development of the SBL since surface roughness determines the amount of drag experienced by the flow. When the flow experiences a sudden roughness change (for example, from forest to open fields) an internal boundary layer develops. In this case wind profiles often show a discontinuity at some level above the surface. In stably stratified conditions the disturbing effects of roughness elements is felt over longer distances than in daytime conditions. Thermal heterogeneity of the surface can cause additional turbulence in the SBL. This occurs when cold or warm patches are present in the SBL, to influence development of meso-scale circulations. This is visualized when patches of fog rise from relatively warm ditches over the cooler meadows in the SBL.

The structure of the SBL is mainly determined by two external forcings: the geostrophic wind speed and long-wave cooling of the earth's surface. The latter depends mainly on the cloudiness condition of the sky. The most stable atmospheric conditions occur during weak geostrophic forcing in combination with clear skies. In this case the SBL is shallow and characterized by strong temperature inversion. On the other hand, when the sky is overcast and geostrophic wind is strong, the surface radiative loss to space is reduced and the SBL is much deeper and only weakly stratified.

In the SBL the underlying soil characteristics influence the cooling rate of the surface layer. During the night, soil heat flux is transported upwards from the soil, (partly) compensating for the radiative loss at the surface. In light wind conditions, when turbulence in the SBL has diminished, this soil heat flux balances the negative net radiation. The soil heat flux depends on the thermal conductivity and the temperature gradient in the soil. A low conductivity means a lower soil heat flux, which results into faster decrease of surface temperature. Dry soils have a lower conductivity than wet soil. Snow layers and vegetation isolate the air from the soil, result into lower temperatures at the surface.

The SBL is characterized by turbulence discontinuity in space and time. On clear nights with weak winds, a frequently observed phenomenon is weak and intermittent character of turbulence. Intermittent turbulence is characterized by brief episodes of turbulence with intervening periods of relatively weak or immeasurable small fluctuations (Garratt, 1992). The intermittent behavior of turbulence causes alternations from the mean evolution of the stratified ABL. As a result of deviation from the mean evolution of stratified ABL, the near surface atmospheric variables such as temperature, wind and humidity will have an oscillatory type of behavior. This is the manifestation of the non-linear character of the turbulent exchange in the SBL. The oscillatory behavior of near-surface atmospheric variables in the SBL has a significant effect on local air quality at hourly to diurnal scales.

According to Steeneveld et al. (2008), temperature profiles in the SBL are determined by both turbulent processes and long-wave radiative flux divergence. The net long-wave radiation at a certain level is determined by the upward radiation from the surface and from the underlying air and the downward radiation received from the overlying air. First hours after the evening radiation divergence dominates the evolution of the near-surface air temperature. In the SBL, availability of atmospheric constituents such as water vapor and carbon dioxide (co_2) reduces the radiative loses to space by absorbing some of long-wave radiations from the earth's surface and re-radiate it back to the earth's surface.

In the SBL, surface temperatures tend to decrease while relative humidity increases. The possible reason for increased relative humidity is that, earth's surface cools to saturation, moisture from the air condenses to the surface as dew hence higher relative humidity. The relative humidity will increase as the air close to the ground continues to cool. When ground cools below the dew point temperature, moisture may condense in the air forming radiation fog (Duynkerke, 1991). It is important to note that in the SBL, highest concentration of liquid water is found near the earth's surface. In many cases when gradually more water condenses near earth's surface the fog layer becomes less transparent for radiation. Then, the level at which the radiative cooling occurs shifts from the surface to the top of the fog layer. This destabilizes the fog layer, which, as a result, becomes well-mixed.

The SBLs is a very complex and turbulent regimes are difficult to study. It is a sensitive and changeable coupling agent where fluxes of energy, momentum and matter between the atmosphere and the sea or land over a broad range of scales are regulated, from local to global scales. A comprehensive Numerical Weather Prediction (NWP), Climate models and Air Pollution (AP) models requires proper inclusion of the stable boundary layer processes/ schemes.

Coupled atmosphere-hydrosphere biosphere models also must include a description of the SBL through specific schemes. SBL have thus become the key element of modern high-resolution models that addresses essential features of the environment at the spatial scale (1 to 100 km). Equilibrium height of the stable boundary layer and its relevance in prediction models has been discussed intensively by Zilitinkevich and Esau (2003) and Steeneveld et al. (2006).

General Circulation Model (GCM) consist of a dynamical part which resolves the synoptic patterns on grids and a package of physical parameterizations that resolves the sub grid processes like turbulence, radiation, convection, precipitation, and the coupling with the land surface (King et al., 2007). Proper parameterizations of model physics of the SBL in GCM are of great practical importance. For example, proper SBL turbulence parameterizations in GCM gives a correct representation of the vertical wind and temperature profiles, but have also influence on the larger atmospheric scale (King et al., 2007).

The SBL has been intensively experimentally and theoretically studied (e.g. Izumi and Caughey, 1976; Cuxart et al., 2000; Zilitinkevich, 2002; Jiménez, 2005; Jiménez and Cuxart, 2005; Zilitinkevich and Esau 2005; Zilitinkevich et al., 2007; Zilitinkevich and Esau 2007). The study by Jiménez (2005) revealed that there are still no enough measurements of the ABL over its entire depth, which could be very important to better understanding of the SBL. This is because; the vertical alterations of the SBL are stronger than for instance within the CBL. As a result, phenomena such as the elevated turbulence are not well characterized.

Modeling of the SBL remains an important tool to understand and harmonize measurements of the SBL. Although modeling remains a useful tool to study the SBL, there are still some difficulties to understand the SBL characteristics from contemporary models, due to its

complexity and lower resolution of the models. In strong stable conditions, the downward heat flux is reduced making the earth's surface colder. In these situations mixing process is inhibited at the lowest levels of the model and enters into a "decoupled" mode, which can lead to runaway characteristics close to the ground (Jiménez, 2005). Also under stably stratified conditions, the use of Kolmogorov theory for the dissipation of kinetic energy from large to small eddies might be no longer valid, due to the fact that the employed theory need to address the dissipation of kinetic energy and is applicable when the grid size falls within the inertial sub-range (Jiménez and Cuxart, 2005). The most energetic eddies in the stably stratified boundary layer are smaller than 1m because of the buoyancy suppression of the vertical motions (Jiménez, 2005). Therefore, model- resolutions of about 1 m are needed to resolve the most energetic turbulence structures in this layer (Jiménez, 2005).

1.3 Problem Statement

Although meteorology of the Highveld has been intensively studied (e.g. Van Gogh et al., 1982; Tyson et al., 1988; Jury and Tosen, 1989; Held et al., 1996; Scheifinger and Held, 1997; Freiman and Tyson, 2000; Tyson and Gatebe, 2001; Tennant and Hewitson, 2002; Freiman and Piketh, 2003; Thomas et al., 2007; Collett et al., 2010; Laakso et al., 2010) there is still need for further experimentation and theoretical analysis to understand the ABL process. Furthermore in none of these publications experimental or theoretical research is done on characterizing the turbulent fluxes which are responsible for the structure and dynamics of the entire ABL.

Highveld region contains most of the coal-power generating plants of South Africa. Therefore the understanding of ABL processes is essential for improved accuracy of dispersions and weather or climate prediction models. NWP, climate models still do not resolve the dynamics of ABL due to its complexity and due to the lack of high resolution models. The first level of the contemporary models in many cases is higher than the depth of SBL. Therefore need arises for data and methods for parameterization of the SBL. There are still insufficient experimental and theoretical studies on the effect of surface inhomogeneous on the ABL structure.

1.4 Study Aim and Objectives

The goal of this research is to characterize the SBL and the role of the surface inhomogeneities on the ABL dynamics over Highveld region, South Africa. In order to meet the above stated aim, the following specific objectives are identified:

i) To use appropriate method for calculating the SBL height using data from automated weather stations and mobile LiDAR technology and compare/validate with Radiosonde data.
ii) To characterize the stability regimes in SBL and study their temporal evolutions
iii) To use the similarity theory approach for calculating the turbulent fluxes of momentum, and heat.
iv) To test the hypothesis of links between spatial and temporal variability of the meteorological variables and existing land use patterns.

This research contributes to understand the following scientific questions:

i) What is the structure and dynamics of SBL over Highveld?
ii) What is the SBL height over Highveld?
iii) What are the spatial and temporal variations of the stability conditions and turbulent fluxes?
iv) How the existing the land use land covers influence on the spatial variations of meteorological quantities over Highveld?

1.5 Study Outline

This study is structured into five Chapters. First Chapter gives a general introduction about the ABL: concept and scientific application of the ABL. The SBL characteristics, scientific application and challenges are also described in this Chapter. Chapter 2 outlines the literature review by giving explanation on SBL height, SBL characteristics, ABL and SBL turbulence, Link between SBL and surface heterogeneity. Chapter 3 discusses the data and methodology used in this study. The Chapter describes the Highveld region in terms of locality, economic activities, topography, and regional climate. Chapter 4, present results on the Stable Boundary

Layer height, dynamics and structure over Elandsfontein and Bethal region, South Africa. The different stability regimes in the stable boundary layer are presented. The spatial distribution of turbulent momentum, heat fluxes and Obukhov length and links between spatial and temporal variability of the meteorological variables and existing land use patterns are presented in this chapter. Chapter 5 presents concluding remarks, recommendations and future perspectives of SBL studies over Highveld region South Africa.

CHAPTER 2

LITERATURE REVIEW

2.1 Near Surface Wind and Stability Characteristics

Numerous studies to characterize the stable boundary layer have been taken on the Highveld (e.g. Van Gogh et al., 1982; Tyson et al., 1988; Jury and Tosen, 1989; Held et al., 1996; Scheifinger and Held, 1997; Freiman and Tyson, 2000; Tyson and Gatebe, 2001; Tennant and Hewitson, 2002; Freiman and Piketh, 2003; Becker, 2005; Thomas et al., 2007; Collett et al., 2010; Laakso et al., 2010). Van Gogh et al. (1982) observed that over the Highveld region, during stable stratification, southwesterly wind dominates due to the passage of cyclonic westerly waves. Topographical induced winds from the sector east to southeast are common at night. Van Gogh et al. (1982) also observed that a low-level wind maximum at night, known as a low-level jet (LLJ), occur under highly stable conditions and ranging in speed from 5m/s-15.5m/s.

Tyson et al. (1988) indicated that the thermal structure over Highveld region is influenced by Continental anticyclones that are formed in the large scale subsidence region. Anticyclones are associated with a strong subsidence motion thus the vertical motion is downward and a general anticlockwise flow results (Tyson et al., 1988; Held et al., 1996). Van Gogh et al. (1986) examined that, high frequency of anticyclonic circulation and associated subsidence in the upper air reaches a maximum in winter. The subsidence leads to the formation of elevated stable layer throughout the year with a frequency of 60% and winter base height of about 1300. Freiman and Tyson (2000) also found that the absolute stable layer over Highveld is found at around 700 hpa (altitude ~ 3000 m). The study also found that primary layer, associated with the level of maximum subsidence occurs in the region of 500 hpa level (altitude ~ 5000 m) with the mean frequency of occurrence on all days of 93% in summer and 78% in winter. However, only non-surface absolute stable layers were considered in this study.

Becker (2005) reported that thermal structure of the stable boundary layer over Mpumalanga Highveld region shows distinctive characteristics with relatively deep stable conditions during the night with inconsistent layering above. Jury and Tosen (1989) described the stable boundary layer characteristics over Highveld region, South Africa in relation to air pollution using Doppler sounder observations and background climatological data. The study revealed that a sharp radiation inversion formed during stable boundary layer just after sunset up to 150-200 m level and grows in depth to reach 300 m on average near sunrise. The inversion cause a reduction in friction drag and influence in the formation of nocturnal low level jet during westerly encroachment. The low level jet overlies the nocturnal temperature inversion. The study also indicated that low level jet increases in strength as the nocturnal surface temperature inversion intensifies through the night. The height of low level jet above the surface also increases as the inversion deepens. Wind speeds in all regions exceed 10 m/s in the jet core, which typically is located between 200 and 300 m above the ground. The study by Held (1996) observed that surface temperature inversions over Highveld are found during most nights. Temperature inversion strength $\leq 3.5°$ with a depth of ≤ 270 m above ground level was observed. Low-level elevated inversions with a base height of 350 to 500 m above the ground level and strength $\leq 3.6°C$ were found on four occasions. The base height of the subsidence inversion varied between 1500 and 2500 m above the ground level. Weak low-level wind maxima just above the surface inversion were observed during most nights, generally with speeds of <10 m s^{-1}.

2.2 Stable Boundary Layer Height and its Application

The SBL height can be defined as the height at which surface-based turbulent stresses vanishes (Fig. 2.1) (Kosović and Curry, 2000). The above definition holds only when surface-based turbulence dominates (Mahrt, 1999; Caughey et al., 1979; and Derbyshire, 1990). Other definitions of the SBL height include, the top of the layer with downward heat flux, the height of the low level jet or minimum wind shear, and the top of the temperature inversion layer or the layer with significant cooling (Vickers and Mahrt, 2004).

The SBL height is an important parameter needed in a number of practical problems such as pollution dispersion, wind engineering, air-sea interactions, and Climate/weather prediction

(Zilitinkevich, 2002). In meso-scale models, a turbulent kinetic energy (TKE) scheme depends heavily on SBL height to parameterize turbulence length scales that is used to describe eddy diffusion coefficients for momentum and scalar mixing (Bloch, 2002). Errors in SBL height estimation can result in gross errors in boundary layer evolution and prediction of turbulent mixing within the BL.

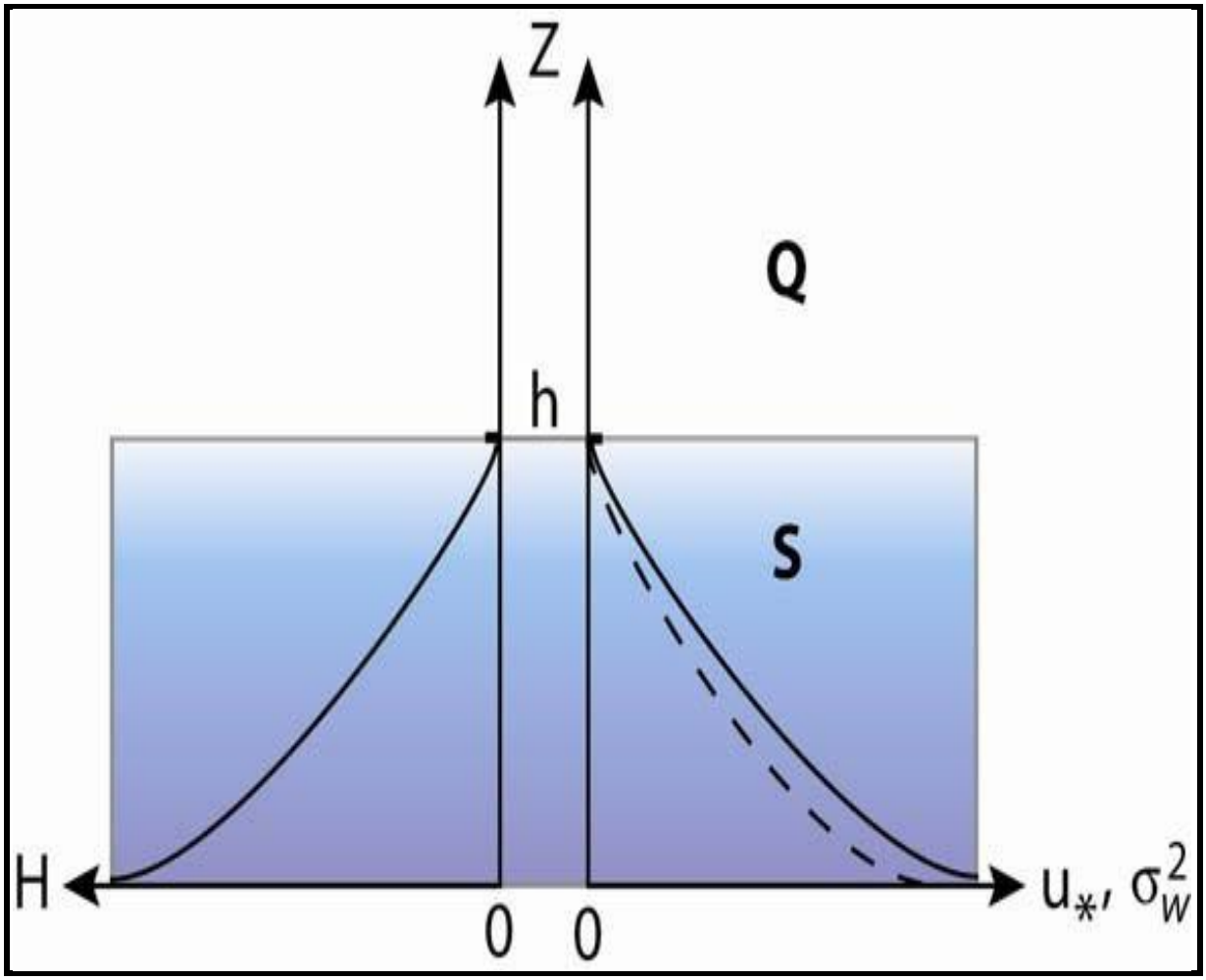

FIGURE 2.1: Schematic profiles of heat flux *H*, vertical velocity variance $2w\sigma$, and friction velocity u_* showing "traditional SBL" structure. Shaded portion marked *S* represents the stable boundary layer (h is the SBL height) and the region above marked *Q* represent a quiescent layer of weaker turbulence aloft (adopted from Banta, 2008).

The SBL height is not a predicted quantity in dispersion and weather or climate models. It is either not a routine measurement from weather stations. It is determined by several methods:

2.2.1 Surface Flux-Based Methods

The SBL height can be expressed as function of turbulent friction velocity and Coriolis parameter as:

$$h = C_n \frac{u_*}{f}, \qquad (2.1)$$

where h is the stable boundary layer height, u_* is the turbulent friction velocity f is a Coriolis parameter and C_n is a constant with value ranging from 0.1 to 0.5 (Vickers and Mahrt, 2004). Small values of C_n are associated with strong stratification and large values are associated with neutral stratification boundary layers (Vickers and Mahrt, 2004).

Kitaigorodskii (1960) derived another formulation for calculating the SBL height which depends on the Obukhov length L:

$$h = C_s L, \qquad (2.2)$$

where h is the stable boundary layer height, L is the Obukhov length and C_s is non-dimension coefficient with value ranging from 100 to 1 (Vickers and Mahrt, 2004). The above formulation is used only when the SBL is dominated by surface fluxes of heat and momentum.

Zilitinkevich (1972) developed an equation for calculating the SBL height which incorporates the influence of the earth rotation and surface fluxes:

$$h = C_{sr} \frac{u_*^2}{(-fB_s)^{\frac{1}{2}}}, \qquad (2.3)$$

where h is the stable boundary layer height, C_{sr} is a non-dimensional coefficient of order 1, $B_s = \left(\frac{g}{\theta_v}\right)\overline{w'\theta'_v}$ is the scaled surface buoyancy flux, f is the Coriolis parameter and u_* is the turbulent friction velocity. Eq. 2.3 is widely used in modeling studies to estimate the SBL height.

In another study, Zilitinkevich (1972) developed an equation for calculating the stable boundary layer height:

$$h = 0.4\left(\frac{u_* L}{f}\right)^{\frac{1}{2}} \tag{2.4}$$

where h is the stable boundary layer height, u_* is the turbulent friction velocity, L is the Obukhov length and f is the Coriolis parameter. The above formulation was derived from Eq. 2.3 assuming buoyancy flux B_s is constant in a very stable BL (Vickers and Mahrt, 2004). The above equation is valid for very stable atmospheric condition:

Nieuwstadt (1981) interpolated the above Zilitinkevich (1972) formula to nearly neutral case of SBL, so that:

$$\frac{h}{L} = \frac{\frac{0.3u_*}{fL}}{1+1.9\frac{h}{L}}, \tag{2.5}$$

where h is the SBL height, L is the Obukhov length and u_* is the turbulent friction velocity and f is the Coriolis parameter. The SBL height derived using Eq. 2.5 approaches Zilinitinkevich's (1972) formulation (Eq. 2.4) only for small L, and is about 0.3 $\left(\frac{u_*}{f}\right)$ for large L.

Pollard et al. (1973), suggested that the SBL height should be a function of turbulent friction velocity, Coriolis parameter and the strength of the inversion at the top of the SBL:

$$h = C_{ir}\frac{u_*}{(fN)^{\frac{1}{2}}} \tag{2.6}$$

where h is the stable boundary layer height, N is the buoyancy frequency or Brunt-Vaisala frequency, $N^2 = \left(\frac{g}{\theta}\right)\frac{\partial\theta}{\partial z}$ and C_{ir} is a non-dimensional constant equal to 1.7 (Vickers and Mahrt, 2004), f is the Coriolis parameter and u_* is the turbulent friction velocity. The above formulation requires free flow measurement and temperature at two levels for the calculation of temperature gradient and hence the buoyancy frequency.

Zilitinkevich and Mironov (1996) employed the TKE equation to derive the SBL height equation:

$$\frac{1}{h_E^2} = \frac{f^2}{C_R^2 \tau_*} + \frac{N|f|}{C_{CN}^2 \tau_*} + \frac{|f\beta F_*|}{C_{NS}^2 \tau_*^2} \quad (2.7)$$

where h_E is the SBL height, $C_R = 0.6$, $C_{CN} = 1.36$ and $C_{NS} = 0.51$ are dimensionless constants, N is the buoyancy frequency or Brunt-Vaisala frequency, τ_* is the shear stress, β is buoyancy parameter, f is the Coriolis parameter and F_* is the buoyancy flux. Recently the above equation is widely used in different numerical models and air pollution models in which two additional terms are introduced. The equation becomes:

$$\left(\frac{f h_E}{C_n u_*}\right)^2 + \frac{h_E}{C_s L} + \frac{N h_E}{C_i u_*} + \frac{|f\beta_s|^{\frac{1}{2}} h_E}{C_{sr} u_*^2} + \frac{|Nf|^{\frac{1}{2}} h_E}{C_{ir} u_*} = 1 \quad (2.8)$$

where h_E is the SBL height $C_n = 0.5$, $C_s = 10$, $C_i = 20$, $C_{sr} = 1.0$ and $C_{ir} = 1.7$ are non-dimensional constant, obtained from field measurement data and large eddy simulations data (LESs), N the buoyancy frequency or Brunt-Vaisala frequency and f is a Coriolis parameter .

2.2.2 Richardson Number-Based Method

The SBL height is also calculated from bulk Richardson number. This is an alternative widely used method for classifying atmospheric condition (Zilitinkevich and Baklanov, 2002). The approach is based on the idea that, the SBL height and strength of mixing in a stratified flow are observed to either increase or decrease depending on whether the Richardson number is less than or greater than some critical value (Vickers and Mahrt, 2004). The SBL height is the lowest level detected at which bulk Richardson number exceeds a critical value. A practical drawback to this approach, in comparison with surface fluxes–based forms, is that the resolved height is only as good as the vertical resolution of meteorological measurements. The only advantage of this method is that the difficult-to-measure surface fluxes are not required to calculate the SBL height.

2.2.3 Remote Sensing-Based Method

In recent years, the importance of a systematic monitoring of the atmospheric structure and dynamics has been demonstrated by several atmospheric programme campaigns over the globe (e.g. Sharma, et al., 2009). The laser radar, more popularly known as LiDAR, is becoming one of the most powerful techniques for active remote sensing of the earth's

atmosphere. Laser systems were deployed for atmospheric studies immediately after the discovery of the laser in 1960. Fiocco and Smullin (1963) were the first to use a laser for atmospheric studies. In 1963, using Ruby laser having energy of 0.5 J, they obtained Rayleigh scattered signals from the atmosphere up to 50 km altitude and also detected dust layers in the atmosphere. Ligda (1963) made the first LiDAR measurements of cloud heights in the troposphere height region. Since these pioneering attempts, laser remote sensing of the atmosphere has come a long way. Discovery of different laser sources, improvements in detector technology, data collection and analysis techniques have made the LiDAR a reliable tool for atmospheric science research. LiDAR remote sensing systems are very attractive for studying the atmospheric boundary layer (ABL), where high-resolution is necessary to capture variations in parameters of interest.

FIGURE 2.2: CSIR mobile LiDAR van (adopted from Sharma, et al., 2009).

South Africa's first mobile LiDAR system has being developed at the National Laser Centre (NLC) of the Council for Scientific and Industrial Research (CSIR) in Pretoria (25°45'S; 28°17'E) (Sharma, et al., 2009) (Fig.2.2). The system is designed primarily for remote sensing

of the atmosphere. At present, the system is being optimised for measuring vertical atmospheric backscatter profiles of aerosols and clouds (Sharma, et al., 2009).

2.3 Stable Boundary Layer Characteristics

2.3.1 Outgoing Long Wave Radiation

One of the key variables for the SBL characteristics is the Outgoing Long wave Radiation (OLR) (Fig.2.3). It is defined as that energy leaving the earth as infrared radiation. Greenhouse gases, such as methane (CH_4), nitrous oxide (N_2O), water vapour (H_2O) and carbon dioxide (CO_2), absorb certain wavelengths of OLR and part of the absorbed OLR is converted into heat energy adding heat to the atmosphere. The heat in turn causes the atmosphere to emit more OLR. Some of this radiation is directed back towards the Earth. This influences an increase of average temperature near the earth's surface.

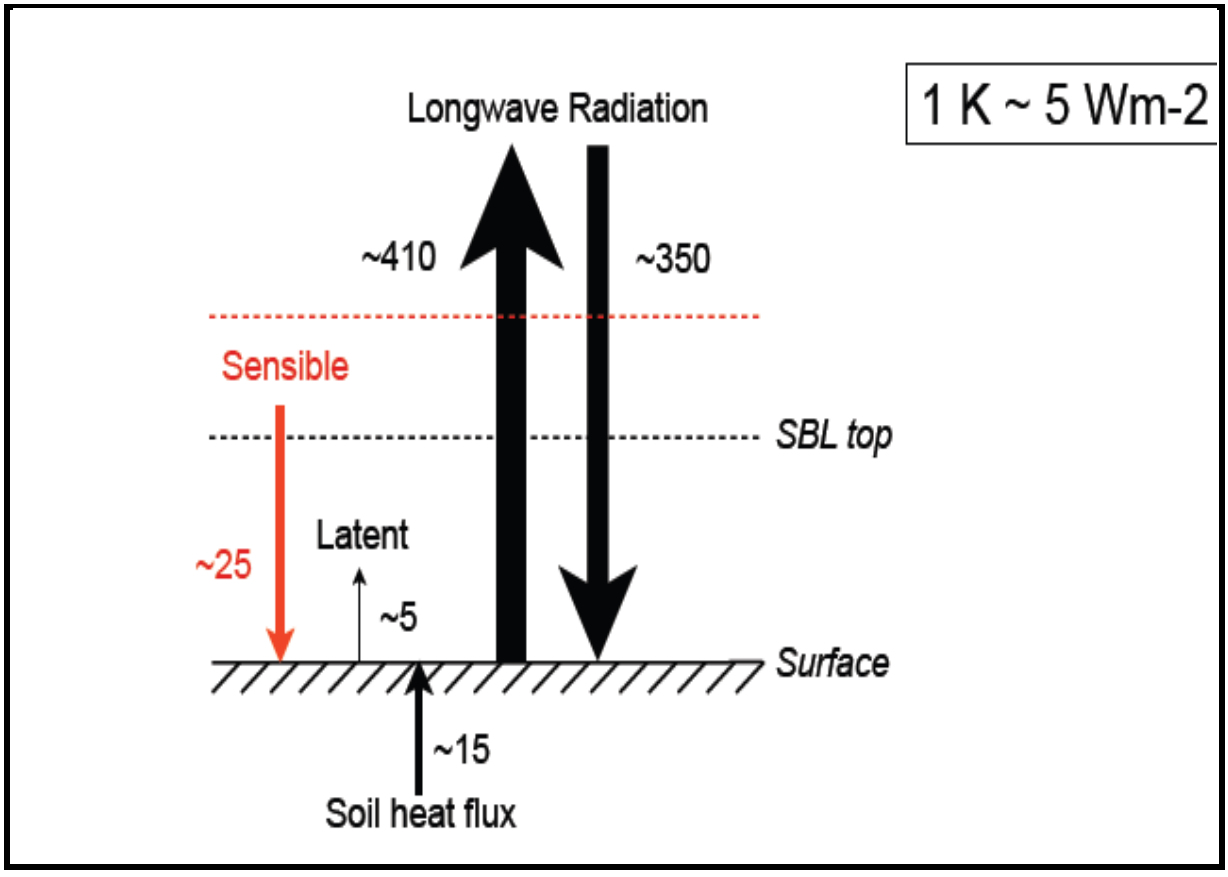

FIGURE 2.3: Long wave radiation in the SBL (adopted from Mauritsen, 2011).

Steeneveld (2007) indicated that, OLR governs the evolution of the SBL. The amount of radiation that is absorbed or emitted by different layers of air in the SBL depends on the absorptivity, emissivity and its temperature. In turns emissivity depends on the concentration of absorptivity gases such as water vapour, carbon dioxide, ozone, methane and nitrous oxide in different layers of the SBL. The difference in emitted absorbed long wave radiation between layers of the SBL results in a net radiative flux, and is pronounced in this layer because temperature gradient near the surface can become extremely large, and the emitted radiation differs strongly between different layers in SBL. Potential temperature at a certain level in the SBL is governed by the divergence of turbulent heat flux and divergence of the net long wave radiative. Measurements indicate that the latter contribute to Clear Air Cooling (CAC) in the SBL.

Sun et al. (2003) observed that, nocturnal SBL long wave radiative flux divergence is strongest at late evening/beginning of night. At this time the ground cools rapidly and the wind is weak. Under weak-wind and clear-sky conditions in the early evening, following a day with high surface radiation temperature and warm boundary layer, the ground cools very quickly while the rest of the SBL stays warm.

Sun et al. (2003), also indicated that there is vertical difference on long wave radiation divergence in the SBL. Small impacts of long wave radiation divergence are observed in the deep layers in the SBL and large impacts of long wave radiative divergence are observed close to the ground. The reason for these differences is questionable; it is speculated to result from vertical variation of radiative fluxes divergence as suggested by radiation models. Vertical variation of the long wave radiative cooling implies that the relative contributions of the sensible heat divergence and the temperature advection (both horizontal and vertical) vary with height. The radiative cooling is the primary heat sink at night. This is a classical observation of the vertical variation radiative flux and sensible heat fluxes and validates the importance of the temperature advection in local cooling at night. In their studies Sun et al. (2003) observed that previous studies of SBL heat balance based only on vertical variations of the radiative fluxes and assuming no advection may lead to wrong conclusions about the role of sensible heat fluxes in local cooling. The outgoing long wave radiation from the ground tends to fluctuate with wind speed due to surface heterogeneity. Changes of outgoing long

wave radiations from the ground influence fluctuations of radiative fluxes divergence. This is not simulated by all of the radiation models; all of vertical variations of the long wave and radiative flux divergent in the SBL complicate the modeling of this layer.

2.3.2 Stability Regimes of the SBL

In current literature surveys, often a distinction of the SBL is made between weakly stable regime and very stable/ strong regime conditions (Mahrt et al., 1998; Van de Wiel et al., 2003; Steeneveld et al., 2006). The weakly stable regime is characterized by strong winds and cloudy conditions. Shear generation of turbulence is large and radiative cooling of the surface is small. In this layer turbulence is continuous and the structure of the SBL is dominated by turbulent processes. Very stable regime is characterized by clear skies and light wind conditions. Under this conditions turbulence is very weak and the SBL structure is mainly determined by radiative flux divergence and soil heat flux (Baas, 2009). Most studies separate the weakly stable and very stable regimes by a transition/ neutral regime,where turbulent activity shows a rapid decrease with stability. Periods of turbulent activity alternate with periods of weak or immeasurably small fluctuations (Mahrt, 1999). Under neutral regime the SBL is dominated with intermittent turbulent (Van de Wiel, 2002).

Van de Wiel et al. (2007) illustrated the difference between the weakly stable regimes and the very stable regimes by considering the feedbacks between the temperature gradient and the heat flux. In case of a weakly stable stratification a sudden increase in the vertical temperature gradient will generally be followed by an increase in the vertical heat flux. The increased flux tends to restore the original weaker stratification. This is a negative feedback between the stratification and the heat flux during weak stable stratification. In very stable boundary regime a positive feedback exists between stratification and the heat flux, where increased stratification inhibit heat flux demanded by the surface net radiative cooling. At this stage SBL is decoupled from the surface.

2.3.3 Turbulence in the SBL

In the SBL turbulence is generated by shear and destroyed by negative buoyancy and viscosity, viscous decay is effective on small scale turbulent eddies. This competition between

shear, buoyancy and viscosity effects reduces strength of turbulence in the stable boundary layer. This is why turbulence in the SBL is much weaker in comparison to the neutral and convective boundary layers. The turbulence energetic eddy in the SBL can be in a delicate and precarious balance. It is extremely sensitive to changes in the mean wind profile which is the source of shear and change in mean temperature profile which is the source of negative buoyancy energy as the limit of vertical motion (Steeneveld, 2007). Therefore similarity statements /arguments made about the structure of the SBL differ from those of CBLs and Neutral Boundary layers (NBLs).

Mahrt (1999) indicated that on clear night and weak wind condition, a frequently observed phenomenon in the SBL is the weak and intermittent character of turbulence. This is characterized by brief episodes of turbulence with intervening periods of relatively weak or immeasurable small fluctuations. The intermittent turbulence causes non-linear interactions in the mean evolution of the near surface atmospheric variables. This may results in oscillatory behavior of the mean atmospheric variables. An example of intermittent turbulence in the SBL and its effect on heat flux in a particular night is described in Fig. 2.4. In this figure there is a difference between small scales intermittency of the velocity gradients organized by the individual large eddies and global intermittency associated with patchiness of turbulence on scales larger than the large eddies. The thick line in Fig. 2.4 represents a case with discontinuous turbulence, observed in conditions with light surface winds. The dashed line represents a case with continuous turbulence, observed in conditions with strong surface winds.

The physical mechanism of SBL intermittent turbulence is complex. The intermittent behavior of turbulence in this layer is influenced by several physical mechanisms. Some of these mechanisms are the formation and breaking of gravity waves (Van de Wiel et al., 2002). In the SBL, as previously pointed out buoyancy is negative and prevents vertical mixing of the atmospheric quantities. Therefore any fluid particles (eddy) displaced vertically from equilibrium state will vibrate around its mean position and the net vertical displacement of a parcel particle over a phase period is zero (Staquet, 2000), but in so doing the parcel transport vertical energy and angular momentum in form of waves (gravity waves).

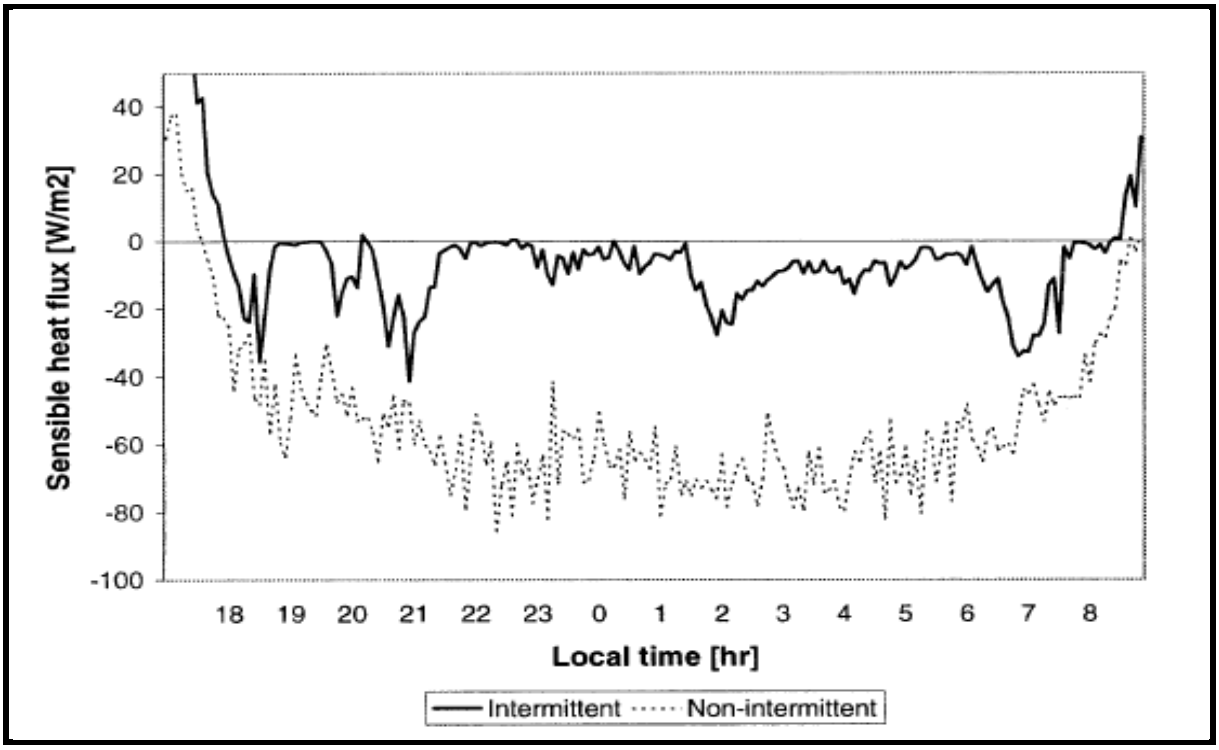

FIGURE 2.4: Turbulent heat fluxes in SBL (Van De Wiel et al., 2001).

In Steeneveld (2007) paper, it is indicated that gravity waves are the general property of stratified geophysical flows. Any stratified geophysical flow support and propagate gravity waves. Gravity waves can then be defined as waves generated within a fluid medium or at the interface between two media (e.g., the atmosphere and the ocean) which has the restoring force of gravity or buoyancy. In the SBL, gravity waves are generated by a variety of features; sudden surface roughness changes, convection and undulating topography (see Fig. 2.5). Since the gravity waves are able to redistribute energy and momentum, they are important in determining the vertical structure of the atmosphere and the coupling of meso-scale motions to the micro scale phenomena. In the SBL gravity waves start to break at the top and transport positive momentum down wards. A certain level in SBL is reached, called critical level, where wind speed in the direction of the wave motion vanishes and as a result the wave breaks into turbulence. In fact, this mechanism removes momentum from the mean flow, and thus acts as a drag on the flow. Breaking of gravity wave in stably stratified BL occurs intermittently in space and time. Therefore gravity waves are the principle sources of intermittent turbulence in

SBL as it breaks intermittently. This type of intermittent turbulence in stratified stable flow achieved a lot of attention from a theoretical and observational point of view.

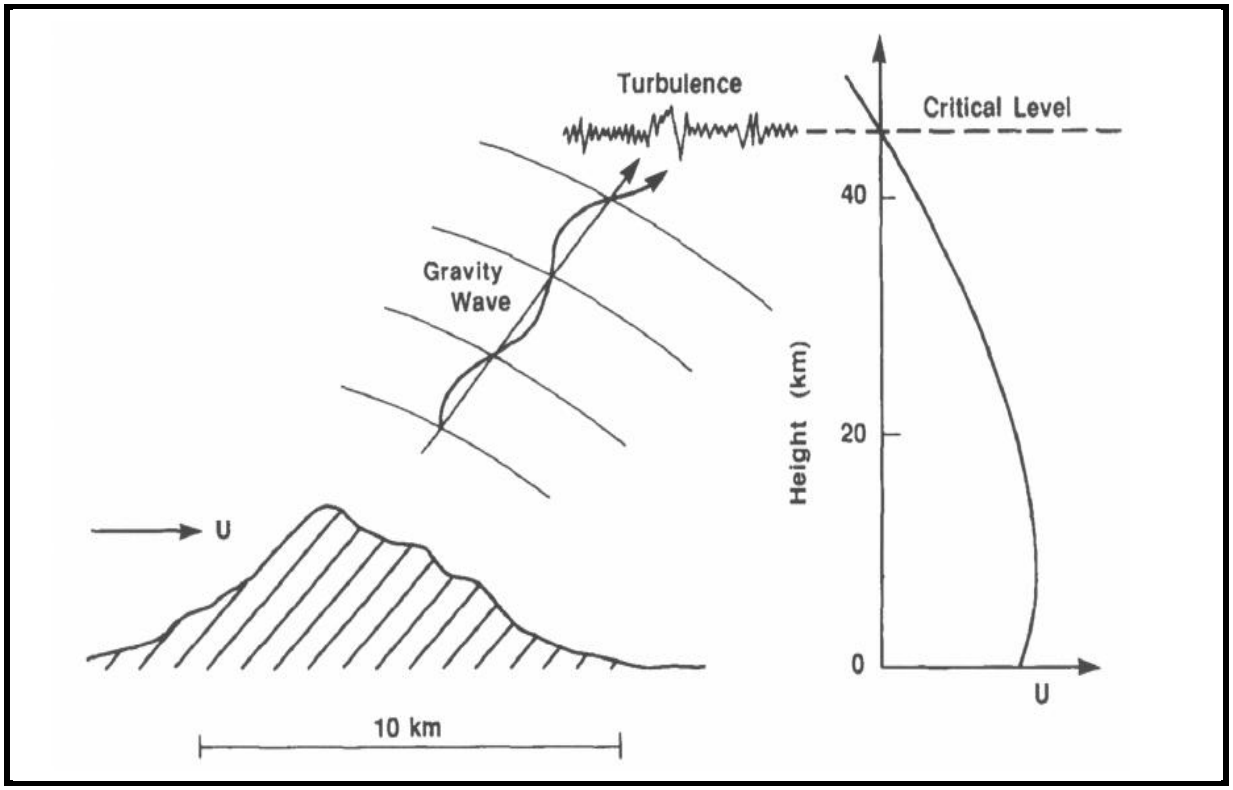

FIGURE 2.5: Illustration of propagating gravity waves caused by orography. At a critical level (where the wind speed is 0), the waves starts to break up into turbulence (Adopted from Steeneveld 2007)

Van de Wiel et al. (2002) described another type of intermittent turbulence generating mechanism in the SBL, created by the direct atmosphere-surface interaction. This kind of intermittency is referred to as Atmosphere-Surface Intermittency (ASI). Van de Wiel et al. (2002) in their publication described the mechanism of ASI as follows: On clear night due to long wave radiative cooling of the earth's surface, thermal stability may increase fast. This influences the gradient Richardson number to increase considerably. In this atmospheric condition turbulence will be suppressed and will eventually collapse. This results in a decoupling of the air from the surface. Little friction force acting on the air influences the omnipresent pressure gradient force to start accelerating the air mass. Thus, shear increases until the Richardson number is below critical value where turbulences are eventually

regenerated. As a result of this turbulence shear is reduced quickly and soon thermal stability dominates over shear, the Richardson number increases and turbulence is suppressed again. At this point the whole process will start over again.

Several cycles of the behavior outlined in the above paragraph results in an intermittent character of the turbulence in the near-surface stable boundary layer and oscillations in the near surface atmospheric variables. The intermittency mechanism described by Van de Wiel et al. (2002) is closely related to the decoupling phenomenon in the SBL, with the exception that in the intermittency case the SBL turbulence is able to 'recover' by an increase of wind shear. Then, the understanding of both phenomena is of great importance for numerical weather predicting modeling in stably stratified boundary layers.

Low level jet is another source of intermittent turbulence in the SBL, encountered with fair regularity in mid-latitudes. The low-level jet is primarily a SBL phenomenon, occurring in conjunction with increased radiative cooling at the surface and the subsequent decoupling of the stable layer from the residual layer above. The low-level jet tends to occur at the top of the stable layer, characterized by high velocity flow, and the nose of the jet can at any times disrupt the top of the stable layer, resulting in a burst of turbulence (Julie, 2008). It is these turbulent events that are responsible for most of the vertical energy transfer in the stable layer.

A turbulence characteristic in the stable boundary layer strongly influences the concentration of pollutants in this layer. At the time of turbulence break, pollutants are mixed and distributed vertically and horizontally. At quiet (calm) condition, normally concentration of pollutant increases provided there is continuous emission of pollutant in the surface layer. This is because any pollutant is trapped close to the surface in a small volume of air with limited vertical and horizontal dispersion.

2.4 Link between Spatial Variability of the Meteorological Quantities and Existing Land use Patterns.

It has been recognized (Pielke, 2001; Patton et al., 2005; Horlacher et al., 2012) that heterogeneity of land use has a significant impact on land-air interaction and atmospheric dynamics in the planetary boundary layer (PBL). Several studies (e.g. Esau and Lyons, 2002;

Sogalla et al., 2006; Scanlon et al., 2007) have found strong connections between land use patterns and the largest scales of atmospheric turbulent convection. For instance, Scanlon et al. (2007) revealed a positive feedback to the atmospheric meso-scale and planetary boundary layer dynamics linked to the clustering of vegetation in arid areas of the Kalahari desert in southern Africa. Starting from homogeneously to randomly distributed vegetation, they arrived to strongly localized vegetation clusters in their model. The process has been attributed to a redistribution of atmospheric convective motions, and therefore, precipitation.

A major deficiency of such modeling studies is that the links between the atmospheric dynamics and land use types are implicitly incorporated into the corresponding (e.g. atmospheric convection and dynamical vegetation) model parameterizations. Hence, independent observationally based validation and calibration are required.

Statistical analysis of observations and their associated meteorological modeling is often disclosing non-linear and climatologically significant effects caused by turbulence self-organization and excitation of meso-scale circulations (land breezes) over different types of surface heterogeneity. For instance, Heerwaarden and Vila-Guerau de Arellano (2008) studied the sensitivity of PBL turbulent dynamics to surface heterogeneities with the aid of turbulence-resolving models, where the transport of specific humidity was varied. Their results clearly indicated that despite the higher temperature and lower surface relative humidity of warm land patches, the heterogeneity-induced convection facilitate the penetration of air parcels to higher elevations where additional condensation enhanced cloud formation. Horlacher et al. (2012) performed a combined statistical analysis on meteorological observations and the simulated output by two meso-scale models, and demonstrated greatly enhanced spatial variability of screen-level variables under stably stratified boundary layer conditions. This variability decreases with height, but at low levels (up to 10 m) it manifested local temperature differences as large as 5^{o}C, which are significant and therefore important for agricultural and other social economic activities.

The SBL characteristics are highly dependent on the spatial distribution of land surface properties such as temperature, aerodynamic roughness and soil moisture (Stoll and Agel, 2006). Natural landscapes are covered with patches of different vegetation and soil properties

(Steeneveld, 2007). Each of them becomes in equilibrium with the local net radiative cooling. As such it might occur that differently stably stratified and unstably stratified patches exist next to each other. This influences on the non-linear dynamics of the stable boundary layer. The non-linear interaction between surface heterogeneities and atmospheric turbulence limits the applicability of similarity theories (e.g., the log-law), commonly used to model turbulent fluxes, and strictly is only applicable in homogeneous boundary layers (Stoll and Agel, 2006). Under stable atmospheric conditions, the effect of stratification on local turbulence scales further complicates the ability to parameterize the effects of surface heterogeneity on ABL fluxes.

Weather forecast models need to represent all patches within a single grid cell. Due to the non-linear nature of the turbulent exchange (Steeneveld, 2007); grid cell averaging results in different exchange coefficients compared to the local approach. Secondly, differential cooling due to land surface inhomogeneities might generate small-scale baroclinicity and consequently meso-scale circulations. These cannot be resolved in Numerical Weather Prediction (NWP) models, although these flows can generate wind shear and as such additional turbulent exchange (Steeneveld, 2007).

CHAPTER 3

DATA AND METHODS

3.1 Description of the Study Area

3.1.1 Geography

Highveld plateau region is situated in Central-North-Eastern part of South Africa. It extends across parts of Gauteng and Free State provinces to the East of the highly urbanized Gauteng Province including the largest cities Pretoria and Johannesburg, and occupies area of about 30000 km^2 at about 1400 m–1700 m above sea level. The surface of the plateau over Highveld region is rather flat but its morphology is very heterogeneous. At small spatial scales, depressions and hills could be found with the elevation difference of 10-20 m and the typical elevation gradients of 5-10 m km^{-1}.

About 70% of the Highveld area is covered by grassland and the rest is utilized for agricultural (maize, cattle and sheep, and crop production), urban and industrial activities. Fig. 3.1 exemplifies the surface heterogeneity. It shows the normalized digital vegetation index (NDVI) for 20 km by 20 km patch within the Highveld obtained from the Landsat platform 7 satellite on July 3, 2006. Typical elements of the surface heterogeneity in Fig. 3.1 are seen as green and yellow patches –agricultural fields (wheat and maize); gray and black patches – coal transporter; blue patches – water reservoirs; magenta patches – build-up areas; and reddish and grayish patches – natural bush and harvested fields.

3.1.2 Climate of the Region

Over South Africa as a whole, and Highveld in particular, the general circulation of the atmosphere is anti-cyclonic throughout the year above 700 hpa (Held et al., 1996). In summer season, surface radiation facilitates the development of near-surface troughs in the region, dominated by upper air subsidence.

FIGURE 3.1: Surface heterogeneity over Highveld region detected using normalized digital vegetation index (NDVI) for the tile e29s26 obtained by the Landsat platform 7 with the sensor ETM+ at 03 July 2006. Pixel size – 30 m. The size of the shown area is 20.6 km by 20.6 km. Data source is FAO FRA Landsat Imagery Database http://globalmonitoring.sdstate.edu/projects/fao/index.html.

On the synoptic-scale clockwise circulation around these troughs lead to moisture advection from the tropics which is a major contributor to summer rains when local instabilities often lead to the development of convective thunderstorms (Freiman and Tyson, 2000). In dry winter season the anti-cyclonic circulation dominates throughout the entire troposphere (Jury and Tosen, 1989). A ridging high pressure that extends from the Atlantic High pressure system and propagates eastwards along the South African coastline, behind a cold front might result in moisture advection from south-east and cloud development against the eastern escarpment of the Highveld.

The Highveld region climate is cooler than climate of other areas of similar latitude, which is mainly due to the Highveld high altitude. Highveld weather is characterized by hot summer daytime temperatures (25 to 32°C) and frequent late afternoon thundershowers. Winter daytime average temperatures ranges from 15 to 19°C, but night time temperatures often drop below freezing and morning frost is common. Closer to the mountain ranges the incidence of frost is even higher. Frost occurs regularly during the winter months and ranges from about 30 days in the Mpumalanga province to about 70 days in the southern Free State. Temperature inversions in winter occur almost every night at the surface, while elevated inversions are with high frequency (Van Gogh et al., 1982; Freiman and Tyson, 2000; Becker, 2005). The elevated inversions occur on 60% of all days at a mean height above the ground of 1700 m with a depth of just under 200 m and strength of 1.5^{o}C. In winter the depth of the surface inversion varies from 300 to 500 m at around sunrise, which is the time of maximum depth and when the average strength of the inversion is about 5 – 6^{o}C. Tyson et al. (1988) present climatological data on the stability regime at Bloemfontein which reveals at midday: stable (25%), unstable (74%), inversion (1%) and stable (19%), unstable (2%), inversion (79%) at midnight. Precipitation, which ranges from 600 - 800 mm per annum, has its maximum during December and January (the austral summer season). Winds are highly variable but easterly and westerly winds are more prevalent.

3.2 Data

3.2.1 Micro-Meteorological Experiment in the Highveld Priority Area

The data used in this study were sampled continuously from 01.01. 2008 to 30.12.2010 using 5 automatic weather stations deployed in the Highveld Priority Area (HPA). This area is associated with poor air quality and elevated concentrations of criteria pollutants occur due to the concentration of industrial and non industrial sources (Held et al., 1996; Scheifinger and Held, 1997). Data samples from temperature, pressure, humidity and wind sensors are averaged automatically by meteorological stations over 10 minute's intervals and stored on the station's digital data loggers. The data collected by all automatic weather stations during the Norway–South Africa bilateral research project constitute the Micro-Meteorological Experiment in Highveld (MMEH) data set. The South African Department of Environmental

Affairs (DEA) provided data from 2008 to 2010 collected by another 5 automatic weather stations placed in the HPA. This data set is very similar to the MMEH data set but some systematic differences can be observed due to the preferable location of the DEA automatic weather stations within urbanized areas. Fig. 3.2 presents the map of Highveld region indicating locations of the automatic weather stations where MMEH and DEA automatic weather stations are identified by symbol "S", "D" respectively. The horizontal data resolution in Fig. 3.2 is 1 arcsec (~ 30 m along longitude). Color shading gives the elevation in meters above sea level (scale bar at the right side). White dots are the automated weather stations installed over Highveld region during MMEH and square dots are DEA automatic weather stations. Table 3.1 lists the meteorological stations and their geographic coordinates. Table 3.2 gives the geodetic distances between the stations. CSIR-Mobile LiDAR-back scattered radiation data were collected to assess temporal variations of SBL height over Elandsfontein region on the 1st -2nd of December 2010.

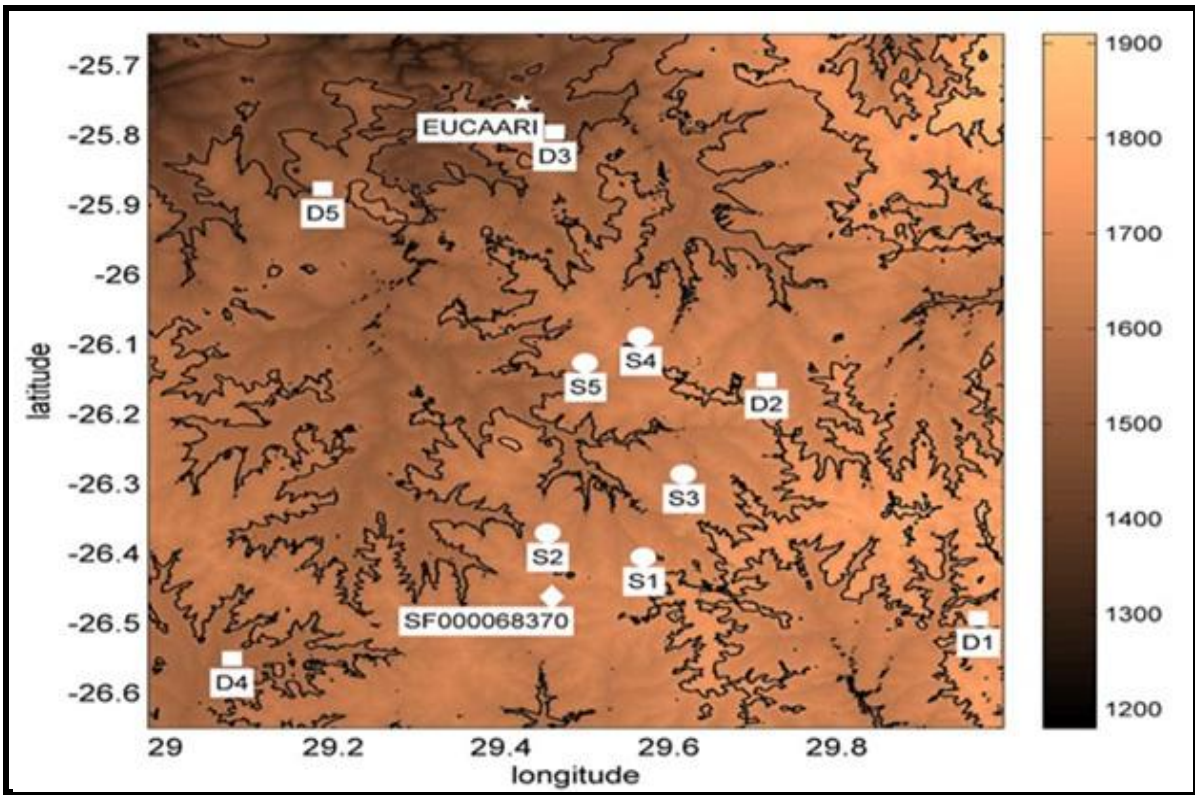

FIGURE 3.2: Digital elevation map of the Highveld region in Republic of South Africa. The map is based on the ASTER data base (http://www.gdem.aster.ersdac.or.jp/index.jsp).

TABLE 3.1: The list of automatic meteorological stations, their coordinates, altitudes and completeness of the data in the database

Station and farm name	Latitude (S)	Longitude (E)	Altitude (m)	Completeness (%)	Completeness (%)	Completeness (%)
DEA stations (D)				01.01.08-31.12.10	01.06.09-31.07.09	01.01.09-28.02.09 01.01.10-31.07.10
D1.Ermelo	26.493	29.968	1760	55	100	60
D2. Hendrina	26.151	29.716	1660	43	100	0
D3. Middleburg	25.796	29.464	1510	47	100	80
D4. Secunda	25.877	29.187	1570	50	100	90
D5. eMalahleni	26.550	29.079	1500	47	100	90
S1. Jan de Jager, Banklaagte	26.405	29.569	1650	19	80	70
MMEH stations (S)						
S2. Anton VanTonder,Yzervarkfontein	26.370	29.455	1660	19	0	70
S3. Bram Jordan, Rietkuil	26.286	29.616	1670	15	0	0
S4. Anton Pelse,Driefontein	26.089	29.566	1706	50	100	100
S5. Daleen vonWieligh, Bultfontein	26.127	29.499	1656	18	0	0

TABLE 3.2: Distances (in km) between the Davis Automatic Weather Station (DAWS) (S) and DEA stations

	S1	S2	S3	S4	S5	D1	D2	D3	D4
S2	12	-	-	-	-	-	-	-	-
S3	14	19	-	-	-	-	-	-	-
S4	35	33	23	-	-	-	-	-	-
S5	32	27	21	8	-	-	-	-	-
D1	41	53	42	60	62	-	-	-	
D2	32	36	18	17	22	46		-	-
D3	69	64	57	34	37	92	47	-	-
D4	51	42	61	71	63	89	77	92	-
D5	70	61	62	45	42	104	61	29	76

Data from both MMEH and DEA automatic weather stations have significant gaps. But the gaps are rather regular in time (see Fig. 3.3); this figure indicates the overall data completeness on daily basis. The regularity of gaps is the result of unattended automatic data collection. The automatic weather stations were inspected on the monthly basis during the first year of operation and once in three months in the following years. During the first year of operation and installation of the automatic weather stations, the gaps were minimal as the stations were repaired and reset almost in real time. In the following years, failures became more serious. All stations, except S4, had to be taken for repair (300 km from the observation site). By January 2010, the stations were installed again but failed in 1-3 months. DEA stations also revealed technical problems but the DEA budget (about 100 larger than the MMEH budget) allowed for more reliable (expensive) equipment and larger cost of maintenance.

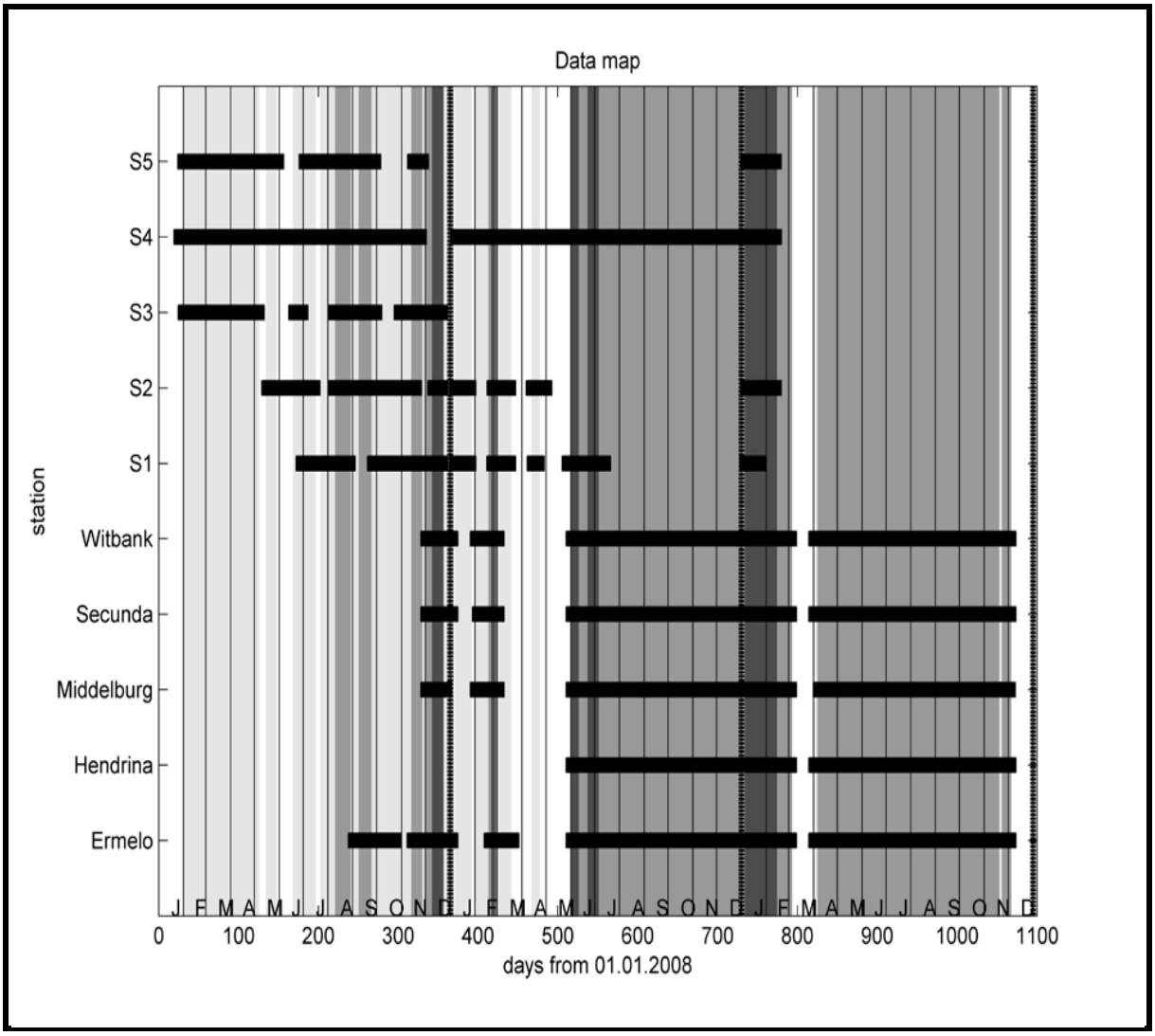

FIGURE 3.3: Data completeness on daily basis collected from MMEH and DEA automatic weather stations.

3.3 Instrumentations

3.3.1 Davis Vantage Pro 2 Automatic Weather Station

The MMEH used Davis Vantage Pro 2 automatic weather stations with independent energy supply from solar panels and wireless data transmission from a set of configurable meteorological sensors to autonomous storage and display module (Fig. 3.4). This equipment has several advantages. It is relatively inexpensive, the stations are automatic.

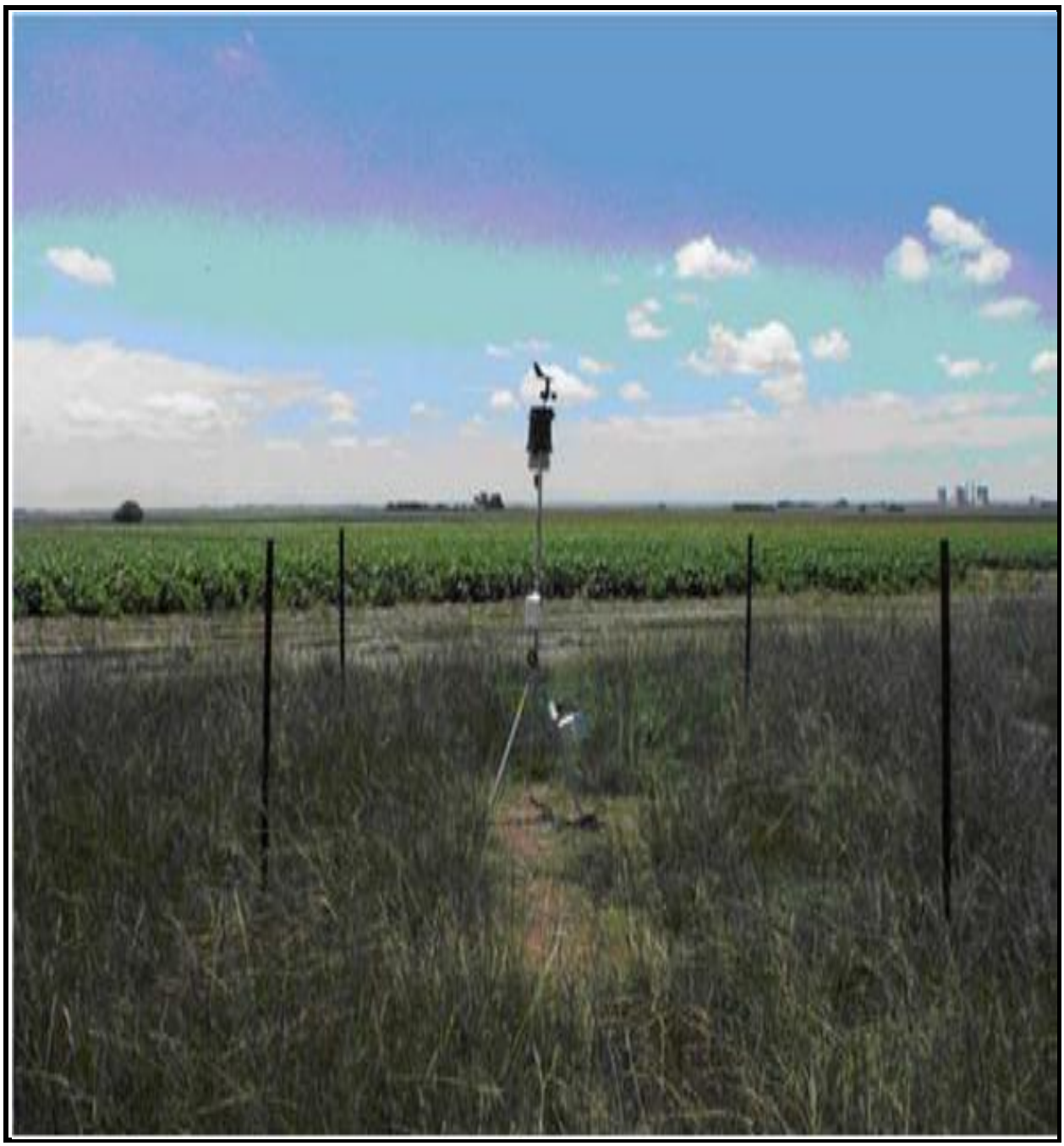

FIGURE 3.4: A typical view of weather station site, site S1 on Jan de Jager's farm (Esau et al, 2010).

They can operate, collect, record and store data without manual maintenance, without external source of the energy supply and without frequent access to sensors and data. All these features are not only reducing the cost but also make it possible to place stations in areas with little or

no infrastructure. The wireless transmission of data with the frequency hopping spread spectrum radio is able to support high transmission rate up to 1000 Hz. It does not require application for a special permit and works effectively with a transmission range up to 120 m. Each of the stations are equipped with a pressure sensor, 2 temperature sensors, humidity sensors, wind anemometers, rain collection gauges and radiation measurements.

An important issue of the experimental meteorology is the quality characteristics of data and stability of the sensors' readings. Massen (2003) studied the performance of Davis automatic weather stations. He concluded that temperature sensors demonstrated good behavior with the scaling factor ~1.0 and negligible offset. Humidity sensors demonstrated acceptable behavior with the scaling factor above 0.9 and the offset ~6 %. The pressure sensor measures atmospheric pressure (not barometric pressure reduced to sea level), when the location altitude is entered, the station stores the necessary offset value to consistently translate atmospheric pressure into barometric pressure. Wind anemometers are working acceptably well with the scaling factor 0.89 and negligible offset. The overall conclusion (Massen, 2003) can be formulated as follows. Certainly the Davis Automatic Weather Station accuracy is way too low to detect minor long-time trends in meteorological parameters. This conclusion opposes the statement of the producer on the station abilities. Thus, the equipment is not suitable for representative meteorological observations, at least without frequent calibration. Nevertheless, the equipment can be used for short-time micrometeorological observations, which rely on statistically significant features but not on the individual readings. The data format is not carefully designed. A lot of important information is missed or stored improperly. At the same time, the format reserves bytes for many derived parameters that can be computed by request. It creates significant complications for the data processing as well as reduces the amount of data to be stored in the limited logger memory. The Davis Vantage Pro equipment has been already used in many educational and scientific projects, e.g. in the Citizen Weather Observer Program (CWOP). In Africa, the equipment has been used in BodEx-2005 (Bodele (in Chad) Experiment. Meteorological experiment (Giles, 2005; Washington, et al., 2005) aimed to quantify the dust aerosol production. As the publications disclose the choice of the Davis Vantage Pro equipment was scientifically justified.

3.3.2 LiDAR System

FIGURE 3.5: NLC-CSIR-Mobile LIDAR system.

Remote sensing measurements from the Council for Scientific and Industrial Research (CSIR) National Laser Centre (NLC), Pretoria (25°5′ S; 28°2′ E) mobile LiDAR were used to study the SBL structure. The system is primarily designed for atmospheric remote sensing. LiDAR uses mono chromatic light (laser) into the atmosphere (see Fig. 3.5). Part of the radiation is scattered back to the LiDAR receiver. This part is being processed to detect the SBL structure. LiDAR provides high temporal variation of BL height in comparison to other techniques. The

detection of ABL height/SBL using laser offers a great advantages over conventional light in terms of peak power, narrow spectral width as well as narrow beam width. LiDAR use 532nm; class IV level and high-single-shot backscatter signal-to-noise ratio performance. The system favors for rapid scan of the atmosphere and provides the measurements almost continuously.

The mobile LiDAR system comprises of a laser transmitter, optical receiver and a data acquisition system. The complete LiDAR system is custom fitted into a van using a shock absorber frame. Hydraulic stabilizer feet have been added to the vehicle suspension to ensure stability during measurements. A Nd: YAG laser is used for transmission which is presently employed at the second harmonic (532 nm) at a repetition rate of 10 Hz. The receiver system employs a Newtonian telescope configuration with a 16 inch primary mirror. The backscattered signal is subjected to fall on the primary mirror of the telescope and is then focused to a plane mirror kept at an angle of 45 degrees. It is detected by the Photo-Multiplier Tube (PMT) and the PMT output is transmitted to the transient digitizer and PC for analysis and archival. A multimode optical fiber is used to couple the received backscatter optical signal from the telescope to the PMT. To accomplish accurate alignment of the fiber tip, a motorized 3-D translation stage is used. The optical fiber is connected to an optical baffle which is positioned by the stage. The PMT is installed in an optical tube which incorporates a collimation lens and a narrow band pass filter. This tube is thermally stabilized with the use of Thermo-Electric Cooler (TEC) cooling. The sub-miniature PMT converts the optical backscatter signal to an electronic signal which can be transferred to a PC for storage and analysis. The PMT used is a Hamamatsu® R7400-U20, which operates in the 300 nm to 900 nm wavelength range and has a fast rise time response of 0.78 ns. This specific detector is selected by request for maximum sensitivity and specified with an anode dark current of 0.37 nA. Typical anode dark currents for these devices range from 2 nA to 20 nA.

The data acquisition is performed by a transient recorder which communicates with a host computer for storage and offline processing of data. A Licel® transient digitizer is used for this purpose. The system is favored due to its capability of simultaneous analogy and photon counting detection, which makes it highly suited to LiDAR applications by providing high dynamic range. A software interface is included with the LICEL system which allows the user

to acquire signals without the need for immediate programming. For more details, about the system and capabilities refer to Sivakumar et al. (2009) and Sharma et al. (2009).

3.4 Methodology

3.4.1 Spatial Analysis

Let's consider a pair of stations i and j with the distance d_{ij} between them (see Table 3.2). A spatial fluctuation of u for this pair of stations is defined as:

$$u_i' = u_i - (u_i + u_j)/2 \tag{3.1}$$

The idea behind Eq. 3.1 is similar to the Reynolds idea of decomposing the meteorological variables in turbulent flow as sum of time averaged and turbulent fluctuation. Here u_i' is the deviation of the respective variable from the mean between two stations due to the difference of the surface characteristics. It is apparent that if at $i = j$, $u_i = u_j$ then $u_i' = 0$, this indicates the same surface characteristics at i and$j$. The time averaged variability is defined as:

$$M_{uu}(i,j) = \left[\overline{u'u'}\right]_{ij} = \frac{1}{2}\left(\overline{u'_i\, u'_i + u'_j\, u'_j}\right), \text{ for all i>j} \tag{3.2}$$

, over bar denotes time averaging done over entire considered period of observations.

The quantity in focus here is the maximum variability, which is defined as:

$$\left[\overline{U'T'}\right]_{ij} = \max\left(\frac{1}{2}\overline{(U_i'T_i' + U_j'T_j')}\right) \tag{3.3}$$

It characterizes the maximum variability of the horizontal temperature flux. Variability of the horizontal relative humidity flux $\overline{U'R'}$ is determined in the same manner. It is reasonable to expect that the flux given by Eq. 3.3 maximize on certain spatial scales. At the large scale limit, only the external forced variability, which is the same for all stations in the area, will determine the concrete value of the residual horizontal fluxes. The decay of these fluxes with increasing d_{ij} is however not necessarily monotonic. If there are significant interactions between the land use scales and the scales of the atmospheric dynamics, the fluxes may level

off or even enhance for certain range of scales. The next section will demonstrate that this is the case for the MMEH and DEA data sets in the Highveld region (Bethal). Such an enhancement of the turbulent exchange over heterogeneous surface was previously called a resonant response (Roy et al., 2003; Patton et al., 2005; Esau, 2007; Robinson et al., 2008). This response is expected within the range of normalized scales $1 < d_{ij}/ h < 9$, where h is the ABL depth. The lower limit of scales is more relevant to the initial stages of the ABL convection, whereas the upper limit is more relevant to the well developed convection (Robinson et al., 2008). Taking h = 2 to 3 km in the Highveld region (Freiman and Tyson, 2000), the flux should peak at distances d_{ij} = 5 to 30 km.

3.4.2 Root Mean Square Analysis

The root mean square (RMS) analysis compares the mean variability of a parameter u, which is determined for each station over all time moments, with the mean variability of u, which is determined at each time moment over all stations. Mathematically, if u (i, t) is a matrix at each sampling moment since measurements were reordered at 10 minutes interval i.e. 144 sample for one day n = 1…..144, where the rows index $i = 1 \cdots \cdots \cdots N$ runs over stations and the column index $t = 1 \cdots \cdots \cdots T$ runs over time moments, then temporal and spatial RMS can be defined as

$$\sigma_u^{\,time}(n) = \sqrt{\overline{\langle u - \bar{u} \rangle^2}} \tag{3.4}$$

$$\sigma_u^{\,station}(n) = \sqrt{\overline{\langle u - (\bar{u}) \rangle^2}} \tag{3.5}$$

$$\text{, where } \langle u \rangle (t,n) = \frac{1}{N} \sum_i u(i,t,n), \text{ and } \bar{u}(t,n) = \frac{1}{T} \sum_i u(i,t,n) \tag{3.6}$$

In order to study the diurnal cycle of the land use interaction with the atmospheric dynamics, the time averaging was achieved independently for each of the data sampling moment n across all days available in each data set (60 days for 100% completeness of a station data set).

Both measures, $\sigma_u^{station}$ and σ_u^{time} may rise and fall within the diurnal cycle. Moreover, one may be consistently smaller or larger than the other. Useful information could be extracted from their relative change within the diurnal cycle as defined by the following measures:

$$R_u(n) = \frac{\sigma_u^{station}(n)}{\sigma_u^{station}(n) + \sigma_u^{time}(n)} \tag{3.7}$$

$$D_u(n) = \left(\sigma_u^{station}(n) - \overline{\sigma_u^{station}(n)}\right) - \left(\sigma_u^{time}(n) - \overline{\sigma_u^{time}(n)}\right) \tag{3.8}$$

Here, the over-bar is used to define averaging over of the diurnal sampling moment *n*. The ratio, R_u indicates the relative significance of the internal (local) variability at the stations versus total variability. It should not be confused with the fraction of total variability, which is explained by the internal variability. For small ensembles of data sets (N < 20) and large internal variability, such a fraction would be estimated with a significant error (Ting et al., 2009). The difference of the normalized RMS, D_u indicates relative importance of changes in the external and internal variability across the diurnal cycle. Reduction of D_u in particular to negative values, indicates spatial homogenization and therefore diminishing internal variability. Vice versa, increase of D_u indicates that the internal variability become more pronounced that suggests increasing coupling between the local land surface features and the atmospheric dynamics and decreasing coupling to the large scale dynamics of the free troposphere correspondingly.

3.4.3 Similarity Theory Approach

In this study the calculation of turbulent friction velocity, sensible heat fluxes and Obukhov length is based on similarity theory. First, for the past already 60 years Kolmogorov's (Kolmogorov, 1941) approach for turbulent closure models based on the turbulent kinetic energy (TKE) balance has been a major scientific tool. His hypothesis, however, is theoretically only justified for neutrally stratified turbulent flows. Many attempts to apply Kolmogorov's method for stratified flows have encountered difficulties. The straightforward application of the TKE budget equation leads to the existence of critical Richardson number above which the turbulence is suppressed.

The Kolmogorov's theory for turbulence laid the foundation of the similarity theory developed by Monin–Obukhov (MO) (Monin and Obukhov, 1954). This theory extended the results for neutrally stratified turbulent flow to any stratification conditions. The similarity theory postulates that near any given surface, the wind and thermodynamic profiles should be determined purely by the height z above the surface (which scales the eddy size) and the surface turbulent fluxes which drive turbulence: surface momentum flux which is often expressed as friction velocity $u_* = \left[\left(\overline{(u'w')}_s\right)^2 + \left(\overline{(v'w')}_s\right)^2\right]^{\frac{1}{2}}$, surface buoyancy flux $F_s = \overline{(w'b')}_s$ and the buoyancy parameter $\beta = g/T_0$ (g is the gravity acceleration, T_0 is a reference temperature of absolute temperature). From these dimensional parameters one can construct the Obukhov length described by:

$$L = \frac{-u_*^3}{\kappa F_s} = \frac{-\tau^{3/2}}{\kappa F_s}, \text{ or } L = \frac{u_*^2}{\kappa^2 \beta \vartheta_*} \tag{3.9}$$

, where κ is the Von Karman constant. L, is positive for stable and negative for unstable boundary layers. In the ABL, a typical u_* is $0.3\,ms^{-1}$ and a typical range of buoyancy flux would be $-3x10^{-4}\ m^2s^{-3}$ (night time) to $1.5x10^{-2}\ m^2s^{-3}$ (midday) (i. e. a virtual heat flux $-10\,Wm^{-2}$ at night, $500\,Wm^{-2}$ at midday), giving $L = 200\ m$ (night time) and $-5\,m$ (midday) (Bretherton, 2011). One can form a single non dimensional stability parameter:

$$\zeta = \frac{z}{L} \tag{3.10}$$

According to MO similarity theory the flux-profile gradient relationship for momentum and potential temperature are:

$$\frac{kz}{\tau_*^{1/2}}\frac{\partial \bar{u}}{\partial z} = \left(\frac{kz}{u_*}\right)\frac{d\bar{u}}{dz} = \Phi_m(\zeta) \tag{3.11}$$

$$\frac{k_\theta z \tau_*^{1/2}}{F_\theta}\frac{\partial \theta}{\partial z} = \left(\frac{kz}{\theta_*}\right)\frac{\mathrm{d}\bar{\theta}}{\mathrm{d}z} = \Phi_\theta(\zeta) \tag{3.12}$$

where $\Phi_m(\zeta)$ and $\Phi_\theta(\zeta)$ are universal similarity functions. Other adiabatically conserved scalars should behave similarly to temperature since the transport is associated with eddies

which are too large to be affected by molecular diffusion or viscosity. To agree with the log layer scaling, $\Phi_m(\varsigma)$ and $\Phi_\theta(\varsigma)$ should approach 1 for small ζ. This requires $\Phi_m(\zeta) = \Phi_\theta(\zeta) \longrightarrow 1$ at $\zeta \to 0$. The functional form of the universal stability functions for stable stratification $\zeta \gg 1$ should be $\Phi_m \sim \Phi_\theta \sim \varsigma$ since the turbulence is not affected by the distance to the surface.

From this theory it follows that the Richardson number $Ri = \beta(\partial\bar{\theta}/\partial z)/(\partial\bar{u}/\partial z)^2$ monotonically increases with s z/L and at $z/L \to \infty$ has an asymptote maximum value of $Ri_{cr} = \chi^2 C_{\theta 1} k^{-1} C_{U1}{}^{-2}$. This shows that the universal function range cannot exceed $Ri > Ri_{cr}$. This is a classical result which follows from the equation of kinetic turbulent energy balance accepted by Kolmogorov at the time when MO theory was formulated.

The stability functions in Eq. 3.11-3.12 must be determined empirically. In the 1950- 60s, several field experiments were conducted for this purpose over regions of flat, homogeneous ground with low, homogeneous roughness elements, culminating in the 1968 Kansas experiment. Businger et al. (1971) documented the universal functions for SBL, which are still accepted and widely used:

$$\Phi_m(\frac{z}{L} > 0) = 1 + 4.7\frac{z}{L} \tag{3.13}$$

$$\Phi_\theta(\frac{z}{L} > 0) = 0.74 + 4.7\frac{z}{L} \tag{3.14}$$

The MO similarity theory as expressed by Eq. 3.11-3.12 subject to the universal function Eq. 3.13-3.14 when integrated from the roughness height z_0 , z_1 to z gives the Monin and Obukhov (1954) similarity theory profiles for the mean wind and potential temperature:

$$\bar{u}(z) = \frac{u_*}{k}\left(ln\frac{z}{z_0} + 4.7\frac{z-z_0}{L}\right) \tag{3.15}$$

$$\bar{\theta}(z) - \bar{\theta}(z_1) = \theta_*\left(0.74 ln\frac{z}{z_1} + 4.7\frac{z-z_1}{L}\right) \tag{3.16}$$

Eq. 3.15-3.16 and Eq. 3.9, form a closed algebraic system of equations for θ_*, u_* and L. Its solution lead to the following quadratic equation for u_*

$$\left[0.74ln\frac{z}{z_1}ln\frac{z}{z_0}-\left(ln\frac{z}{z_0}\right)^2\right]u_*^2+\left[\overline{u}(z)k\left(2ln\frac{z}{z_0}-0.74ln\frac{z}{z_1}\right)\right]u_*+\left[4.7(z-z_0)k^2\beta(\theta(z)-\theta(z1))-k2u2(z)=0\right. \quad (3.17)$$

The coefficients of the above quadratic equation are; a=$\left[0.74ln\frac{z}{z_1}ln\frac{z}{z_0}-\left(ln\frac{z}{z_0}\right)^2\right]$

b=$\left[\overline{u}(z)k\left(2ln\frac{z}{z_0}-0.74ln\frac{z}{z_1}\right)\right]$ and c=$\left[4.7(z-z_0)k^2\beta(\theta(z)-\theta(z_1))-k^2\overline{u}^2(z)\right]$

Negative discriminant given by $b^2-4ac<0$, indicates all turbulence is suppressed in SBL. Therefore all data with negative discriminant are not valid for this calculation. Positive discriminant given by $b^2-4ac>0$, indicates turbulence exist in the SBL. Zero discriminant is given by $b^2-4ac=0$, indicates existence of turbulence in the SBL.

θ_*, is solved from the following equation:

$$\theta_*=\frac{u_*}{4.7\kappa^2\beta(z-z_0)}\left[\overline{u}(z)\kappa-u_*ln\left(\frac{z}{z_0}\right)\right] \quad (3.18)$$

After Eq. 3.9, L can be calculated.

Using the experimental data one can calculate u_*, θ_* and L and subsequently the vertical profiles of the meteorological elements in the surface boundary layer.

The performance of the Monin Obukhov similarity theory has been investigated for the wind velocity less than 6m/s and for greater than 6m/s in the stable boundary layer (Fig. 3.6 and 3.7). This figure depicts the dependence of u* on stability (Δθ). Also it indicates that the Monin Obukhov similarity theory gives realistic results of u* if the wind velocity is less than 6 m/s. In the analysis in a few cases wind speed greater than 6 m/s exist in SBL (see Table 3.3) and the decision was to exclude such velocity.

TABLE 3.3: percentage of wind velocity bigger than 6 and less than 6 m/s at different stations.

Stations	% wind >6 m/s	% wind < 6 m/s
S1	0	100
S2	1	99
S3	6	94
S4	0	100
S5	0	100

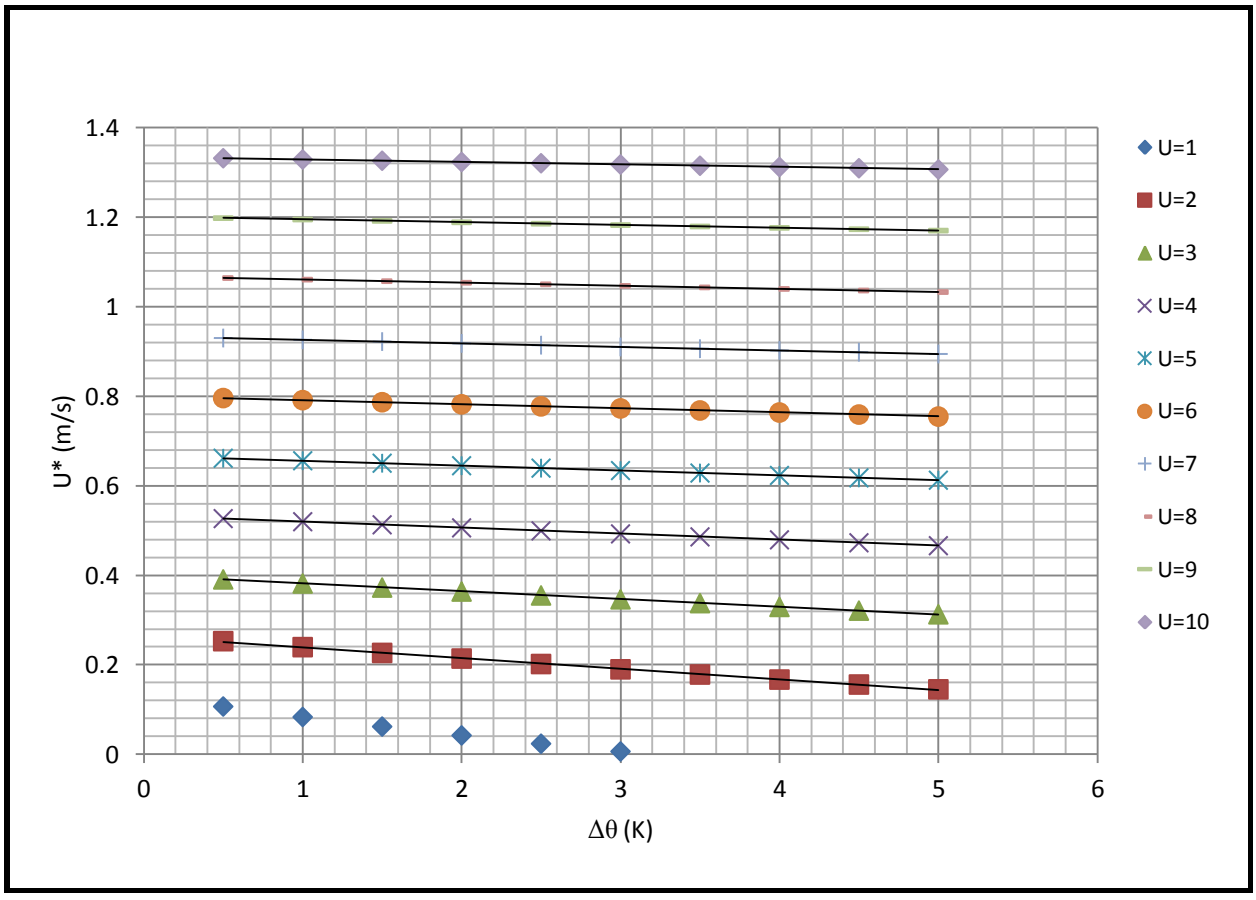

FIGURE 3.6: Variation of u* (m/s) with Δθ (k) at different wind speed.

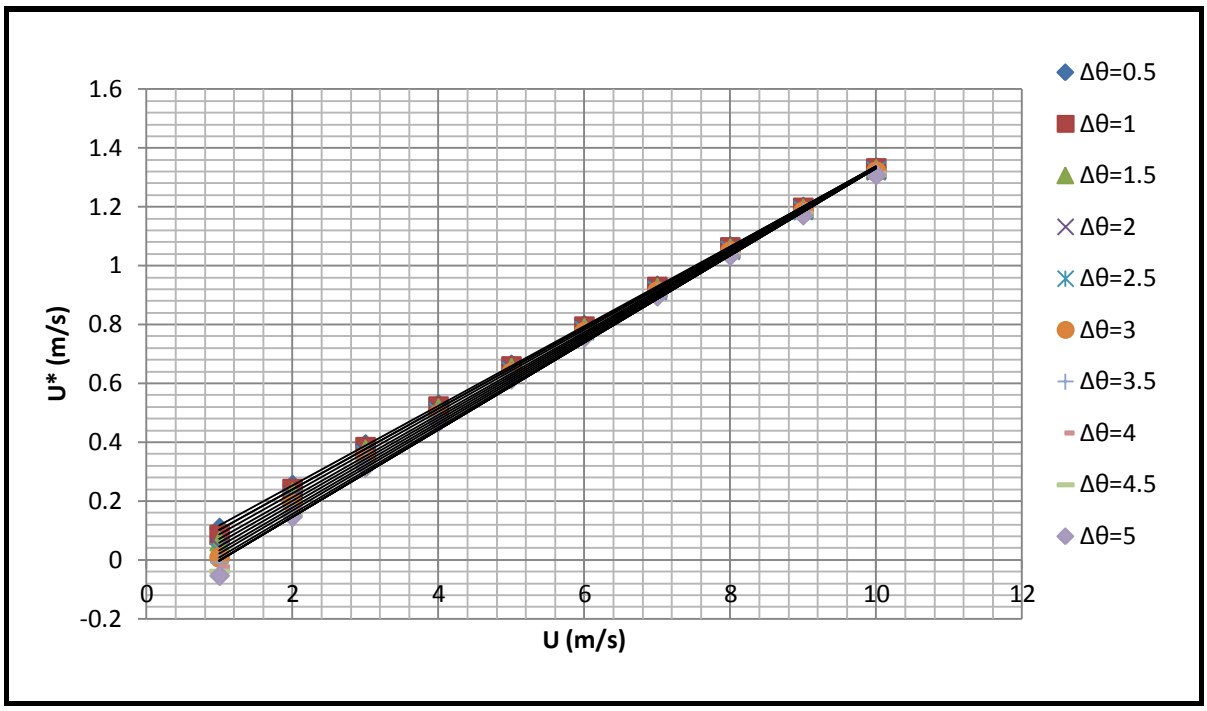

FIGURE 3.7: Variation of u* (m/s) with wind speed at different Δθ (K).

3.4.4 SBL height from Radiosonde Data

A Radiosonde is an instrument package that measures temperature, relative humidity, wind speed and atmospheric pressure. These data are transmitted back to the launch site by radio. Temperature, relative humidity and wind speed can be used to calculate the BL height.

The conventional methods for detecting BL height from Radiosonde data is straight-forward by analysis of the vertical variations of temperature, humidity, wind speed and turbulent fluxes. The ABL height is the height region where there is temperature inversion, or is the height region where wind velocity becomes equal to geostrophic wind. Also ABL height is identified as a region where the turbulent fluxes are negligible.

3.4.5 SBL Height Detection from LiDAR

LiDAR backscatter profiles present the vertical distribution of aerosol concentration in the ABL. Aerosols originates from the earth's surface, producing high concentration in the ABL near the surface relative to the free atmosphere above. There is always a sharp decrease of

aerosol concentration at the top of the ABL this provides method to determine the ABL height using either first gradient method or statistical method.

3.4.5.1 First Derivative Gradient Method

This method is based on the analysis of first derivative gradient of LiDAR back scattered signal. The BL height is identified as the height/altitude at which there is absolute negative minimum of the first derivative of the LiDAR backscatter:

$$h_{AB} = \frac{dP(z)}{dZ} \tag{3.26}$$

$$\mathrm{P}(z) = \mathrm{P}_0 \frac{c\Delta tA}{2Z^2} \eta\beta(z) e^{-2\int_0^z \alpha(z)dz'} \tag{3.27}$$

, where $\mathrm{P}(z)$ is power received from a range Z, P_0 is the transmitted power in watts, c is the speed of light, Δt is the laser pulse width, η is the overall system efficiency, $\beta(z)$ is the volume backscatter function, A is the area of the receiving mirror, $\alpha(z)$ is the volume extinction function and h_{AB} is the ABL height.

3.4.5.2 Statistical Method

This method is also known as standard deviation method. In this method, the standard deviation is calculated from the temporal fluctuations of the range squared corrected signal $\mathrm{P}(z^2)$ at each altitude as follows.

$$\sigma P(z^2) = \frac{1}{N}\sum_i \left(P_i(Z^2) - \overline{P}(Z^2)\right)^2 \tag{3.28}$$

where $\sigma P(Z^2)$ is the standard deviation for the range square corrected signal, $\overline{P}(Z^2)$ is the mean of range square corrected signal N- Correspond to number of profiles, $P(Z^2)$ - is the range square corrected signal. The ABL height is determined as the altitude with maximum standard deviation.

CHAPTER 4

RESULTS AND DISCUSSION

4.1 Stable Boundary Layer Height

First gradient method for detecting the SBL height was applied to CSIR- Mobile LiDAR backscatter measurement over Elandsfontein, Highveld region and one such example is presented in Fig. 4.1. This figure illustrates a "snapshot" view of vertical distribution of passive tracer within the atmosphere over Elandsfontein. Basically the SBL height is identified as the first minimum slope close to surface in the LiDAR backscatter profile.

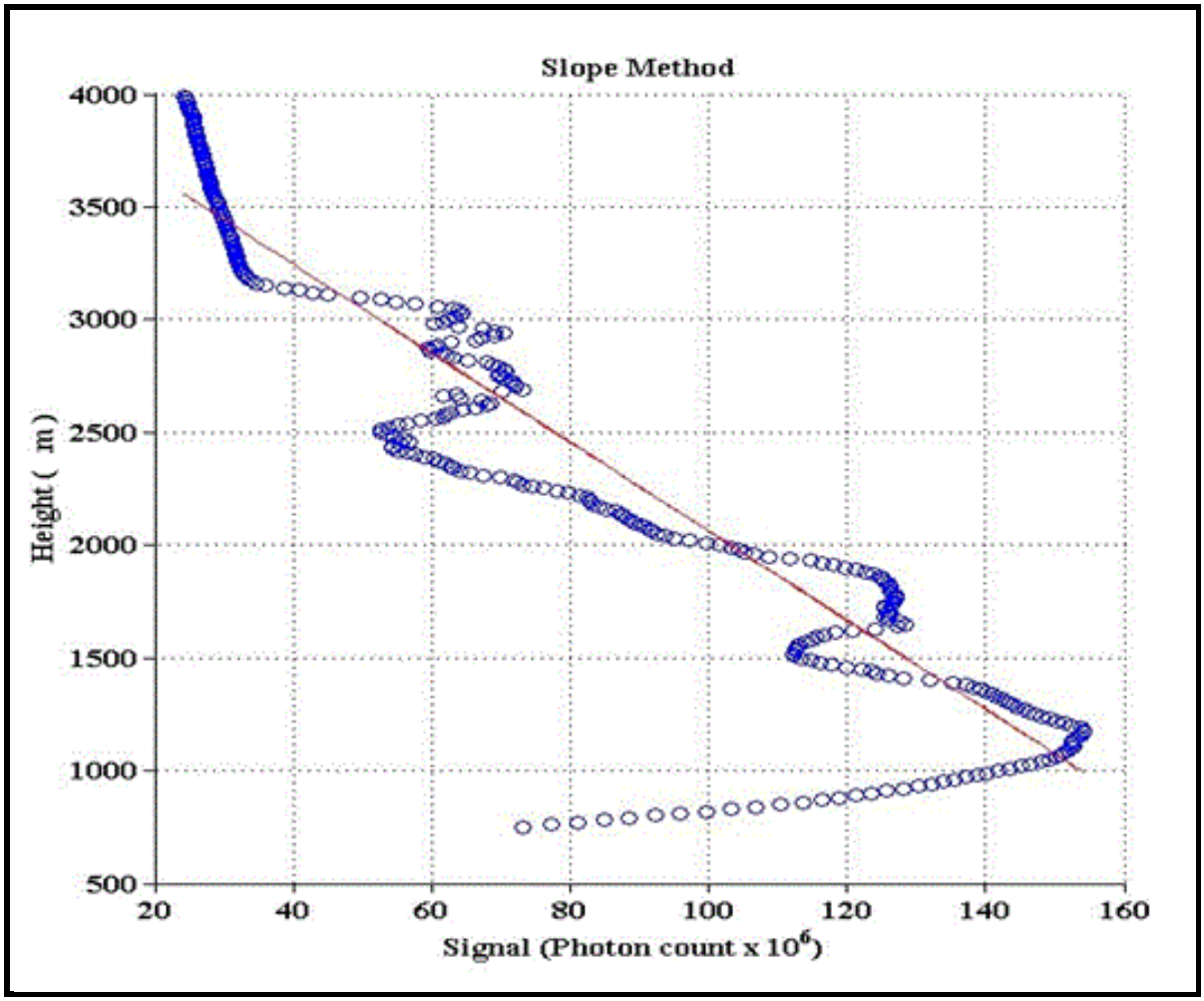

FIGURE 4.1: Height profile of range corrected LiDAR signal returns.

Based on the presented profile in Fig. 4.1 the first minimum gradient is identified at 1200 m. This height does not reflect the actual height of the SBL but complement with the height of the first elevated absolutely stable layer (Van Gogh et al., 1986). The profile also indicates that the backscattered measurement received at the LiDAR site start at around 750 m above the ground level, this height is higher than the typical height of the SBL.

The temporal evolution of the LiDAR backscatter radiation from 23:23 pm to 04:22 am over Elandsfontein on 1st-2nd December 2010 is presented in Fig. 4.2. This figure is produced based on the LiDAR Eq. 3.27. Strong signal LiDAR returns are observed at the high altitude (~ 1200 m-3000 m), this is the height range of elevated absolutely stable layer. Beyond 3000 m LiDAR returns starts to decreases with height due to less scattering particles in the free atmosphere. The evolution of high level clouds at 7 km to 10 km was observed. Other than the cloud structure (at 7-10 km), the aerosol structure evidences the temporal evolution of the elevated absolutely stable layers.

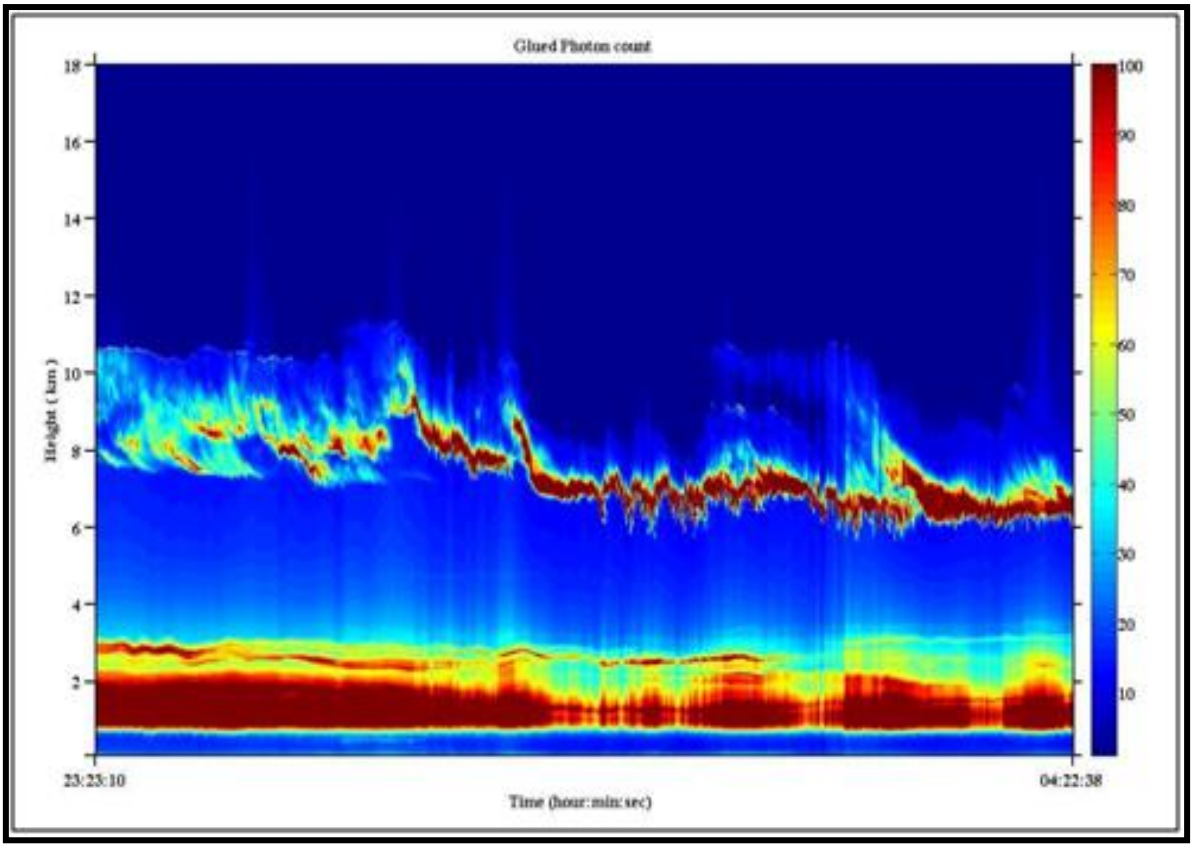

FIGURE 4.2: Height-Time-Color map of LiDAR return signal on 1st-2nd December 2010.

The LiDAR return signals used to plot the height time color map Fig. 4.2 were processed using gradient method for detection of the first minimum gradient of LiDAR backscatter. Result for temporal evolution of the first minimum gradient is presented in Fig. 4.3. In this figure the first elevated absolutely stable layer varies significantly with time and decrease as night progress reaching its minimum value at early morning time (3:00-4:13 am).

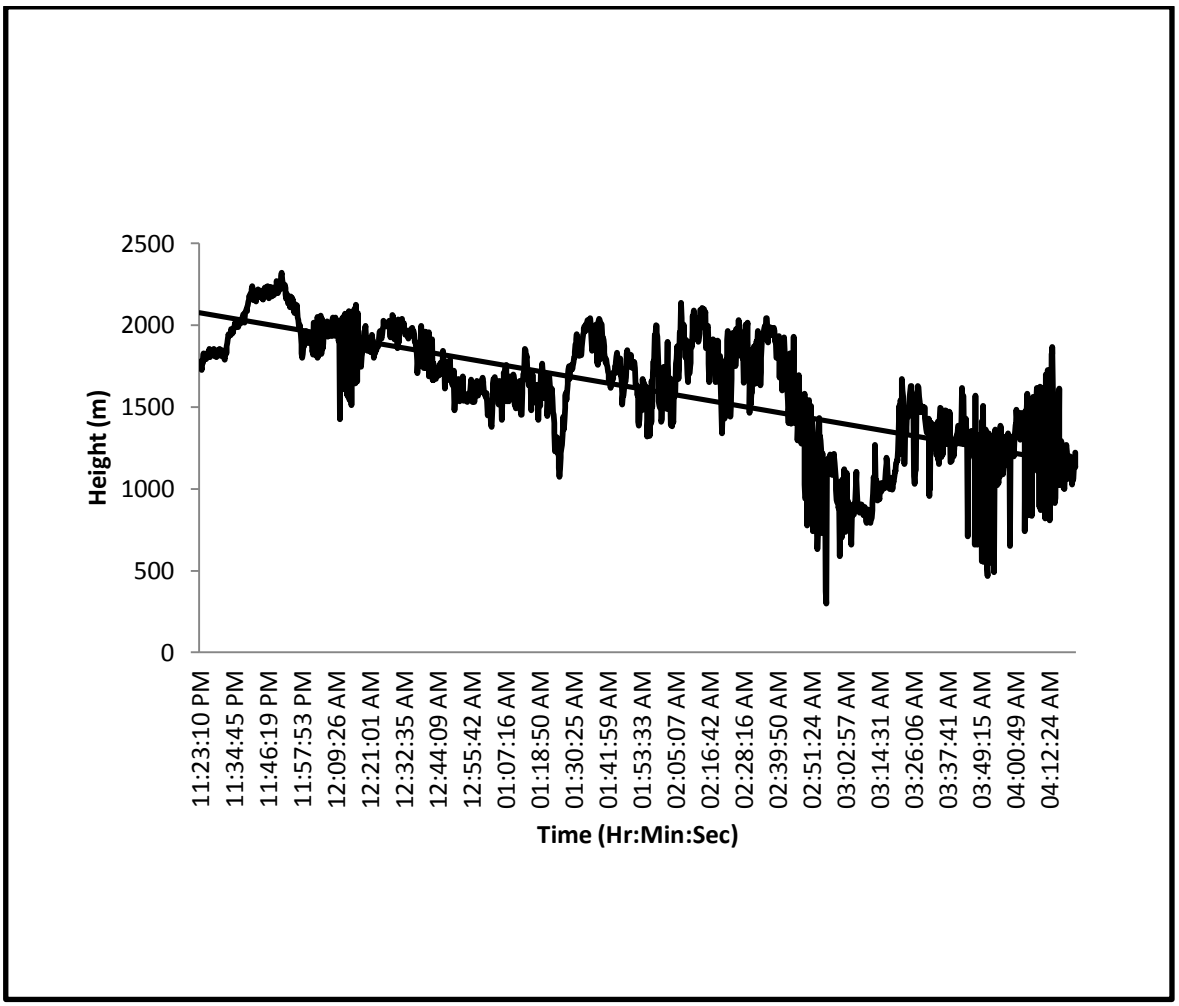

FIGURE 4.3: The elevated absolutely stable layer observed on 1-2 December 2010 over Elandsfontein using gradient method.

Statistical method was also used for deduction of the SBL height. In this method the SBL height is identified as the height where there is maximum standard deviation in the range square corrected signals. Results from this method also indicate too high height of about 3000

km (Fig. 4.4). This height does not reflect the actual height of the SBL but correlate with the height of elevated absolutely stable layer.

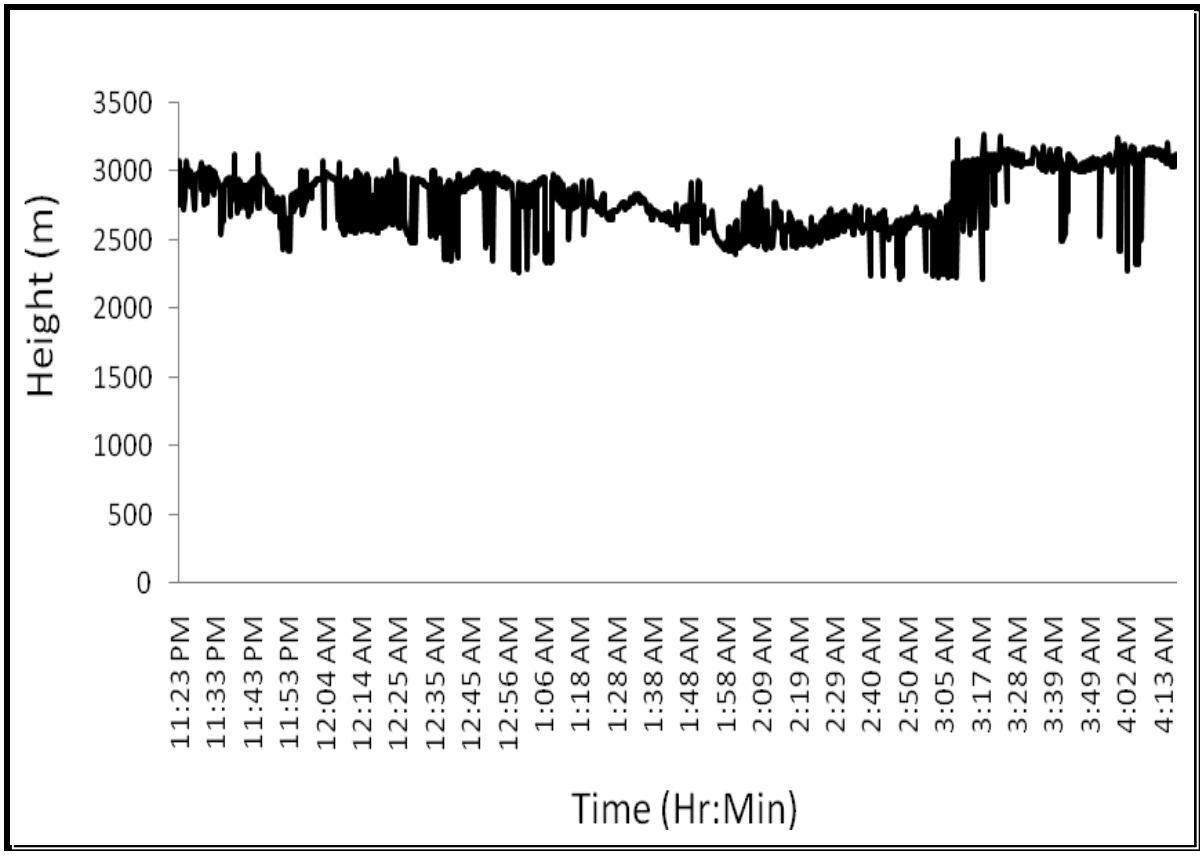

FIGURE 4.4: The height of elevated absolutely stable layer on 1-2 December 2010 over Elandsfontein using statistical method.

LiDAR results were validated using Radiosonde data from Irene weather station (25° 52' 8" S, 28° 12' 59" E) on 1.12.2010 at 02 am (Fig. 4.5). Radiosonde is used in weather balloons to measure various atmospheric parameters at different height and transmits them to a fixed receiver. The temperature variations with altitudes are used for detection of the first minimum gradient in the profile. The first minimum gradient was observed at height region of 166 m (Fig. 4.5). This is the height of the SBL. It is shallow when compared with the first elevated absolute stable layer of about 1250-3000 m observed over Elandsfontein ($26^0$2’ S, $29^0$4167’ E) at 02 am from LiDAR measurements using both, gradient and statistical methods. This concludes that LiDAR cannot measure accurately so close to the surface hence cannot detect the SBL height.

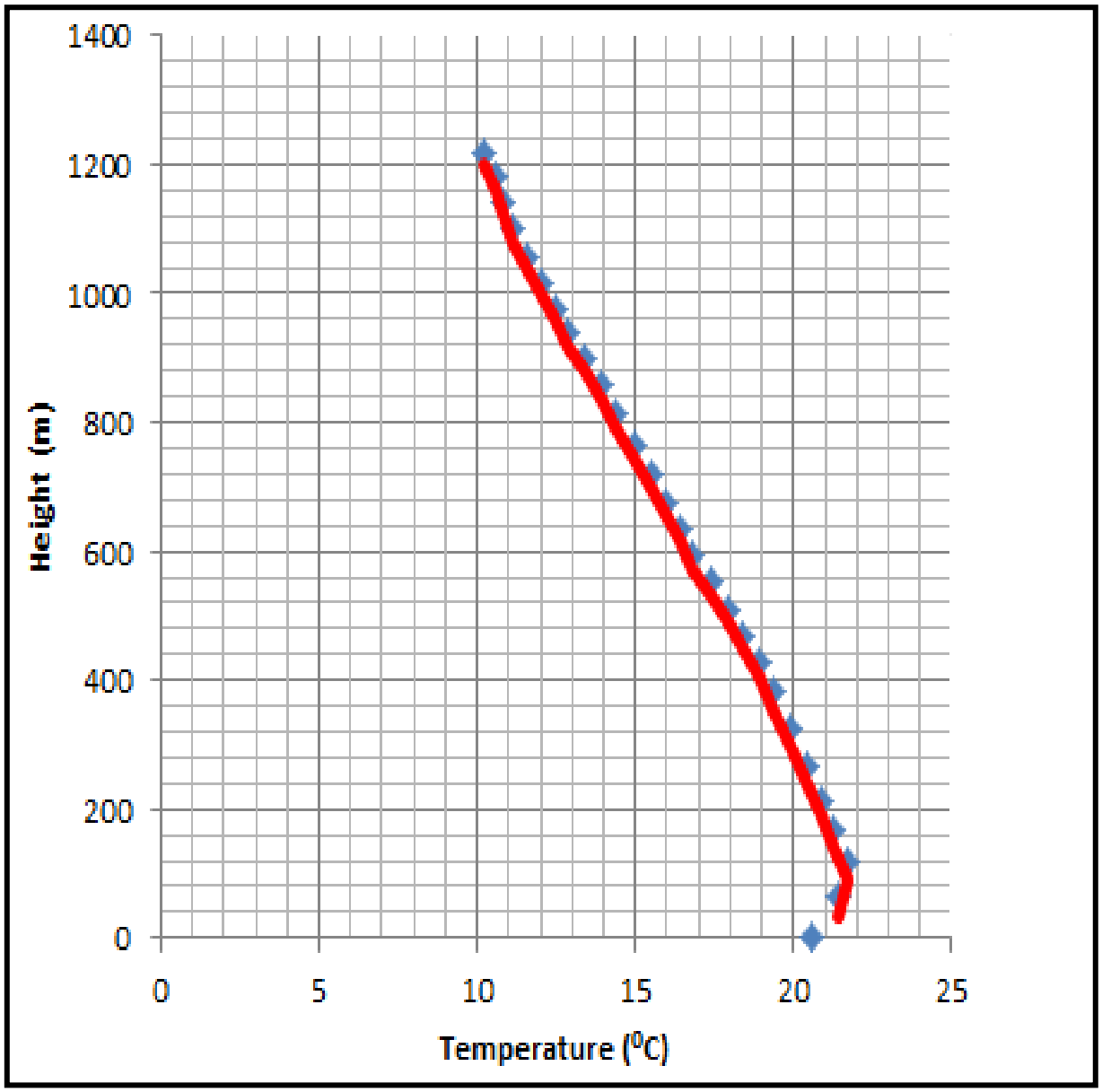

FIGURE 4.5: SBL height derived from sounding data from Irene weather station: 25° 52' 8" South, 28° 12' 59" East.

4.2 Spatial Distribution of Turbulent Momentum and Heat fluxes and Obukhov Length

The spatial distribution of turbulent momentum and heat fluxes and Obukhov length at 2m height in SBL over Highveld region are presented in Fig. 4.6-4.11.

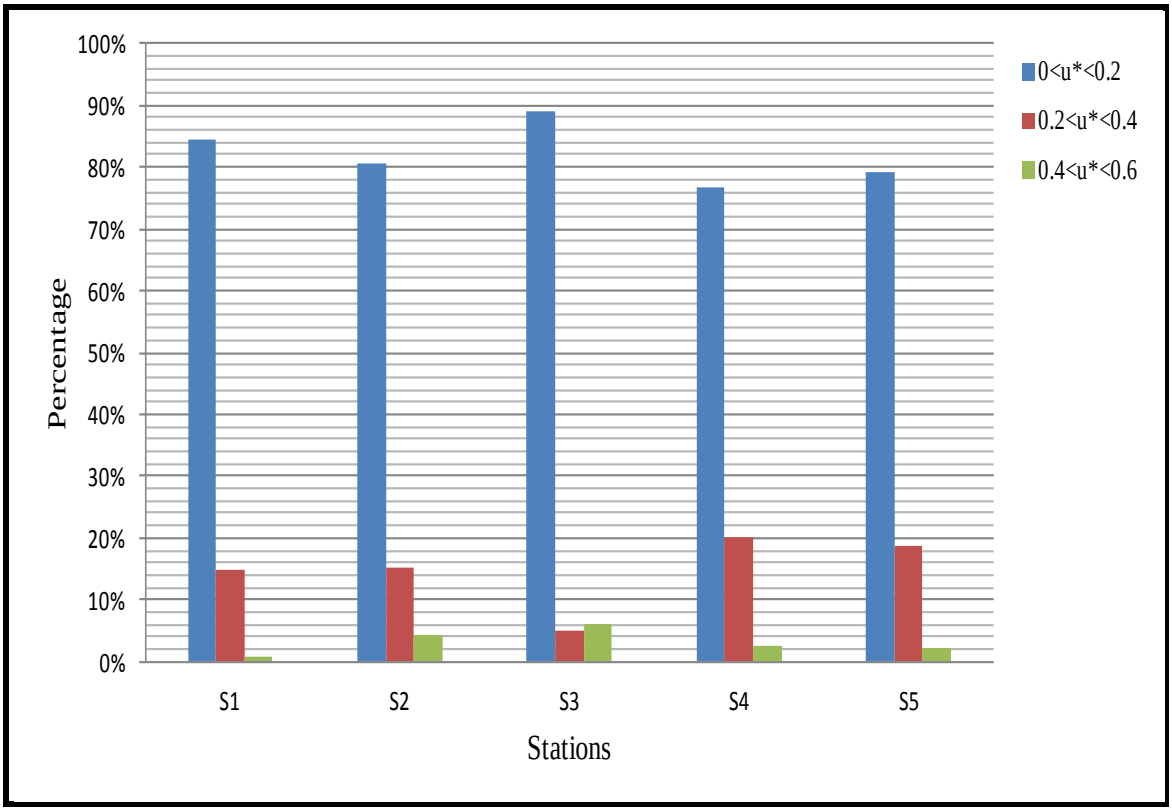

FIGURE 4.6: Spatial distribution of the turbulent momentum fluxes.

Fig. 4.6 presents results obtained from similarity theory using data set collected from 2008 to 2010. The figure presents the distributions of three ranges of turbulent momentum fluxes at micro-meteorological scales that play an important role in local and meso-scale atmospheric circulations. This figure indicates that the distribution of turbulent momentum fluxes at the spatial scales between the stations is almost similar, dominated by small values of momentum fluxes in the range of $0 < u_* < 0.2$ (m/s). Previous published work (Jegede and Løføstrøm, 1997) suggest that the low values of turbulent momentum fluxes indicates that the mechanical contribution to the surface layer turbulence is minimal which is the consequent from the rather weak wind fields in the area. In the figure above about 85% of the turbulent friction velocities are in the range of $0 < u_* < 0.2$ (m/s). This indicates that Highveld is dominated by strong stability regimes.

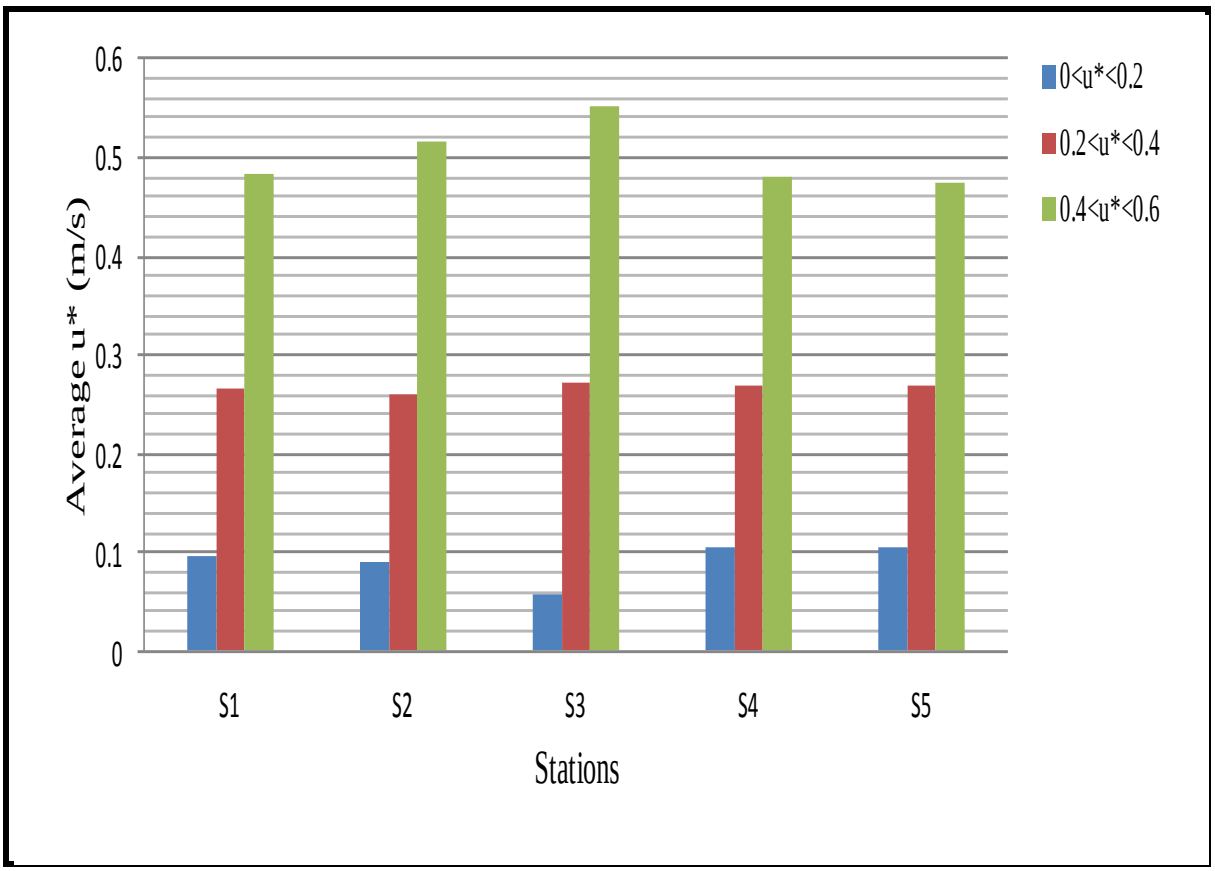

FIGURE 4.7: Spatial distribution of the average turbulent momentum fluxes.

Fig. 4.7 presents results derived using the same data as in Fig. 4.6, but for the average turbulent momentum fluxes. This figure indicates that there is no significant difference of the averaged turbulent momentum fluxes between the stations. Station 3 is dominated with small values of turbulent friction velocity.

Fig. 4.8 presents results produced using the same data and approach as in Fig.4.6 but for the turbulent heat fluxes. Small values of turbulent heat fluxes dominate throughout the stations; roughly 46-59% of values fall in the range of $0 < \theta_* < 0.2$ station 1 and 2, and 39%, 34% and 40% at station 3, 4 and 5 respectively fall in the range of $0.2 < \theta_* < 0.4$. The distribution of these heat fluxes indicates no significant variation between stations. The average distribution of turbulent heat fluxes is presented in Fig. 4.9. This figure indicates similar distribution of average turbulent heat fluxes between stations.

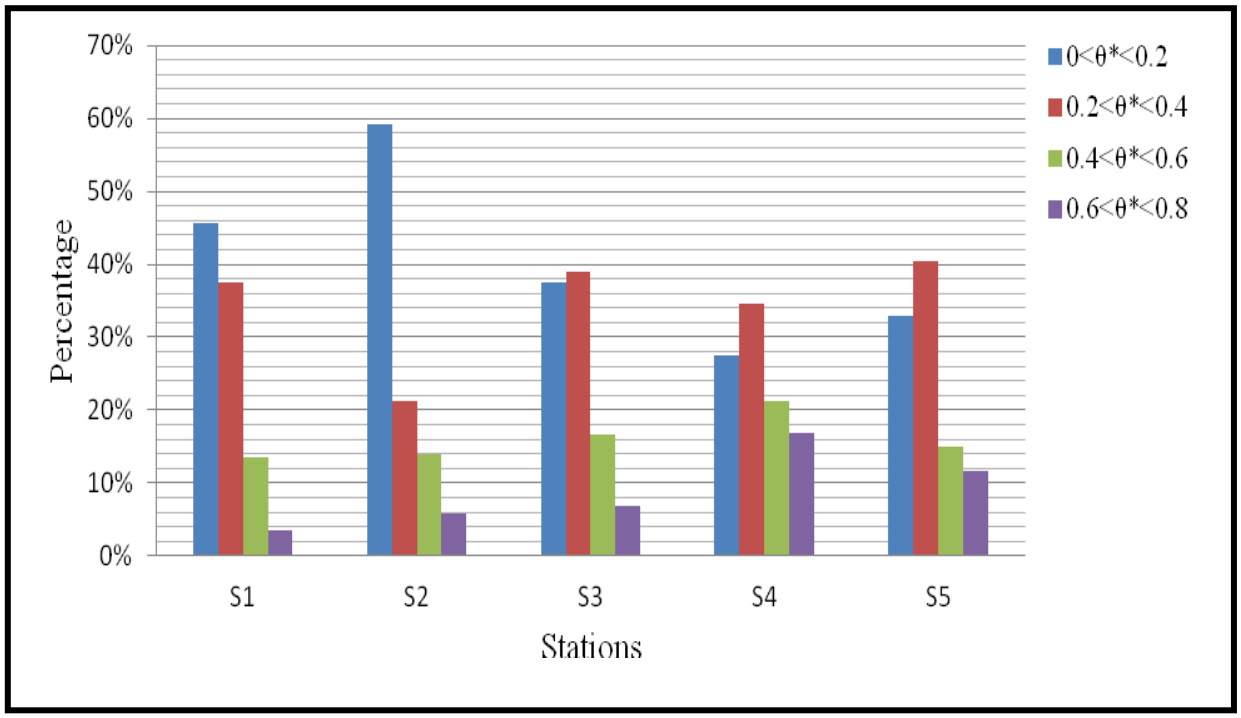

FIGURE 4.8: Spatial distribution of the turbulent heat fluxes

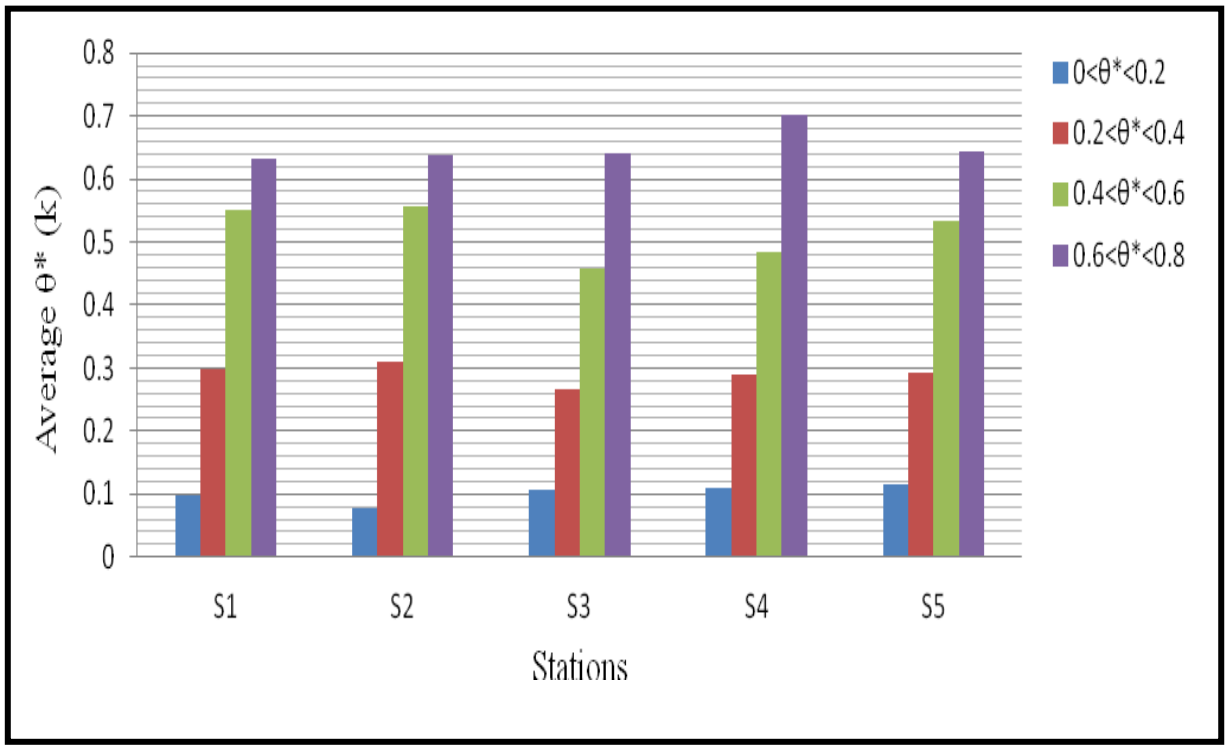

FIGURE 4.9: Spatial distribution of the average turbulent heat fluxes

The Obukhov length was calculated using similar dataset as that used to generate Fig. 4.6. Result indicates that at all stations, the Obukhov length is always between 0 and 16 m. The distribution of average Obukhov length (L) presented in Fig. 4.10 suggests that the stability range of 0 m<L<8 m is almost similar distributed between stations. The Obukhov length is less at station three (S3) because of the dominant weak wind condition as presented by small values of turbulent friction velocity (Fig.4.6). This is the indication of strong stability exists at this station.

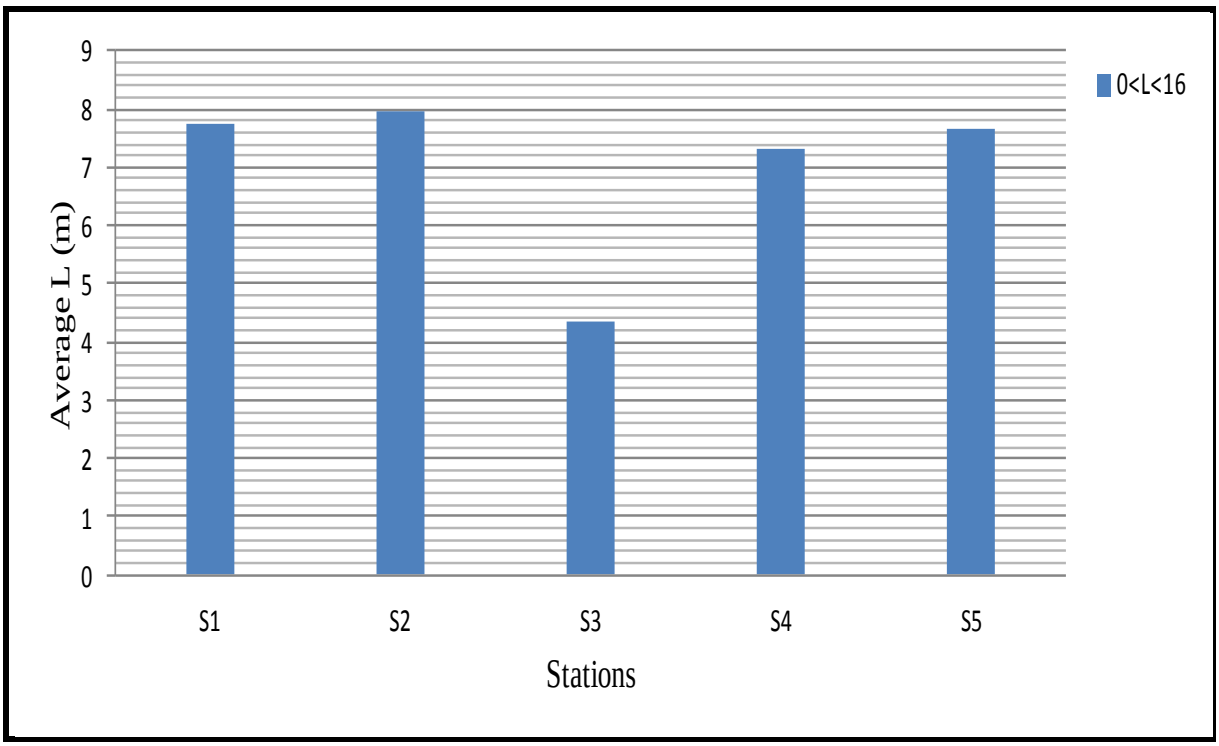

FIGURE 4.10: Spatial distribution of the average Obukhov length.

Distribution of the stability regimes as presented by BRN are indicated in Fig. 4.11. This figure was produced using same data set as used in Fig.4.6, but for calculation of the BRN. The distribution suggests that about 82% of BRN values fall in strong stability regime (BRN>0.25) which are almost similar distributed between stations at micro-meteorological scale.

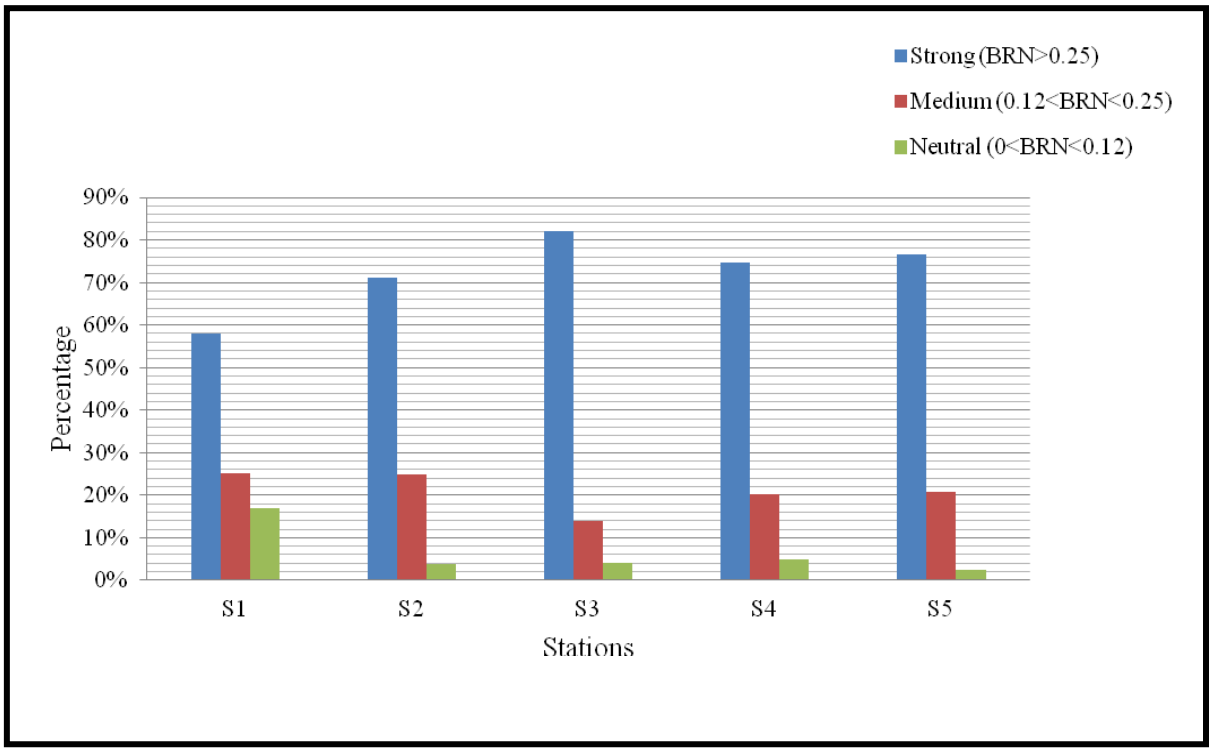

FIGURE 4.11: Spatial distribution of the bulk Richardson number.

4.3 Temporal Variation of Turbulent Momentum and Heat Fluxes and Obukhov Length

Fig. 4.12 depicts the time variation of turbulent momentum flux in the range of $0 < u_* < 0.2$ (m/s). This small values of turbulent momentum fluxes dominate around 15-18 and 18-21 hours then decreases as night progresses reaching their minimum values at 6-15 hours

Temporal variations of turbulent momentum fluxes in the range of $0.2 < u_* < 0.4$ (m/s) are presented in Fig. 4.13. Similar temporal distribution as in Fig. 4.12 is observed for turbulent momentum fluxes in the range of $0.2 < u_* < 0.4$ (m/s).

Temporal variation of turbulent heat fluxes in the range of $0 < \theta_* < 0.2$, $0.2 < \theta_* < 0.4$ $0.4 < \theta_* < 0.6$, and $0.6 < \theta_* < 0.8$ are presented in Fig. 4.14, 4.15, 4.16 and 4.17 respectively.

Similar temporal distribution is observed with turbulent heat fluxes dominates at 15-18 and 18-21 hours.

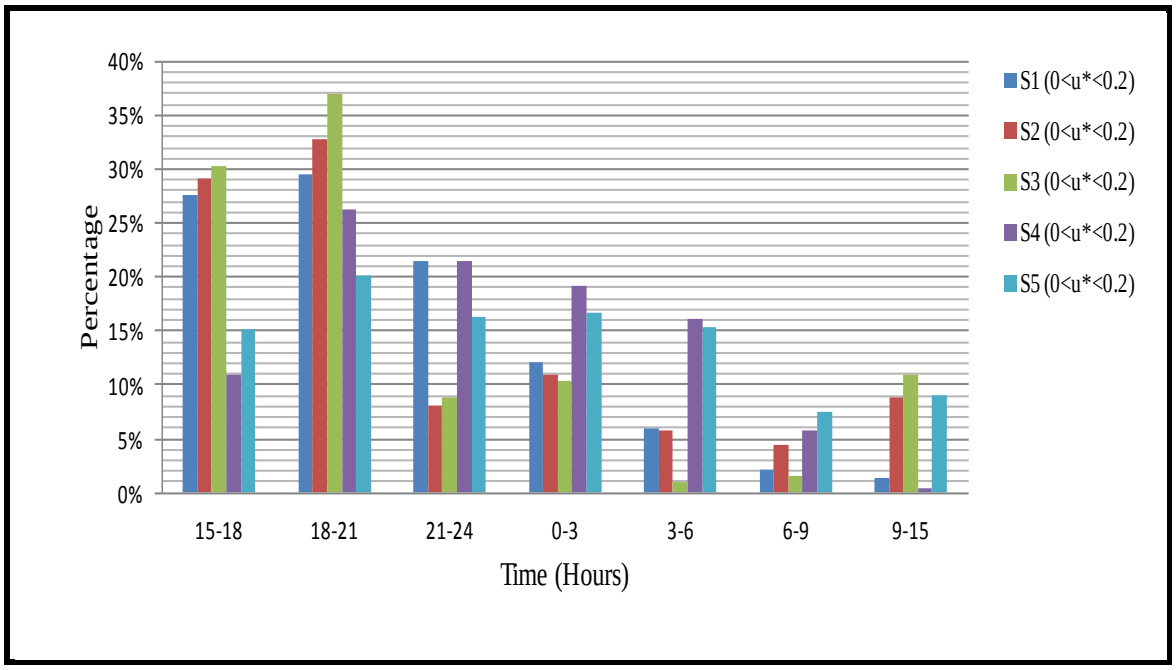

FIGURE 4.12: Temporal variation of the turbulent momentum fluxes in the range of $0 < u_* < 0.2$.

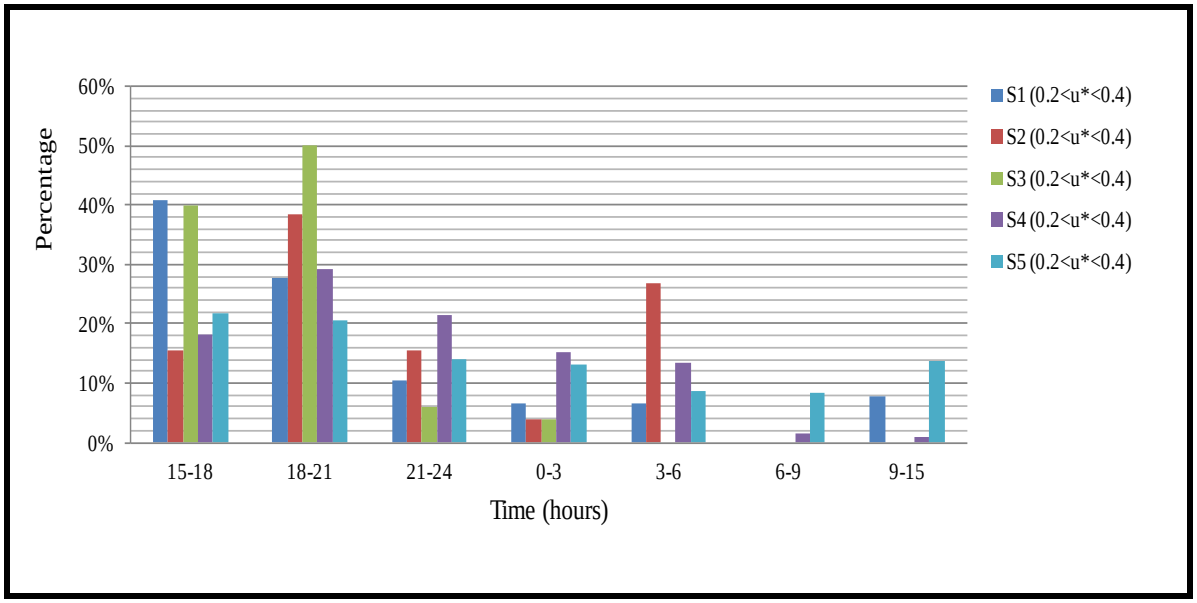

FIGURE 4.13: Temporal variation of the turbulent momentum fluxes in the range of $0.2 < u_* < 0.4$.

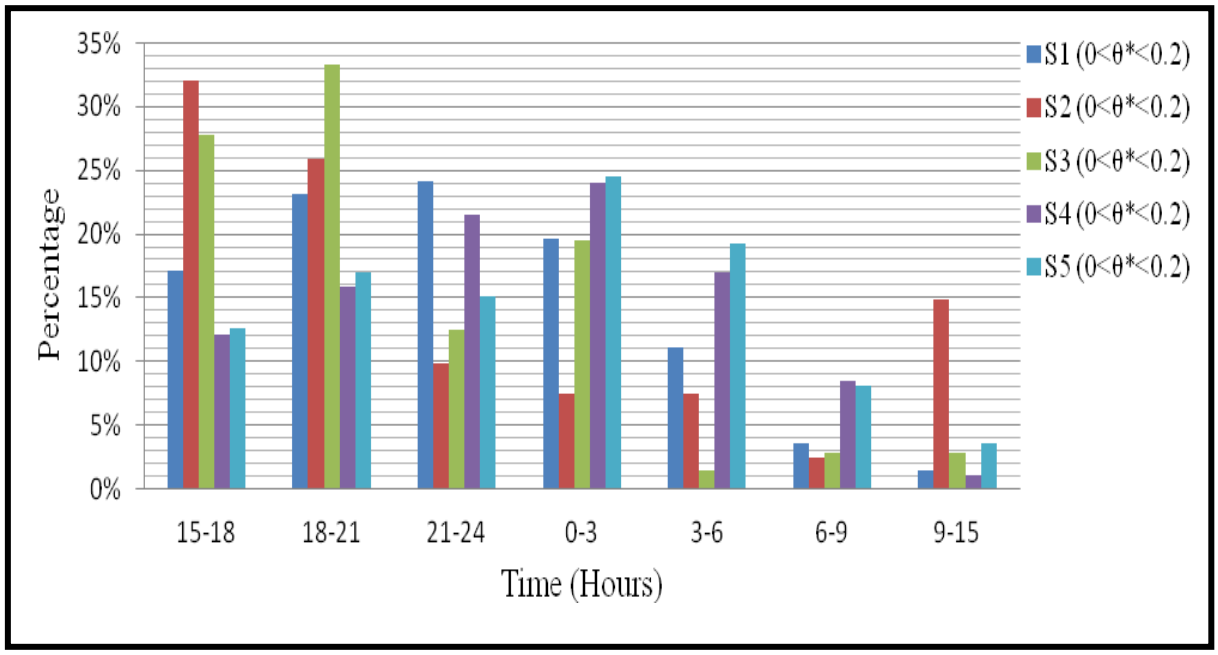

FIGURE 4.14: Temporal variation of the turbulent heat fluxes in the range of $0 < \theta_* < 0.2$.

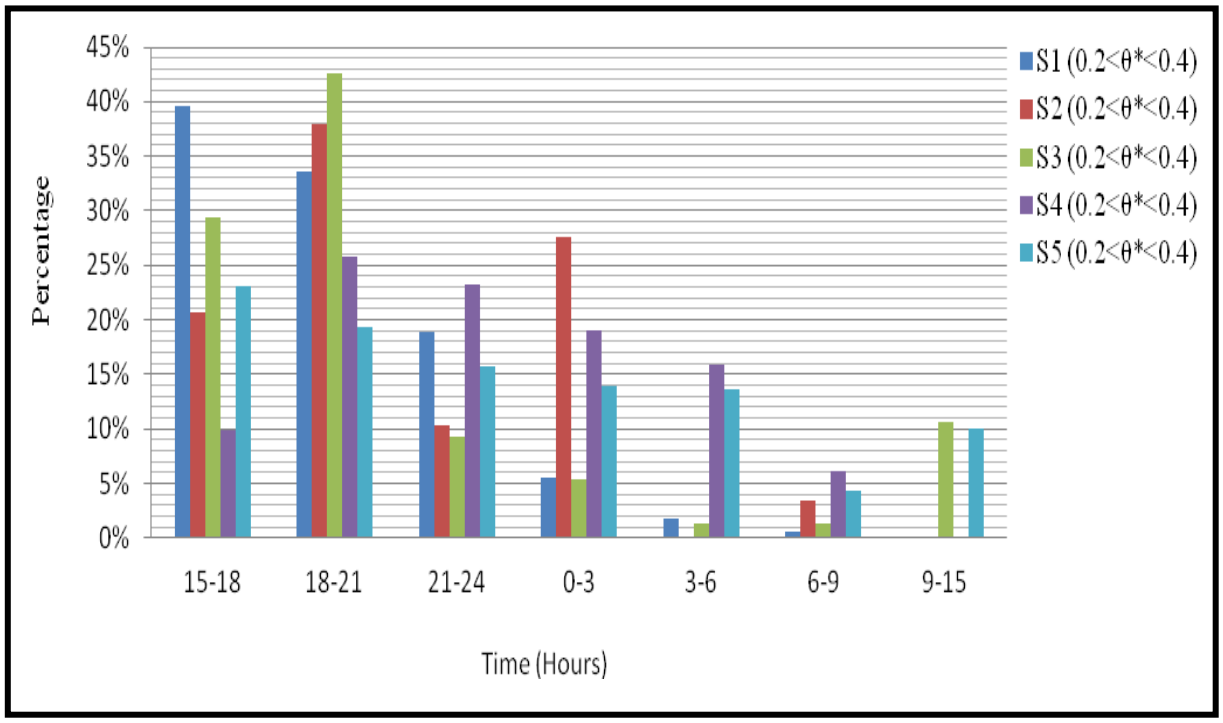

FIGURE 4.15: Temporal variation of the turbulent heat fluxes in the range of $0.2 < \theta_* < 0.4$.

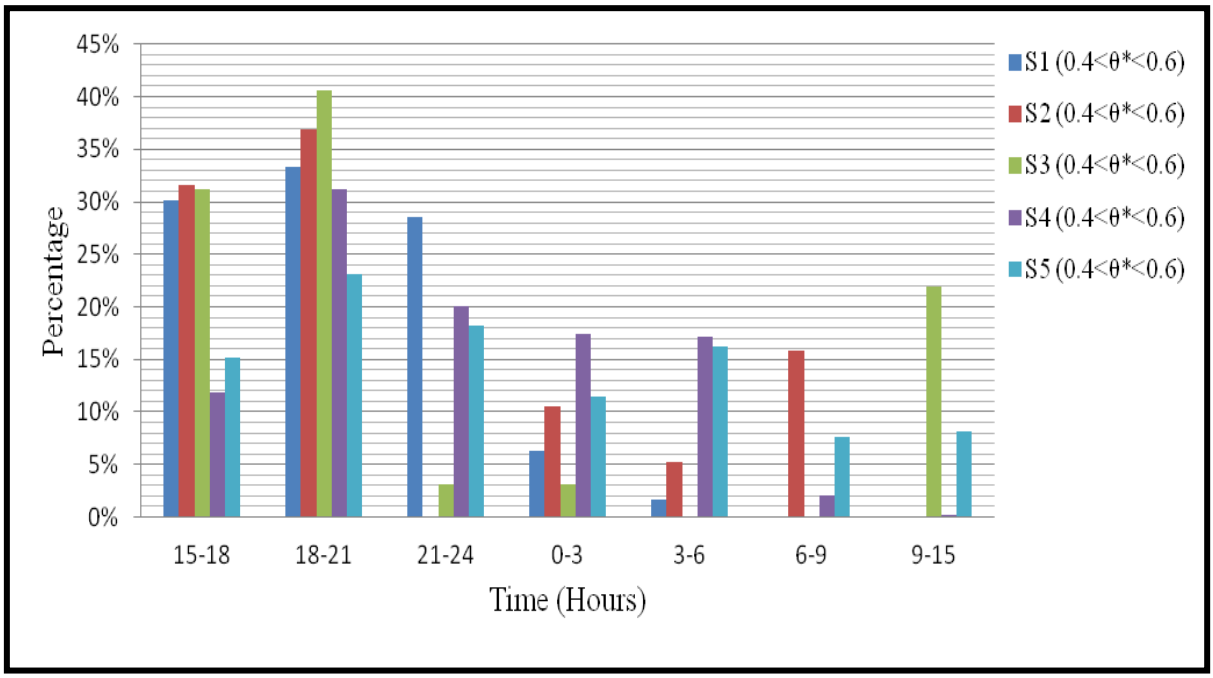

FIGURE 4.16: Temporal variation of the turbulent heat fluxes in the range of $0.4 < \theta_* < 0.6$

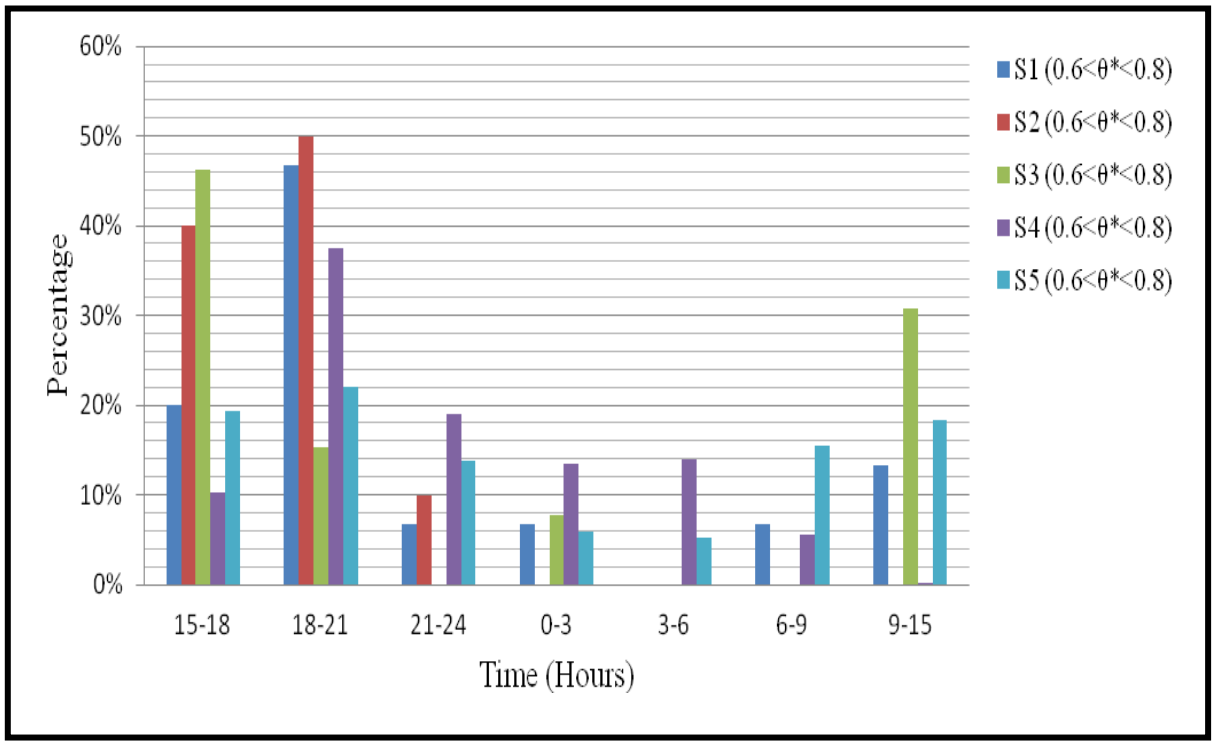

FIGURE 4.17: Temporal variation of the turbulent heat fluxes in the range of $0.6 < \theta_* < 0.8$

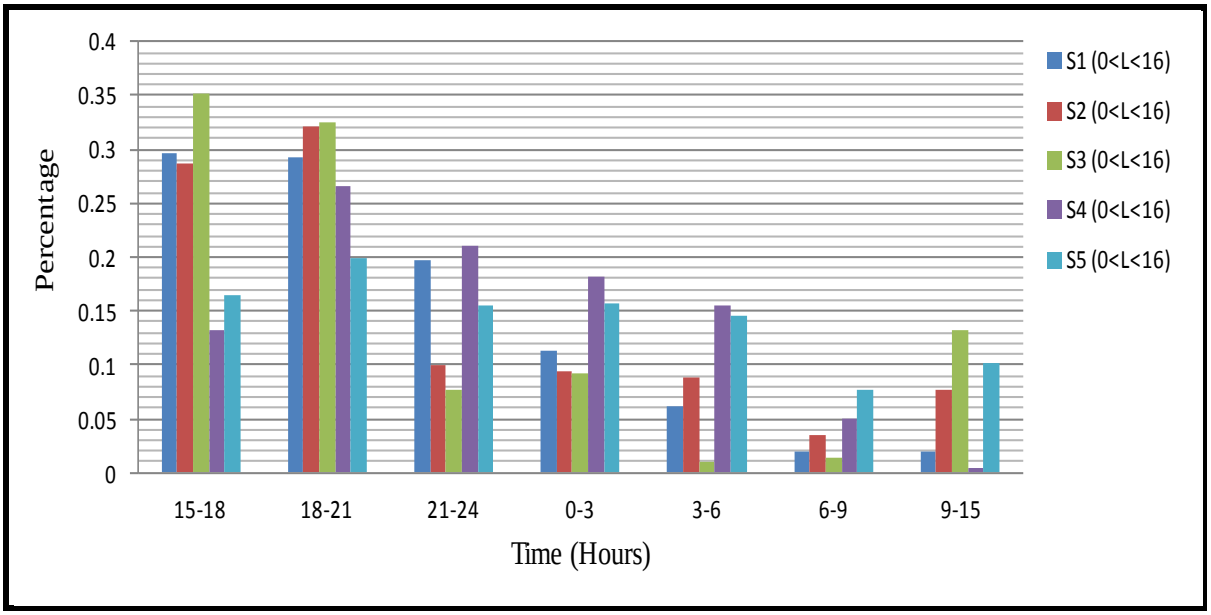

FIGURE 4.18: Temporal variation of the Obukhov length.

Fig. 4.18 indicates temporal of stability regimes as presented by the Obukhov length. This figure indicates that the strong stability regime dominate at 15-18 and 18-21 hours. The results presented in section 4.1 for the stable boundary layer height and in 4.2 to 4.3 for the spatial distributions and temporal evolutions of momentum, heat fluxes and the stability regimes as presented by both BRN and L are important for numbers of practical applications. These results can be used by numerical, dispersion and weather prediction models to use realistic values for the turbulent fluxes within the industrial areas over the Highveld. It is important to mention here that, the low values of turbulent momentum fluxes which are dominant roughly 77-88% is indicative that the mechanical contribution to SBL turbulence generation in the surface layer is minimal. Also the observed values of turbulent heat fluxes and Obukhov length strongly indicates a high probability of occurrence of air pollution episodes over Highveld region for emission from low sources since the dispersion effects by the mean wind flow is very limited. These results also can be used to validate other remote sensing equipments, for example boundary layer flux measurements from aircraft, LiDAR detection of BL height where the BL height can be calculated using momentum fluxes (Venkaraman, 1980) and used to validate LiDAR measurements.

4.4 Links between Spatial and Temporal Variability of the Meteorological Variables and Existing Land use Patterns

In this dissertation, the described methods of the spatial scale and RMS analyses mutually, complement each other. The former selects horizontal scale of optimal land use-atmosphere coupling and the latter show change of coupling strength within a typical diurnal cycle and for winter and summer seasons.

The results of the spatial scale analysis as implemented to the available data sets of the winter and summer seasons are shown in (Fig. 4.19 – 4.20). Previously published works (Patton et al., 2005; Esau, 2007 and Robinson et al., 2008) suggested that the horizontal flux given in Eq. 3.3 should be enhanced on spatial scales of 5 – 30 km in the case of the ABL development over a homogeneous surface. At the same time, Fig. 4.21 revealed that the typical range of the NDVI variability over Highveld is 7 – 20 km. Thus, the range of scales of the expected resonant response in the ABL dynamics partially overlaps with the range of scales of the observed surface morphology variations over Highveld. In winter season, certain enhancement of $\overline{U'T'}$ (Fig. 4.19b) and $\overline{U'R'}$ (Fig. 4.20b) was found within the range scales of 30 – 50 km. Although the number of data sets in the constructed ensembles is small (5 for MMEH and DEA data sets and 10 for composite ensemble), the flux enhancement in this range of scales is rather consistent and as large as 0.5 of the maximum normalized flux magnitude. In summer season, flux enhancement is less pronounced and shifted to larger scales 40 – 60 km (Fig. 4.19a and Fig. 4.20a). This range of scales seems to be unrelated to the NDVI surface heterogeneity (Fig.4.21). This figure indicates the spectral energy normalized for each band. The bold line represents the spectrum of the total pixel brightness. The normalized spectra for the bands 2, 3, 5 and 7 of the satellite image revealed maximum variability on scales of 5 – 10 km. The normalized brightness spectrum in band 4 reveals the maximum variability on scales (10 – 20 km), whereas the spectrum in band 1 reveals the maximum on much smaller sub-kilometer scales. The maximums variability on scales of 5 – 20 km is easily associated with the visual variability of the land use type in the studied area

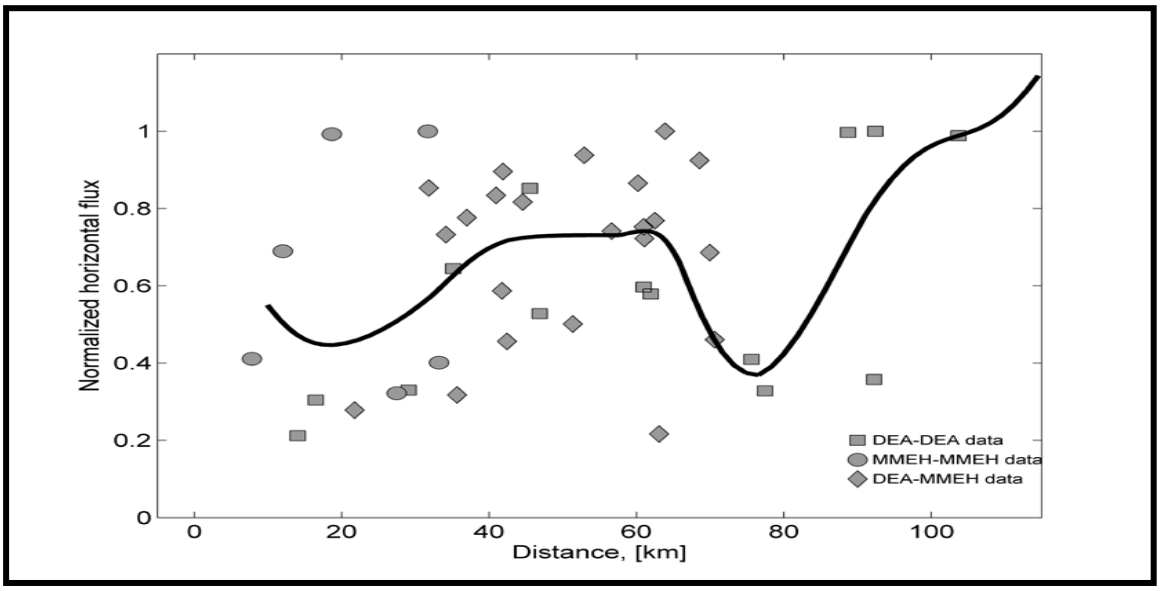

(a)

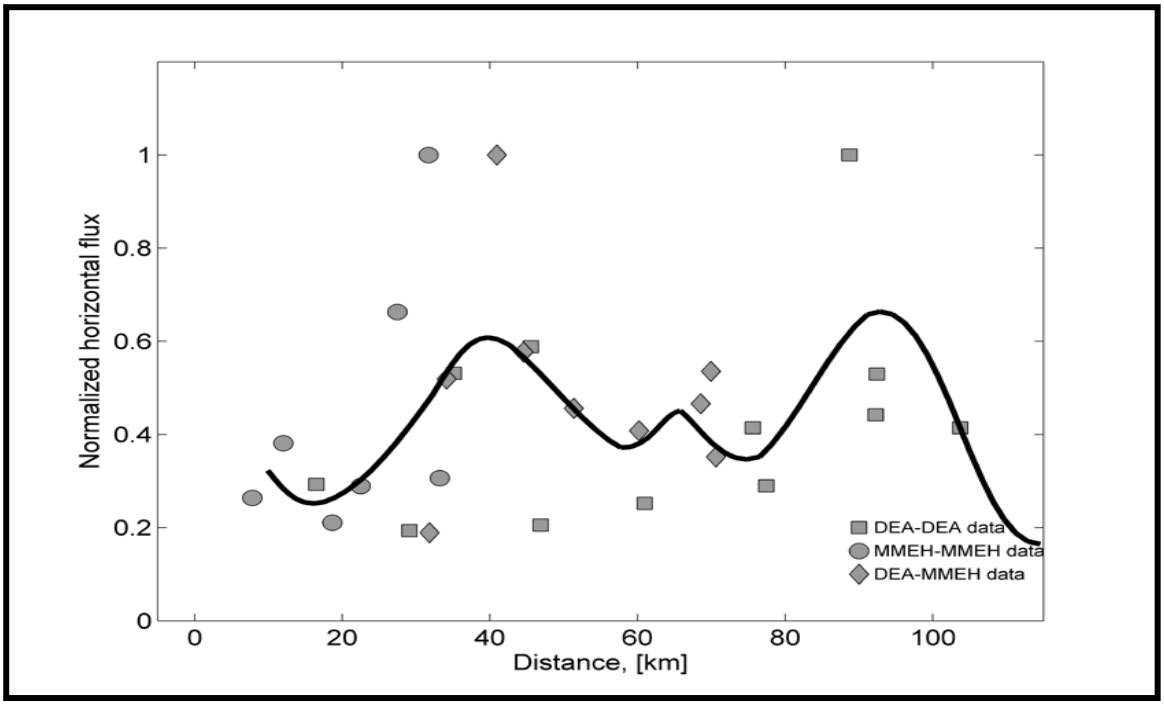

(b)

FIGURE 4.19: Variation of the normalized horizontal temperature flux $\overline{U'T'}$ (a, b) obtained through Eq. 3.3 with the distance between stations. The squares show fluxes obtained for the DEA data set; the circles for the MMEH data set; diamonds for the mixed DEA (one station) – MMEH (another station) data set. The bin-averaged dependence is shown by the black curve. Panel (a) show the variation during the austral summer and panels (b) show variation during the austral winter.

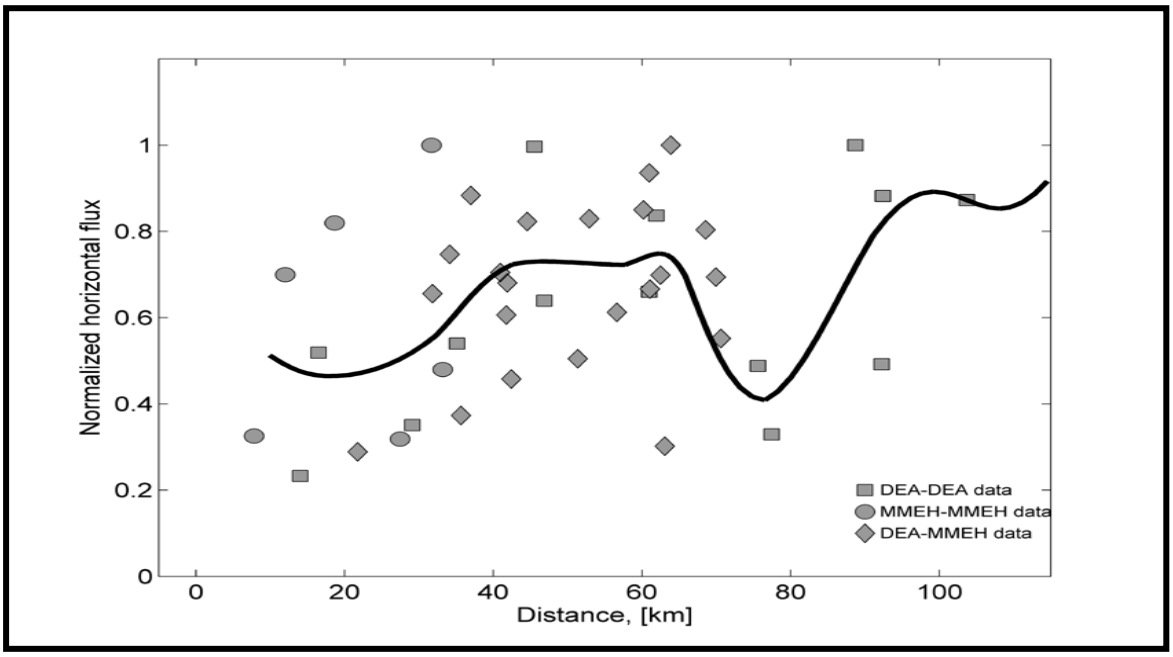

(a)

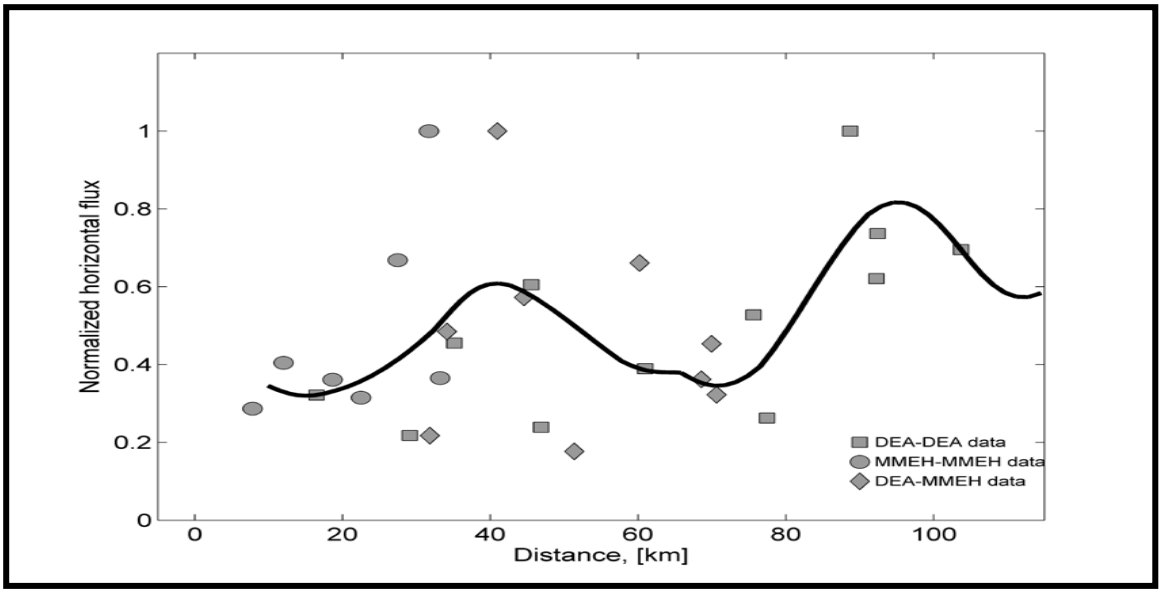

(b)

FIGURE 4.20: Variation of the normalized horizontal relative humidity flux $\overline{U'R'}$ (a, b) obtained through Eq. 3.3 with the distance between stations. The squares show fluxes obtained for the DEA data set; the circles for the MMEH data set; diamonds for the mixed DEA (one station) – MMEH (another station) data set. The bin-averaged dependence is shown by the black curve. Panel (a) show the variation during the austral summer and panel (b) show variation during the austral winter

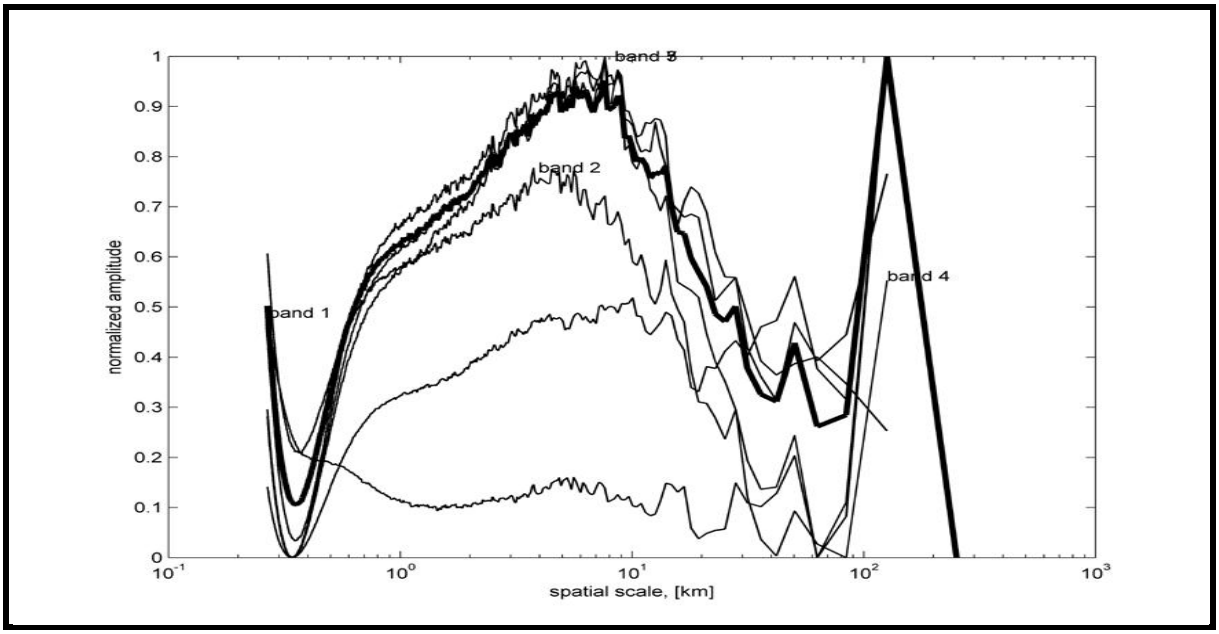

FIGURE 4.21: The spatial spectra of pixel brightness variability for the bands 2, 3, 5 and 7.

The diurnal cycles of the winter and summer RMS values are shown in (Fig. 4.22– 4.25). The common picture of the developing daytime convection (e.g. Zilitinkevich et al., 2006) predicts breakdown of the nocturnal inversions, which prevent mixing of the near-surface air both vertically and horizontally, and development of a deep, well-mixed convective layer, which is well mixed in the core but still may have some local dependences within the layer of super-adiabatic gradients near the surface. The atmospheric convection is however self-organized. Although on the horizontal scales up to the scale of the convective cell, the near surface air is well-mixed, there could be considerable deference between cells (Esau and Lyons, 2002; Junkermann et al., 2009) that is determined by the land surface heterogeneity on larger scales. The growth of a convective cell, observed in the course of the day, results in successive mixing of heterogeneities of increasingly larger scales. Thus, the RMS analysis may reveal enhancement of convection on certain scales when the turbulence (or meso-scale circulations) in the convective cells stronger coupled to the surface. This coupling will occur at certain hours of LST as the horizontal scales are increasing as $L \propto t^{1/2}$. In this dissertation the results for the ensemble composed of all stations in the MMEH and DEA data sets are presented.

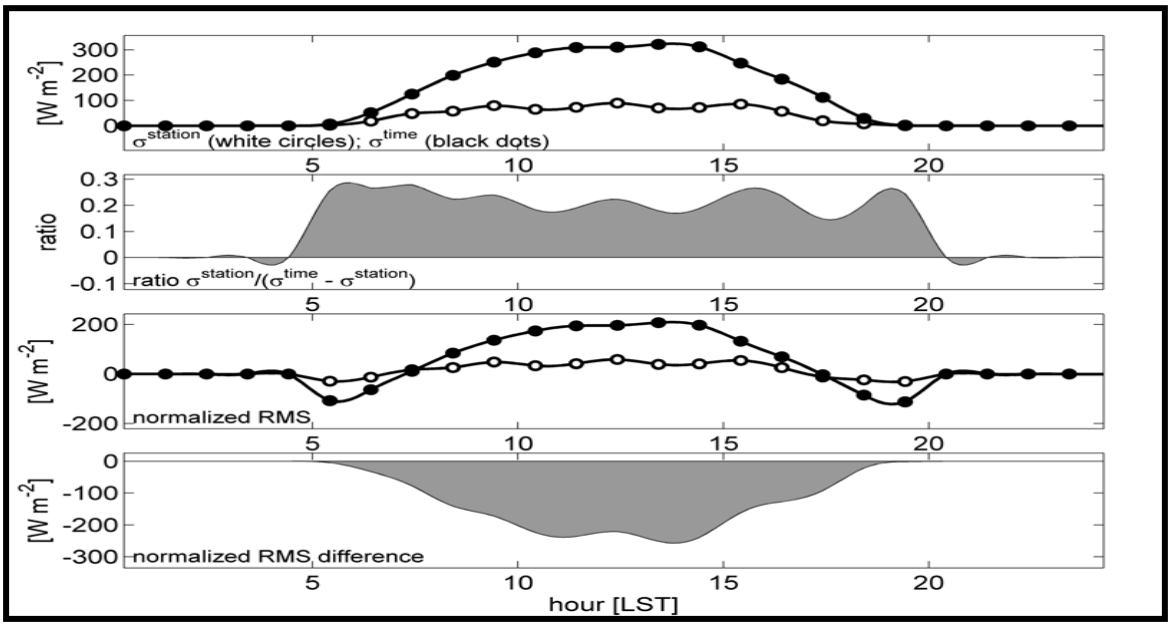

(a)

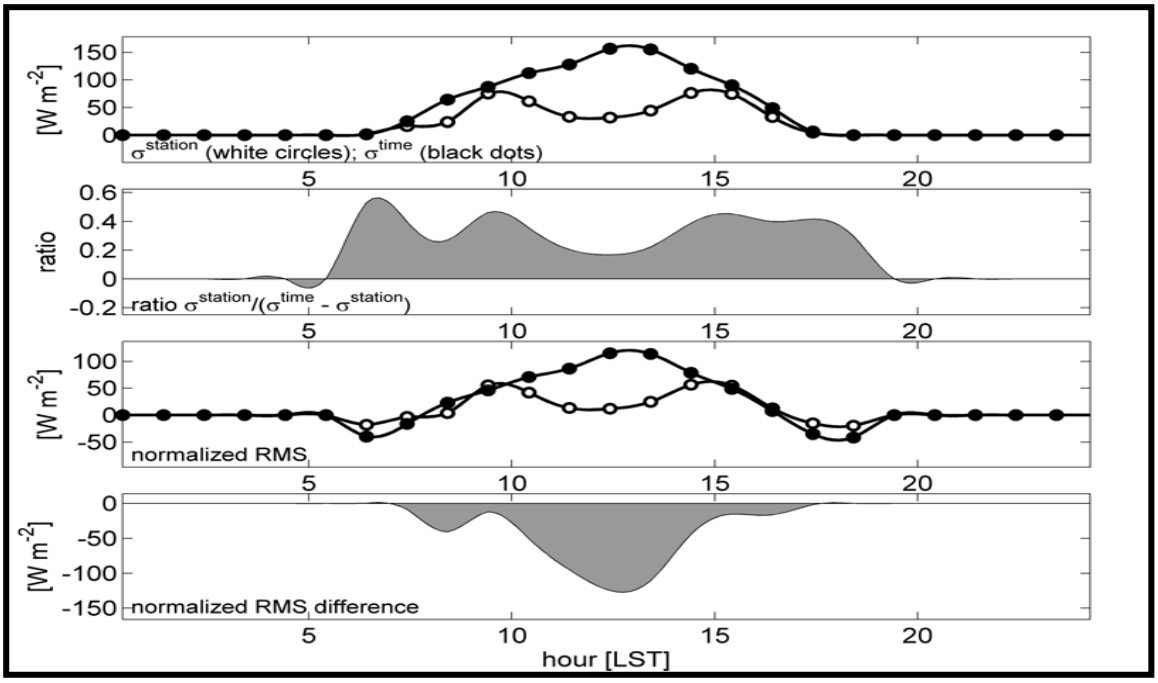

(b)

FIGURE 4.22: Diurnal evolution of: the RMS values for incoming short wave solar radiation, σ_s^{time} (black dots) after Eq. 3.4 and $\sigma_s^{station}$ (white circles) after Eq. 3.5; the ratio of variability *R S* after Eq. 3.7; the normalized RMS values $\sigma_s^{time} - \sigma_s^{time}$ (black dots) and $\sigma_s^{station} - \sigma_s^{station}$ (white circles); and their difference *D S* after Eq. 3.8. Panel (a) present the diurnal cycle for austral summer; (b) – for austral winter

Diurnal variability of the incoming solar radiation is given in Fig. 4.22. This figure is useful to test the proposed interpretation of the RMS analysis as the diurnal course of the incoming solar radiation is well-known. The solar radiation RMS is defined by the presence of clouds with horizontal scales smaller than the distance between stations. The clouds can help to detect the size of the convective cells but in dry atmosphere, the convection may not create them. At sunset and sunrise, the solar radiation RMS will be also defined by the local surface properties such as trees, houses and the orientation of the terrain slope. Fig. 4.22 suggests that in summer, the local surface properties and clouds have little effect on the RMS as the cloud clusters would typically occupy the whole Highveld region (Bethal region) area. In winter, the effect is more pronounced, indicating smaller size of clouds and longer periods with low sun angles.

Fig. 4.23 – 4.25 shows the RMS analysis of the surface air temperature, relative humidity and the wind speed. The most interesting transition occurs during the winter season. The local regime dominated by the internal variability is identified during night and morning time. The internal variability is about 55% – 65% of the sum of RMS in this regime with the average difference between stations reaching 3^0C in temperature, 10% in the relative humidity and only 0.2 m s^{-1} in wind speed. These numbers clearly identify the expected effect of the stable stratification and reduced horizontal mixing. The wind speed RMS reaches its maximum during the afternoon hours (16 LST). This maximum can be interpreted as the time when the horizontal size of the convective cells reached the resonance interval of scales. It means that the turbulent convection is enhanced by the meso scale land breeze motions generated by the heterogeneity of the land use types. This enhancement raises the ABL height locally above the lifted condensation level, which results in cloud development. This interpretation is consistent with Fig. 4.22, as clouds increase the incoming solar radiation RMS, and with Fig. 4.24, as no particular feature in the relative humidity RMS is found. The summer season is characterized by much smaller internal variability so the ratio $R_u(n) = \dfrac{\sigma_u^{station}(n)}{\sigma_u^{station}(n) + \sigma_u^{time}(n)}$ drops to 35% – 45%. The wind speed RMS difference reaches its maximum in the late morning hours (10 LST) and then significantly reduces. Taken in account that the summertime ABL is deeper and develops faster, this time shift of the wind speed RMS maximum can be interpreted as the

discussed enhancement of the turbulent convection, which was observed at 16 LST in wintertime. The following further growth of the ABL destroys the resonance between the turbulent and local circulations. It leads to smaller wind speed RMS.

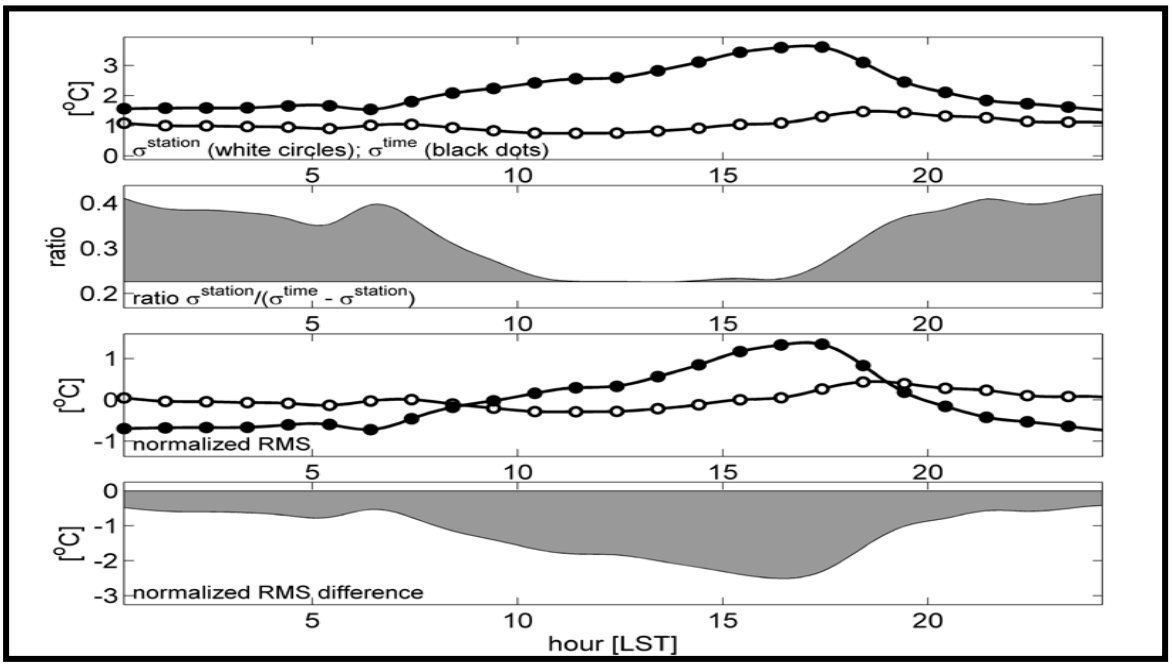

(a)

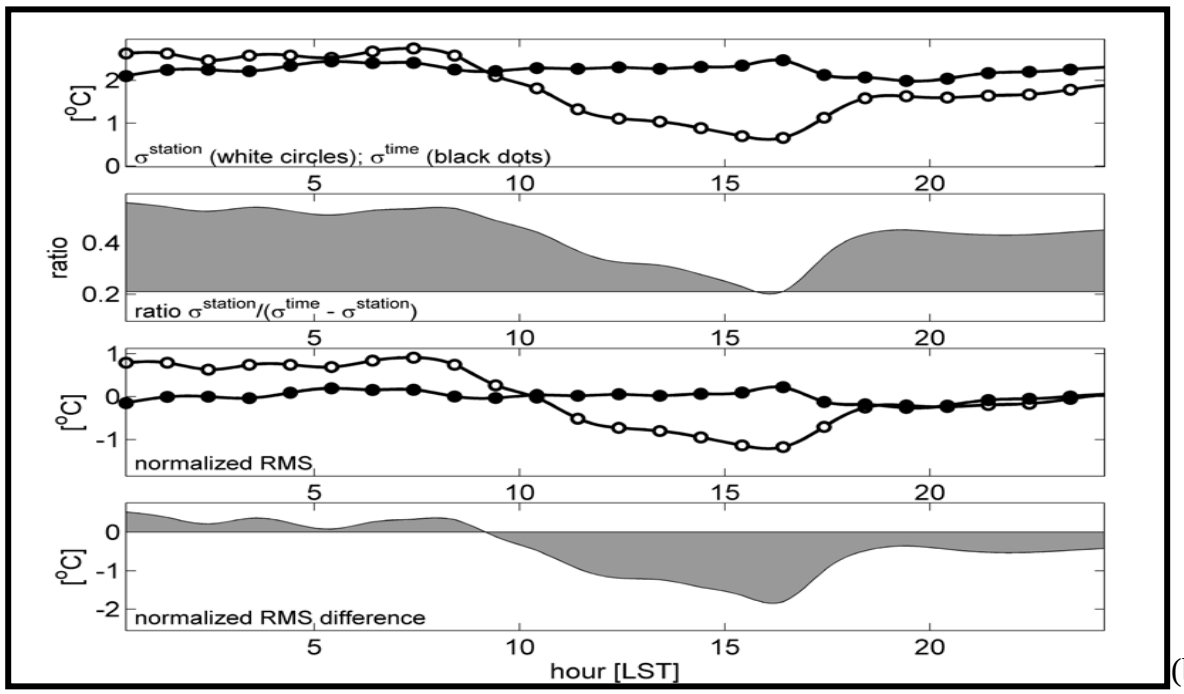

(b)

FIGURE 4.23: The same as in Figure 4.22 but for the RMS of surface air temperature.

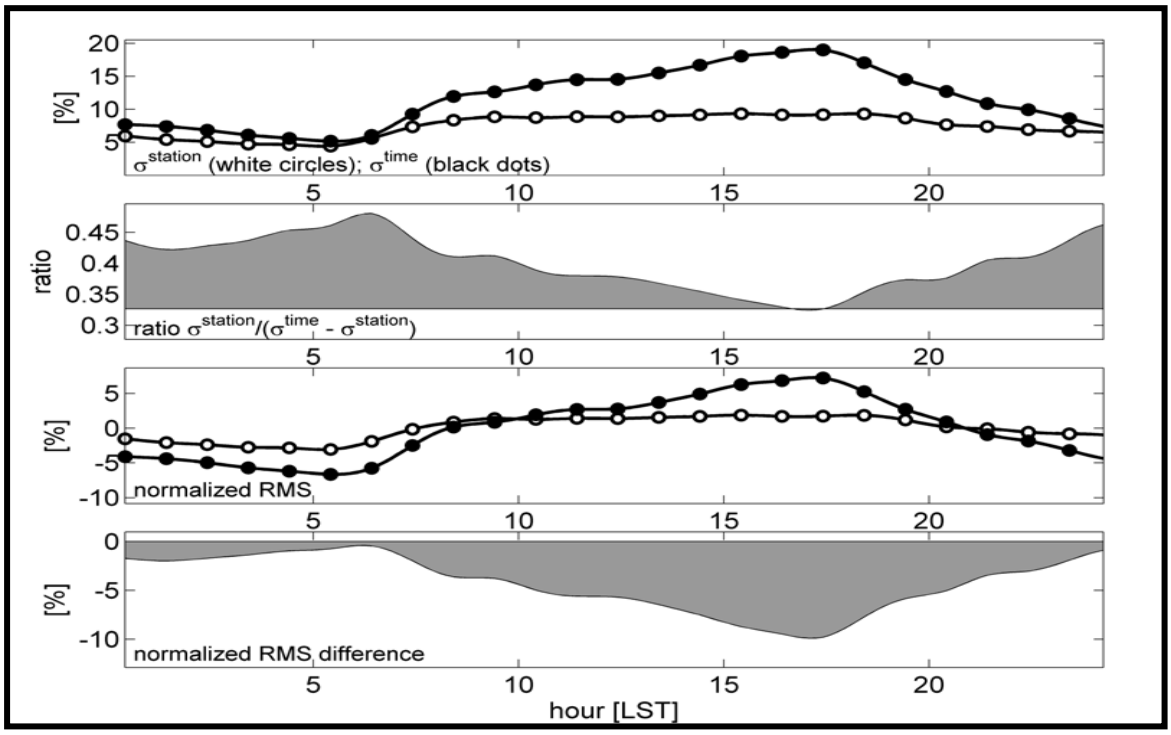

(a)

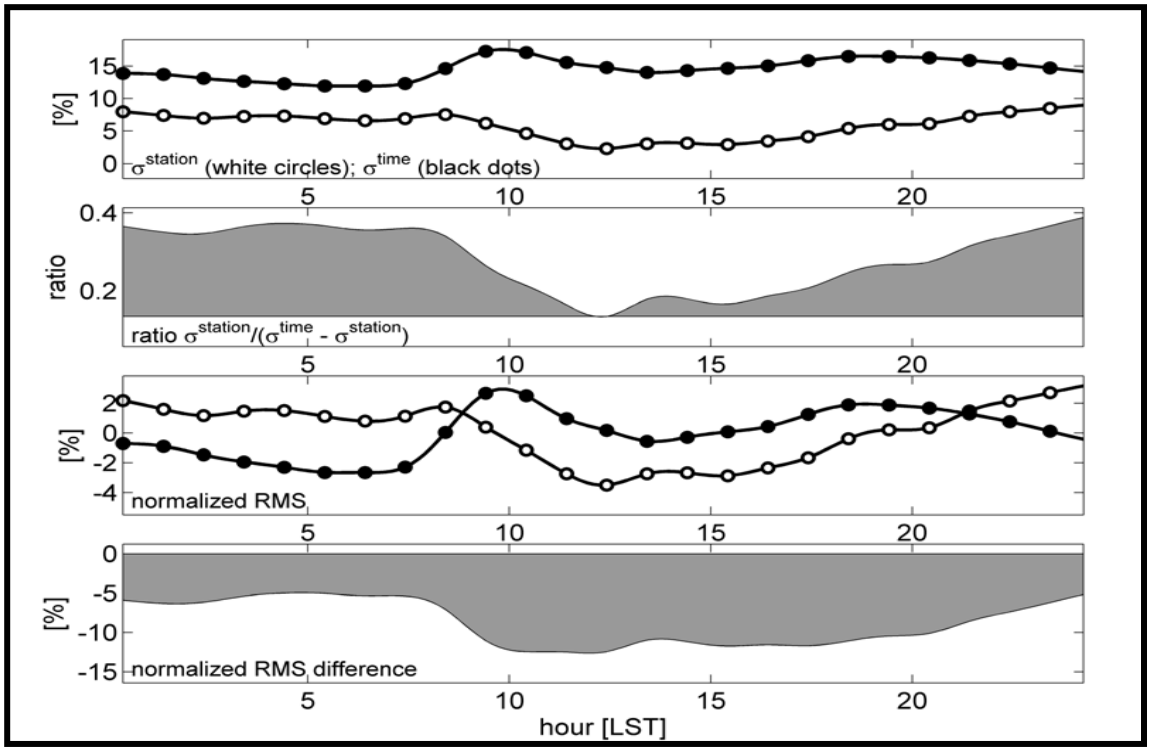

(b)

FIGURE 4.24: The same as in Figure 4.22 but for the RMS of the relative humidity.

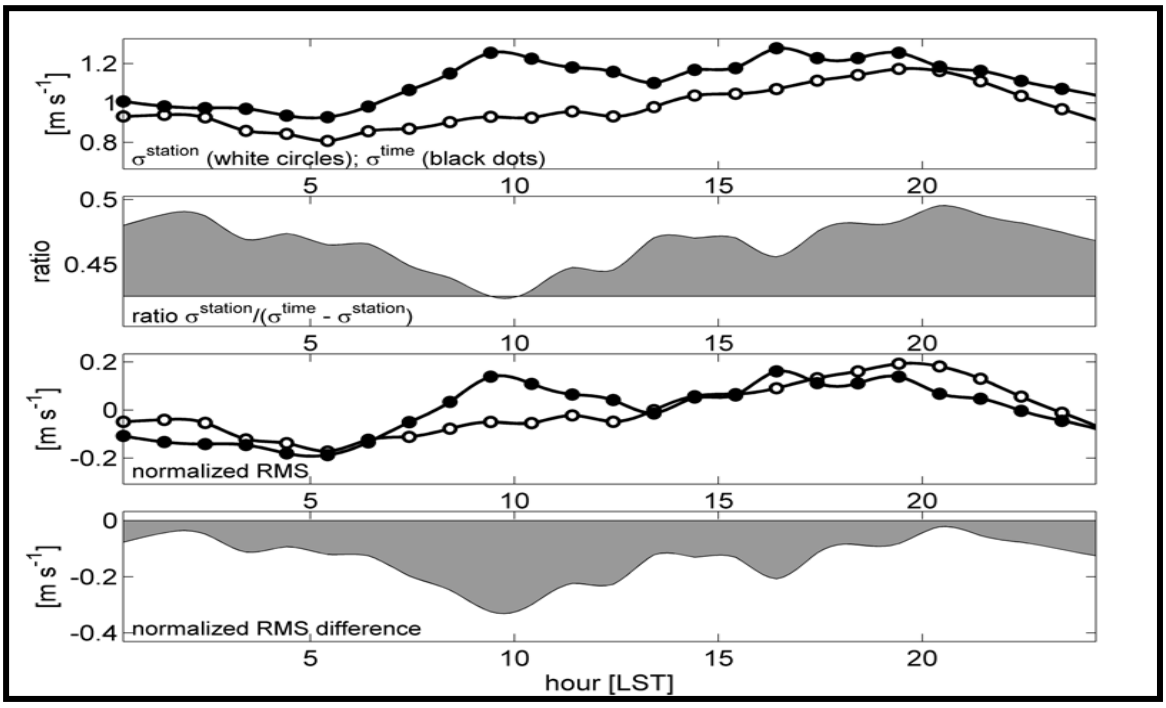

(a)

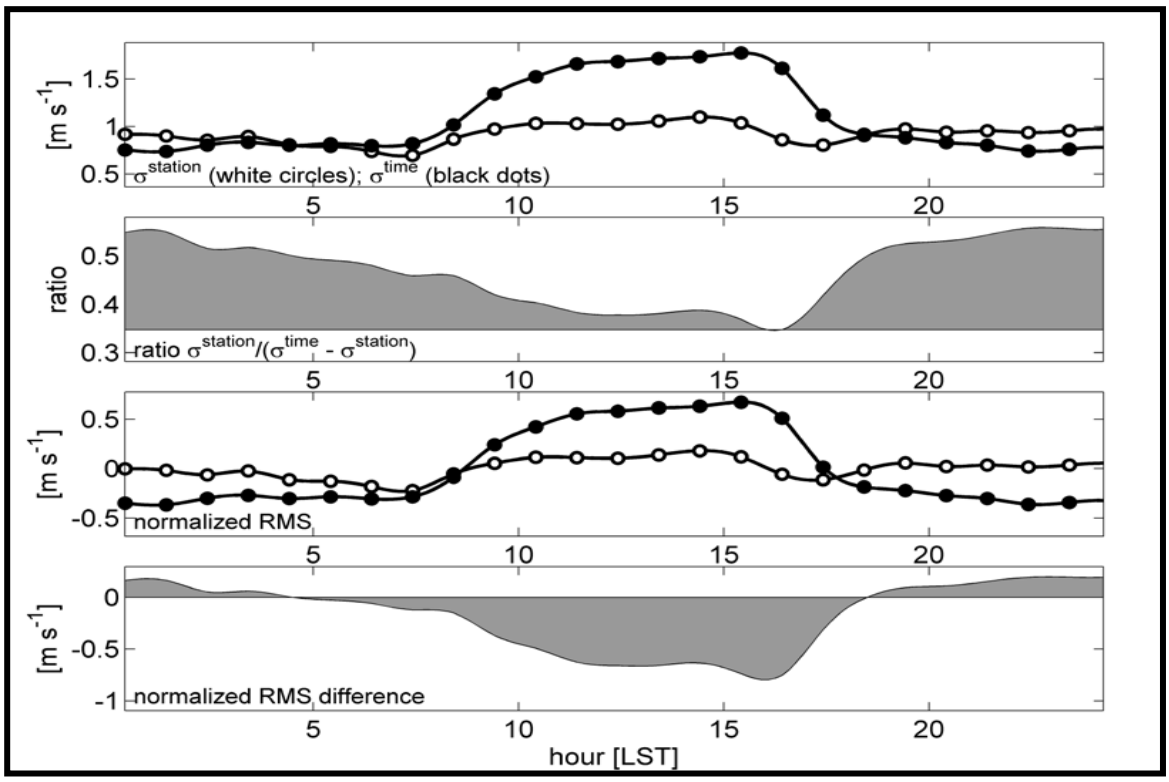

(b)

FIGURE 4.25: The same as in Figure 4.22 but for the RMS of the wind speed.

Results presented in section 4.4 consider dissimilarity of temporal variations in the ensemble members. With respect to the spatial scale analysis, one can observe that the scattered data have the maximum (minimum) of the horizontal flux within the same range of scales for each data set as well as their blending. Although it is difficult to quantify the degree of enhancement of the atmospheric motions in the ABL, it is likely that scales of the enhancement were indentified correctly and that the enhancement itself is not a statistical artifact. The result on enhancement of variability has been interpreted as strengthening of the turbulent convection by the meso-scale breeze motions. Another physically plausible cause of enhancement could be linked to the cloud system development. According to Blamey and Reason (2012), the meso-scale convective storms developing in the Highveld region (Bethal) in the summer season have the initiation time 13–19 LST. It corresponds well to the afternoon maximums for the temperature σ_T^{time}, D_T and the similar maximums for the relative humidity. The wind speed RMS consistently increases with convection developing. The horizontal scale of storms was found to be 200 – 300 km, which covers the entire area of observations. Hence, the convective storms do not generate the internal variability in meteorological quantities with exception for the wind speed, which is affected by sub-cloud micro-fronts. This is different from the RMS behavior in wintertime when all quantities exhibit coherent fluctuations within the diurnal cycle.

CHAPTER 5

CONCLUSSION AND RECOMMENDATIONS

The main objective of this dissertation has been to study the ABL characteristics over Highveld Region South Africa. The specific objectives were to use appropriate method to calculate the SBL height using data from automated weather stations and mobile LiDAR technology and compare/validate with Radiosonde data. Other objectives were to identify different stability regimes available in SBL, to use the similarity theory approach to calculate turbulent fluxes of momentum, and heat and to test the hypothesis of links between spatial and temporal variability of the meteorological quantities and existing land use patterns.

The results obtained in this study suggest that the deduction of the SBL height using LiDAR provides unrealistic results. Strong signal LiDAR returns are observed at the high altitude (~ 1200 m-3000 m). This height does not reflect the actual height of the SBL but is the height of elevated absolutely stable layer. LiDAR results were validated using Radiosonde data from Irene station (25° 52' 8" S, 28° 12' 59" E) on 1.12.2010 at 02 am. The SBL height of 166 m was observed over Irene. This height is too shallow when compared with detected height of about 1250-3000 m over Elandsfontein ($26^0$2’ S, $29^0$4167’ E) at 02 am from LiDAR measurements. This concludes that LiDAR cannot measure accurately so close to the surface hence cannot detect the SBL height.

The fluxes of momentum, heat and Obukhov length are computed using the Monin-Obukhov similarity theory. The momentum and heat fluxes show no significant spatial variation between stations. Spatial distribution of stability regimes as presented by both BRN and L indicates that the dominant stability regime over Highveld is the strong regime. This is indicated by the small values of Obukhov length accounting to 100% and BRN greater than critical value 0.25 accounting to 82%. Other than L and BRN values, small values of momentum and heat fluxes indicate the presence of strong stability regime. This indicates a high probability of occurrence of air pollution episodes over Highveld region for emission from low sources since the dispersion effects by the mean wind flow is very limited.

To understand the general dynamics of the SBL in different time, average diurnal distribution of momentum and heat fluxes and Obukhov length were studied. Results suggest that large percent of momentum and heat fluxes occur around 15-18 and 18-21 hours then decreases as night progresses reaching their minimum values at 6-15 hours.

The statistical analysis of the prepared ensemble obtained from automatic weather station data sets was aimed at investigating variability of meteorological variables at different time and spatial scales. The analysis was seeking for enhancement of the ABL dynamics by the meso-scale circulations. Such an enhancement was found in the data on scales of 30 – 50 km (winter seasons) and 40 – 60 km (summer seasons). These scales are somewhat larger than the scales of surface heterogeneity visually identified on the NDVI Landsat images. Hence, the enhancement links to the surface heterogeneity were identified qualitatively but their quantification requires high resolution numerical model study. The strongest evidence of the land use – atmosphere resonant coupling at certain scales is derived from the diurnal evolution of the RMS transition from internal (local) to externally forced variability regimes. The results suggest that the nocturnal and especially wintertime variability are shaped by the local surface properties. Developing of deeper convective ABL homogenize the internal variability forcing synchronous variations of the meteorological quantities across the stations. When the growing convective cell increases in size to the scale of the meso-scale circulations, a kind of resonance interaction between the convective and meso-scale motions occurs that enhance the horizontal fluxes. The interactions between the surface layer atmospheric dynamics and the land use heterogeneity is a strongly non-linear and complex process. This is one of the reasons why these interactions are not satisfactory included in the meteorological models. The results of this study provide a solid observational material for further model development as well as for more accurate interpretation of the regional climate change. A more applied utility of the analysis is seen in optimization of the land use, calibration of satellite remote sensing data and climate adaptation studies.

REFERENCES

AMS, 2000: *Glossary of Meteorology*, American Meteorological Society, First Edition, USA.

Baas, P., 2009: Turbulence and Low-Level Jets in the Stable Boundary Layer, PhD thesis at Wageningen University, Wageningen, Netherland:

http://edepot.wur.nl/12194.

Banta, R.M., 2008: Stable-boundary-layer regimes from the perspective of the low-level jet. *Acta Geophysica***,** 56, 58-87.

Becker, S., 2005: Thermal structure of the atmospheric boundary layer over the South African Mpumalanga Highveld. *Clim. Res.*, **29**, 129–137.

Blamey, R.C., and C.J.C. Reason, 2012: Mesoscale convective complexes over Southern Africa, *J. Climate*, **25**, 753-766.

Bloch, A. L., 2002: Evaluation of daytime Boundary Layer Heights from a Mesoscale Model using Profilers/rass measurements, dissertation at Naval postgraduate school, Naval postgraduate school, California:

http://www.dtic.mil/cgi-bin/GetTRDoc?AD=ADA479824.pdf.

Bretherton, C., 2011: Lecture 5. The logarithmic sub layer and surface roughness, University of Washington, Washington, breth@atmos.washington.edu:

http://www.atmos.washington.edu/academics/classes/2011Q1/547/lect5.pdf.

Businger, J. A., J.C. Wyngaard, Y . Uzumi, and E.F. Bradley, 1971: Flux-profile relationship in the atmospheric surface layer. *J. Atm. Sci*., 28, 181-189.

Chimonas, G., 2001: On internal gravity waves associated with the stable boundary layer. *Boundary Layer Meteorology*, 102:139-155.

Collett, K.S., S.J. Piketh, and K.E. Ross, 2010: An assessment of the atmospheric nitrogen budget on the South African Highveld. *South African J. of Sci.*, 106(5-6), 1 – 9.

Cuxart,J., C.Yague, G. Morales, E. Terradellas, J. Orbe, J. Calvo, A. Fernandez, M.R. Soler, C. Infante, P. Buenestado, A. Espinalt, H.E. Joergensen, J.M. Rees, J. Vila, J.M. Redondo, I.R. Cantalapiedra, and L.Conangla, 2000: Stable Atmospheric boundary layer experiment in Spain (SABLES 98). *Boundary layer Meteorology*, 96, 337-370.

Derbyshire, S. H., 1990: Stable boundary layer revisited. *Quart. J. Roy. Meteor. Soc*., 116, 127–158.

Duynkerke, P.G., 1991: Radiation fog: a comparison of model simulations with detailed observations. *Mon. Wea. Rev*., **119**, 324-341.

Esau, I., 2007: Amplification of turbulent exchange over wide Arctic leads: Large-eddy simulation study. *J. Geophys.l Res.*, **112**, D08109, doi:10.1029/2006JD007225

Esau, I., and T.J. Lyons, 2002: Effect of sharp vegetation boundary on the convective atmospheric boundary layer. *Agricult. Forest Meteorol.*, **114**(1-2), 3-13

Esau, I.N., Zilitinkevich, S.S., Djolov, G.D and J. deW. C. Rautenbach, 2010: A micro-meteorological experiment in the atmospheric boundary layer in Highveld region, IOP Conf. Series: Earth and Environmental Science 13 (2010) 012012 doi:10.1088/1755-1315/13/1/012012

Fiocco, G., and L.D. Smullin, 1963: Detection of scattering layers in the upper atmosphere (60-140 km) by optical radar. *Nature*, **199**, 1275-1276.

Freiman, M.T., and P.D. Tyson, 2000: The thermodynamic structure of the atmosphere over South Africa: Implications for water vapour transport. *Water SA*, 26(2), 152-158

Freiman, M.T., and S.J. Piketh, 2003: Air transport into and out of the industrial Highveld region in South Africa. *J. Applied Meteorol.*, 42, 994 – 1005

Garratt, J.R., 1992: The atmospheric boundary layer, Cambridge university press, New York.

Giles, J., 2005: Climate science: The dustiest place on Earth. *Nature*, 434, 816-819.

Held, G., H.Scheifinger, G.M. Snyman, G.R. Tosen, and M. Zunckel, 1996: The climatology and meteorology of the Highveld. *Environmental Scientific Association, Cleveland*, 144 pp.

Held, G.,1996: Wind and temperature profiles in the boundary layer above the Kruger National Park during SAFARI-92. *J. Geophys. Res.,* 101*(*D19*),* 23737–23743, *doi:*10.1029/95JD02274.

Hooper, W. P., and E. W. Eloranta,1986: Lidar measurements of wind in the planetary boundary layer: the method, accuracy and results from joint measurements with radiosonde and Kytoon. *J. Climate Appl. Meteorol*. 25, 990-1001.

Horlacher, V., S. Osborne, and J.D. Price, 2012: Comparison of two closely located meteorological measurement sites and consequences for their areal representability. *Boundary-Layer Meteorol*, **142**, 469-493

Izumi, Y., and J.S. Caughey, 1976: Minnesota 1973 Atmospheric boundary Layer Experiment Data Report. *Environmental research papers*, No 547, Air Force Cambridge Research Lab., Bedford, USA, 79p.

Jiménez, M.A., 2005: Stably stratified atmospheric boundary layer: study through large-eddy simulations, mesoscale modelling and observations, PhD thesis from Universitat de les Illes Balears (UIB), Universitat de les Illes Balears, Spain:

http://www.tesisenred.net/bitstream/handle/10803/9433/tmajc.pdf?sequence=1.

Jiménez, M.A., and J. Cuxart, 2005: Large-eddy Simulations of the Stable Boundary Layer: study of applicability using experimental data. *Boundary- Layer Meteorology*, 115, 241-261.

Julie, A.P., 2008: Bursting Events in the Stable Atmospheric Boundary Layer, MSc thesis at Texas Tech University, Texas Tech University, Texas:

http://thinktech.lib.ttu.edu/ttuir/bitstream/handle/2346/12200/Phillipson_Julie_Thesis.pdf?sequence=1

Junkermann, W., J. Hacker, T. Lyons, U. Nair, 2009: Land use change suppress precipitation. *Atmos. Chem. Phys.*, **9**, 6531 – 6539

Jury, M.R., and G.R. Tosen, 1989: Characteristics of the winter boundary layer over the, African Plateau: 26 ° S. *Boundary-Layer Meteorol*, 49(1-2), 53-76

King, J.C., A. Jrrar, and W.M. Connolley, 2007: Sensitivity of modeled atmospheric circulation to the representaion of stable boundary layerprocesses. *Geophys. Res. Letters*, **34**, L06708.

Kitaigorodskii, S. A., 1960: On the computation of the thickness of the wind-mixing layer in the ocean. *Izv.Akad.NaukUz SSSR. Ser. Geofiz*., 3, 425–431

Kolmogorov, A.N., 1941: Energy dissipation in locally isotropic turbulence. *Doklady AN SSSR*, 32(1):19-21.

Kosović, B., and J. A. Curry, 2000: A large eddy simulation study of a quasi-steady, stably stratified atmospheric boundary layer. *J. Atmos. Sci*., 57, 1052–1068.

Laakso,L., V. Vakkari, H. Laakso, A. Virkkula, M. Kulmala, J. P. Beukes, P. G. van Zyl, J. J. Pienaar, K. Chiloane, S. Gilardoni, E. Vignati,A. Wiedensohler, T. Tuch, W. Birmili, S. Piketh, K. Collett, G. D. Fourie, M. Komppula, H. Lihavainen, G. de Leeuw, and V.M. Kerminen, 2010: South African EUCAARI – measurements: a site with high atmospheric variability. *Atmos. Chem. Phys. Discuss*., 10, 30691 – 30729.

Ligda, M.G.H., 1963: Meteorological Observation with Pulsed Laser Radar. *Proc. Conf. Laser Technol.,1st, San Diego, U.S. Navy, 63*.

Mahrt, L., 1999: Stratified atmospheric boundary layers. *Bound. Layer Meteor.*, **90**, 375-396.

Mahrt, L., J .Sun, W. Blumen, T. Delany, and S. Oncley, 1998: Nocturnal boundary-layer regimes. *Boundary-Layer Meteorology* 88, 255–278.

Massen, F., 2003: A short calibration study of the Vantage Pro Plus weather station, Physics Lab, U.S.A, francis.massen@education.lu:

http://meteo.lcd.lu/papers/comparison_vantage/vantage_calibration.html

Mauritsen,T., 2007: On the Arctic Boundary Layer, PhD thesis at Stockholm University, Stockholm University, Sweden:

http://www.mpimet.mpg.de/fileadmin/staff/mauritsenthorsten/Thesis_Thorsten_Mauritsen_introduction.pdf.

Mauritsen,T., 2011: Views on Advancing turbulence closure models under stable stratification, ECMWF GABLS Workshop on Diurnal cycles and the stable boundary layer. Leading, United Kingdom. 7-10 November 2011

http://www.ecmwf.int/newsevents/meetings/workshops/2011/GABLS/presentations/Mauritsen.pdf.

Monin, A.C., and A.M. Obukhov, 1954: Fundamental laws of turbulent mixing in the atmospheric surface layer. *Annals of the Geophysical Institute, AN USSR*, No.24 (151), 163-187.

Nieuswstadt, F. I. M., 1981:"The steady-state height and resistance laws of the nocturnal boundary layer: theory compared with Cabauw observations". *Boundary Layer Meteor*., 20: 3-17 (1981).

Panofsky, H.A., and J.A. Dutton, 1984: Atmospheric turbulence, John Wiley and Sons, Inc, Canada.

Patton, E.G., P.P. Sullivan, and C. H. Moeng, 2005: Influence of idealized heterogeneity on wet and dry planetary boundary layers coupled to the land surface. *J. Atmos. Sci.*, **62**, 2078–2097

Pielke, R.A., 2001: Influence of the special distribution of vegetation and soils on the prediction of cumulus convective rainfall. *Rev. Geophys*., 39, 151-178

Pollard, R. T., P. B. Rhines, and R. O. R. Y. Thompson, 1973: The deepening of the wind-mixed layer. *Geophys. Fluid Dyn*., 3, 381–404.

Robinson, F.J., S.C. Sherwood, Y. Li, 2008: Resonant response of deep convection to surface hot spots. *J. Atmos. Sci*., 65, 276-286.

Roy, S.B., C.P.Weaver, D.S. Nolan, and R. Avissar, 2003: A preferred scale for landscape forced mesoscale circulations?, *J. Geophys. Res*.,108(D22),8854, doi:10.1029/2002JD003097.

Scanlon, T.M., K.K. Caylor, S.A. Levin, and I. Rodriguez-Iturbe, 2007: Positive feedbacks promote power-law clustering of Kalahari vegetation. *Nature*, **449**, 209-212

Scheifinger, H., and G. Held, 1997: Aerosol behaviour on the South African Highveld. *Atmos. Environ.*, **31**(21), 3497-3509.

Sharma, A., V. Sivakumar, C. Bollig, C. van der Westhuizen and D. Moema, 2009: System Description of the mobile LIDAR of the CSIR, South Africa. *South African J. of Science*, 105, 456-462..

Sivakumar, V, M.,Tesfaye, W. Alemu, D. Moema, A. Sharma , C. Bollig and G. Mengistu, 2009: CSIR South Africa Mobile LIDAR – First scientific results : comparison with satellite, sun photometer and model simulations. *South African J. of Science*, 105, 449-455, 2009.

Sogalla, M., A. Krüger, and M. Kerschgens, 2006: Meso scale modelling of interactions between rainfall and the land surface in West Africa. *Meteorology and Atmospheric Physics*, 91, 211-221.

Staquet, C., and P.B. Aubertot, 2001: Mixing in weakly turbulent stably stratified flows. *Dynamics of Atmospheres and Oceans*, 34 (2001) 81–102.

Staquet, C., 2000: Mixing in a stably stratified shear layer: two-and three-dimensional numerical experiments. *Fluid Dyn. Res*. 27, 367–404.

Steeneveld, G.J., B.J.H. van de Wiel, and A.A.M. Holtslag: 2006. Diagnostic equations for the stable boundary layer height: evaluation and dimensional analysis. *J. Appl. Meteorol. Clim.* in press.

Steeneveld, G.J., B.J.H. van de Wiel, and A.A.M. Holtslag, 2008: Long term observations of Long Wave Radiative Flux Divergence in the Stable Boundary Layer. *AMS Boundary Layer and Turbulence Conference, 9 – 13 June 2008,* Stockholm,

Steeneveld, G.J., A.A.M. Holtslag, C.J. Nappo, B.J.H. van de Wiel, and L. Mahrt, 2008: Exploring the possible role of small-scale terrain drag on stable boundary layers over land. *J. Appl. Meteor. Climatol*., 47, 2518-2530.

Steeneveld, G.J., B.J.H. van de Wiel, and A.A.M. Holtslag, 2006: Modeling the Evolution of the Atmospheric Boundary Layer Coupled to the Land Surface for three Contrasting Nights in CASES-99.*J. Atmos. Sci.*, 63, 920–935

Steeneveld, G.J.,2007: Understanding and Prediction of Stable Atmospheric Boundary Layers over Land, PhD thesis at Wageningen Universiteit, Wageningen Universiteit, Netherland:

http://www.met.wau.nl/medewerkers/steeneveld/PhDThesis.pdf

Stoll, R., and F.Port ´e-Agel, 2006: Dynamic subgrid models for momentum and scalar fluxes in large-eddy simulationsof neutrally stratified atmospheric boundary layers over heterogeneous terrain. Water Resources Res.,42, W01409, doi:10.1029/2005WR003989.

Stull, R.B., 1988: An introduction to Boundary Layer Meteorology, Kluwer Academic Publishers, Netherlands.

Sun, j., P.B. Sean, C. D. Anthony, P.O. Steven, W.H. Thomas, and H.L. Donald, 2003: Diurnal variations of thermal roughness height over a grassland. *Bound.-Layer Meteor.*, 92, 407–427.

Tennant, W.J., and B.C. Hewitson, 2002: Intra-Seasonal Rainfall Characteristics and their Importance to the Seasonal Prediction Problem. *Int. J. Climatol*., **22**, 1033-1048

Thomas, D.S.G., C. Twyman, H. Osbahr, and B.C. Hewitson, 2007: Adaptation to climate change and variability: farmer responses to intra-seasonal precipitation trends in South Africa. *Climatic Change*, **83**, 301–322.

Ting, M., Y. Kushnir, R. Seager,C. Li, 2009: Forced and internal Twentith-Century SST trends in the North Atlantic. *J. Climate*, **22**, 1469-1481.

Tyson, P.D., and C.K.Gatebe, 2001: The atmosphere, aerosols, trace gases and biogeochemical change in southern Africa: A regional integration. *South African J. of Science*, 97, 106-118.

Tyson, P.D., F.J.Kruger, and C.W. Louw, 1988: Atmospheric pollution and its implications in the Eastern Transvaal Highveld, National Scientific Programmes Unit: CSIR, SANSP Report 150, pp 123.

Van de Wiel, B. H., R.J.Ronda, H.A.R. Moene, and A.A.M.Holtslag, 2001: Intermittent Turbulence and oscillations in the Stable Boundary Layer over Land. *Journal of Atmospheric Sciences*, 59, 942-958.

Van de Wiel, B. J. H., A. F. Moene, R. J. Ronda, H. A. R. De Bruin, and A. A. M. Holtslag, 2002: Intermittent turbulence and oscillations in the stable boundary layer. Part II: A system dynamics approach. *J. Atmos. Sci.*, **59**, 2567-2581.

Van de Wiel, B., 2002: Intermittent turbulence and oscillations in the stable boundary layer over land. Ph.D. thesis at Wageningen University, Wageningen University, Netherland:

http://edepot.wur.nl/121360.

Van de Wiel, J. H., A. F. Moene, O. K. Hartogensis, H. A. R. De Bruin, and A. A. M. Holtslag, 2003: Intermittent turbulence in the stable boundary layer over land. Part III: A classification for observations during CASES-99. J. *Atmos. Sci., 60, 2509– 2522*.

Van de Wiel, B., A. Moene, G. Steeneveld, O. Hartogensis, and A. Holtslag, 2007: Predicting the collapse of turbulence in stably stratified boundary layers. *Flow Turbulence Combustion*, **79**, 251–274.

Heerwaarden, C.C. and J. Vilà-Guerau de Arellano, 2008: Relative humidity as an indicator for cloud formation over heterogeneous land surfaces. *J. Atmos. Sci.*, **65**(10), 3263 - 3277.

Verkaik, J. W., and A. A. M. Holtslag, 2007: Wind profiles, momentum fluxes and roughness lengths at Cabauw revisited. *Bound.-Layer Meteor.*, **122**, 701-719.

Vickers,D., and L.Mahrt,2004:Evaluating Formulations of Stable Boundary Layer Height.*Journal of applied meteorology*, 43,1736-1749.

Van Gogh, R.G., H.Landenberg, K.Brassel, and I. Danford, 1982: Dispersion climatology and characteristics of sulphur dioxide pollution in Eastern Transvaal Highveld, ATMOS/82/3, Atmospheric Science Division, CSIR, Pretoria, 117 pp.

Washington, R., M.C.Todd, S. Engelstaedter, S. Mbainayel, and F. Mitchell, 2005: Dust and the Low Level Circulation over the Bodélé Depression, Chad: Observations from BoDEx 2005. *J. Geophys. Res.*, **111**(D3), D03201.

Zilitinkevich, S., and I.N. Esau, 2005: Resistance and heat transfer laws for stable and neutral planetary boundary layers: old theory advanced and reevaluated. *Quart J Roy Meteorol Soc.* , 131, 3339-3356.

Zilitinkevich, S.S., and L.N.Esau, 2007: Similarity Theory and calculation of turbulent fluxes at the surface for the stably stratified atmospheric boundary layer. *In Atmospheric Boundary Layers*, Spingler,37-49.

Zilitinkevich, S.S., T. Elperinm, N.Kleeorin and I. Rogachevski, 2007: Energy- and flux-budget (EFB). Turbulence closure model for stably stratified flows, Part I: teady-state, homogeneous regimes. *In Atmospheric Boundary Layers*, Spingler, 5-35

Zilitinkevich, S.S., and I.N. Esau, 2003: The effect of baroclinicity on theequilibrium depth of the neutral and stable planetary boundary layers.*Q. J. R. Meteorol. Soc.* **129**: 3339–3356.

Zilitinkevich, S., and D. V. Mironov, 1996: A multi-limit forumulation for the equilibrium depth of a stably stratified boundary layer. *Bound.-Layer Meteor.*, 81, 325–351.

Zilitinkevich, S. S.,1972: the Determination of the Height of the Ekman Boundary Layer. *Boundary Layer Meteor.*, 3:141-145.

Zilitinkevich, S., 2002: Third-order transport due to internal waves and non-local turbulence in the Stably stratified surface layer. *Quart, J. Roy. Met. Soc*. 128, 913-925.

Zilitinkevich, S., A. Baklanov, J. Rost, A.-S. Smedman, V. Lykosov, and P. Calanca, 2002: Diagnostic and prognostic equations for the depth of the stably stratified ekman boundary layer. *Quart. J. Roy. Meteor. Soc.*, **128**, 25–46.

Zilitinkevich, S.S., J. C .R. Hunt, A.A. Grachev, I. Esau, D.P. Lalas, E. Akylas, M. Tombrou, C.W. Fairall, H.J.S. Fernando, A. Baklanov, and S.M. Joffre, 2006: The influence of large convective eddies on the surface layer turbulence. *Quarterly J. Royal Meteorol. Soc.*,**132**, 1423-1456

Zilitinkevich, S.S., J.C.R. Hunt, A.A. Grachev, I., Esau, D.P. Lalas, E. Akylas, M. Tombrou, C.W. Fairall, H.J.S. Fernando, A. Baklanov, and S.M. Joffre, 2006: The influence of large convective eddies on the surface layer turbulence. *Quart. J. Roy. Meteorol. Soc., 132, 1423-1456.*

Zilitinkevich, S., and A. Baklanov, 2002: A Calculation of the height of stable boundary layers in practical applications. *Boundary-Layer Meteorology*, 105, (3), 389–409.